

**Study on High Functionality, Durability Verification and
Insulation Diagnostic Techniques for Superconducting Maglev
Ground Coil**

March 2014

Masao Suzuki

Table of Contents

Chapter 1. Introduction	1
1.1 Background of research	1
1.1.1 Types and outline of magnetically levitated railway	1
1.1.2 Configuration of superconducting Maglev	1
1.1.3 Subject for research and development	2
1.2 Purpose of this study	5
1.3 Contents of thesis	6
Chapter 2. Operational Environments of the Ground Coil	9
2.1 Introduction	9
2.2 Mechanical load	10
2.2.1 Continuous load	10
2.2.2 Fluctuating load	12
2.3 Electrical load	19
2.3.1 Power-frequency withstand voltage	19
2.3.2 Impact withstand voltage	19
2.4 Environmental load	20
2.4.1 Deterioration due to water absorption	20
2.4.2 Ultraviolet degradation	20
2.4.3 Others	21
2.5 Summary	22
Chapter 3. Cost Reduction of Ground Coils	23
3.1 Introduction	23
3.2 RIM system coil	24
3.2.1 Characteristics of the RIM method	24

3.2.2	Development history	26
3.2.3	Development of the practical levitation and guidance coil	27
3.2.4	Durability evaluation	32
3.2.5	Cost reduction effect	36
3.2.6	Application study of the propulsion system coil	37
3.3	PLG system coil	41
3.3.1	Principle of PLG system	41
3.3.2	Development of PLG coil for practical use	42
3.3.3	Development of surface protection layer	46
3.4	Summary	51
3.4.1	RIM system coil	51
3.4.2	PLG system coil	52
Chapter 4. High Functionality of the Ground Coil		53
4.1	Introduction	53
4.2	Small cable joint with high-reliability	54
4.2.1	Development point of linear connecting part	54
4.2.2	Prototype test results of PLG coil connecting portion	55
4.2.3	Durability evaluation	56
4.3	High reliability of the coil fastening portion	60
4.3.1	Background of development	60
4.3.2	Development of the vibration resistance fastening portion	61
4.3.3	Durability evaluation	64
4.4	Reduction of the eddy current loss	65
4.4.1	Magnetic drag due to eddy currents	66
4.4.2	Quantitative evaluation of eddy current loss	67
4.4.3	Application of compression molding to the winding coil	72
4.4.4	Development of real-scale ground coil	74
4.5	Labor saving on the maintenance management of the ground coil by applying IT	81
4.5.1	Ground coils individual information management method using IC tags	81

4.5.2 Ground coil self-diagnostic method	86
4.6 High functioning of mold resin material	93
4.6.1 Functional improvement by a combination of different materials	93
4.6.2 Prototype test of toughness resin material	94
4.7 Summary	96

Chapter 5. Durability Verification of the Ground Coil 99

5.1 Introduction	99
5.2 Basic configuration of durability verification	100
5.2.1 Material property test	101
5.2.2 Investigation by actual use	101
5.2.3 Actual verification tests in stationary	101
5.3 Durability verification of the mold resin	103
5.3.1 Required functions of mold resin	103
5.3.2 Environmental degradation characteristics of the epoxy resin for molding	104
5.3.3 Water absorption characteristics	113
5.3.4 Verification of the reaction kinetics	118
5.3.5 Evaluation of fatigue strength	120
5.4 Durability verification of actual coil	126
5.4.1 Dynamic durability verification	126
5.4.2 Accelerated weathering verification	132
5.4.3 Thermal durability verification	135
5.5 Summary	137

Chapter 6. Effective Insulation Diagnostic Technique for the Ground Coil 139

6.1 Introduction	139
6.2 Insulation abnormality that should be considered in the propulsion ground coils	140

6.2.1 Voids and foreign substances	140
6.2.2 Separation of conductor from molded resin	140
6.2.3 Exfoliation of shield coating	141
6.2.4 Improper on-site installation	141
6.3 Insulation properties of the defect simulated ground coils	142
6.3.1 Exfoliation of shield	142
6.3.2 Construction defect at cable connection	145
6.3.3 Internal defect by the simulated void	148
6.4 Locating the defect position by the PD detection	151
6.4.1 PD detection by the AE sensor	151
6.4.2 PD detection by the UHF sensor	151
6.5 Development of effective insulation diagnosis technique based on the EM wave detection	156
6.5.1 Problems in insulation diagnosis of propulsion ground coils	156
6.5.2 Locating defect by using interferometer system	157
6.5.3 Preliminary examination in outdoor environment	162
6.5.4 Driving test in Miyazaki Test Line	170
6.5.5 Insulation diagnosis configuration intended for commercial operation	179
6.6 Summary	184
Chapter 7. Conclusions	187
References	193
Acknowledgement	200
List of Publications	202
List of Patents	214

Chapter 1 Introduction

1.1 Background of research

1.1.1 Types and outline of magnetically levitated railway

The magnetically levitated railway (it is also referred to as Maglev: Magnetically levitated transportation system) supports and guides its vehicles by electromagnetic (EM) force and is driven by a linear motor. There are two streams of magnetically levitated railway: one is a type aimed at ultra-high speed taking advantage of the characteristics of non-stick drive that is difficult to achieve by traditional railway, the other is a type aimed at urban and suburban transport of low-cost and low pollution although the speed is about the same as a conventional railway. They are classified according to the type of linear motor used. An ultra-high speed system supplies primary traveling power to the ground side. On the other hand, a middle to low speed system supplies primary traveling power to the vehicles. The attraction force between the magnet and iron or the electrodynamic force is used for supporting and guiding the vehicles. Presently, Transrapid, Germany, has started commercial operation of the ultra-high-speed system in Shanghai, China. Furthermore, the superconducting Maglev of the Japan Railway (JR) system is preparing for starting commercial operation from 2027. In addition, HSST, the system of middle to low speed type, began commercial operation in the Aichi Rapid Transit Eastern Hills Line (pet name "Linimo") from 2005 (Fig. 1.1) ⁽¹⁾.

1.1.2 Configuration of superconducting Maglev

A superconducting Maglev vehicle has no iron wheels or pantograph. The ultra-high-speed traveling is achieved by the state of complete non-contact with the ground. The electromagnets called "superconducting magnet (SCM)" mounted on the vehicle and "the ground coil" laid on the guide-way

make the ultra-high-speed traveling possible. The ground coil can be classified as levitation and guidance coil to support the vehicle during traveling and the propulsion coil giving power to the vehicle (Fig. 1.2). Prolonged outdoor use and a huge number of ground coils being laid over the whole track are required. Therefore, ensuring high reliability and stable performance in addition to cost reduction are important issues for the development of ground coils.

1.1.3 Subject for research and development

Because the ground coil, which is made with the resin-molded winding, does not have a core in the structure, the ground coil must be exposed to the EM force directly. Of course, electrical isolation is also required for the molding materials in addition to the mechanical strength of the coil. Therefore, it is necessary to verify the mechanical and electrical reliability from materials to the actual ground coil product level as referred by the degradation process shown in Fig. 1.3 by performing various durability tests as assumed in a commercial operation ⁽²⁾. In addition, the continuous cost reducing considerations through researching and developing the ground coil as described above will be required. On the other hand, the efforts based on the comprehensive point of view, considering not only the initial construction cost but also the energy cost for traveling and maintenance cost during commercial service operation, are also important. Improvement of the weakness of the ground coil under special operational environment and optimization of maintenance work are essential challenges. Optimization of overall efficiency will certainly improve the entire system cost.

Drive system	Levitation system	Development target, Feature
LSM (Linear Synchronous Motor)	EDS system Using Superconducting magnet Gap: 100mm	JR Maglev (Japan) • Miyazaki Test Line (1977~1996) • Yamanashi Test Line (1997~) Max. speed: 581km/h
	EMS system Using normal Electromagnet Gap: 10mm or less	Transrapid (Germany) • Emsland Test Line (1983~) • Shanghai Maglev (2003~) Max. speed of business: 430km/h
LIM (Linear Induction Motor)		HSST (Japan) • Pet name: Linimo (2005~) Max. speed of business: 100km/h

EDS: Electrodynamic Suspension
EMS: Electromagnetic Suspension
HSST: High Speed Surface Transport

Fig. 1.1 Classification of Maglev systems ⁽¹⁾

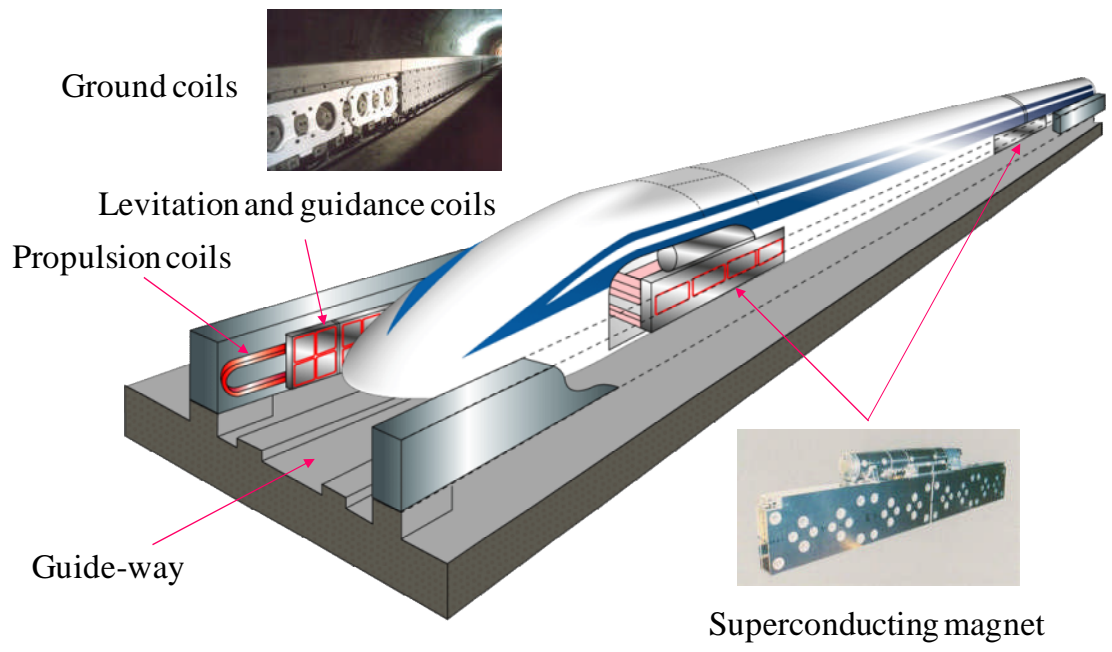


Fig. 1.2 Basic configuration of superconducting Maglev

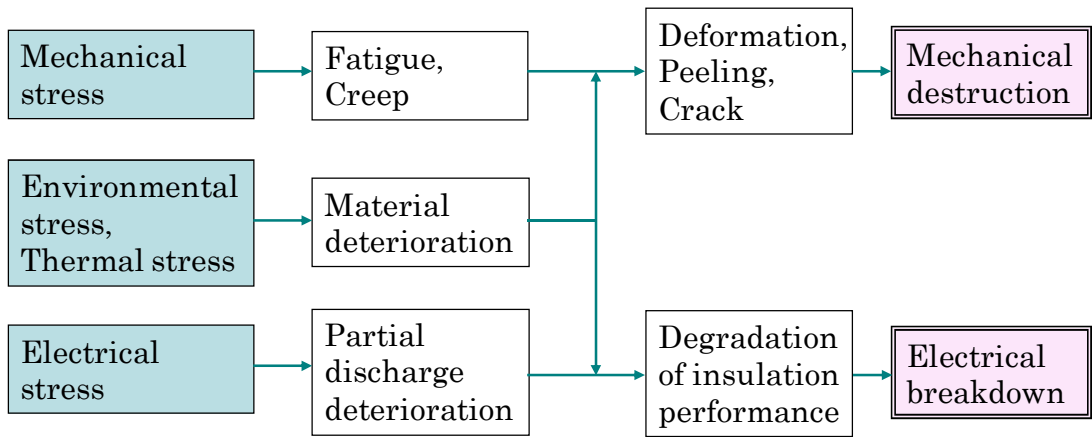


Fig. 1.3 Degradation process of the ground coil

1.2 Purpose of this study

The limit design is required for optimizing the EM force characteristics against the SCM and reducing the cost of the huge number of ground coils. Furthermore, because mechanical, electrical and environmental complex loads are applied for a long period of time to the air-core molded ground coil, its operating condition will be extremely severe. It is an important issue how the reliability of the ground coil should be verified for practical commercial operation of the system. It is necessary to organize unique verifying procedures. In this study, high functionality and a systematized durability verification method for practical commercial operation were examined while considering the conflicting proposition of cost reduction against stable performance. Furthermore, the insulation diagnostic method using EM wave detection to the propulsion coil was studied and a new diagnostic technique to identify the insulation abnormality of laying coils from the ultra-high-speed running vehicle was examined.

1.3 Contents of thesis

This paper is formed in seven chapters. The classification and outlines of Maglev systems are introduced in Chapter 1 "Introduction". The basic configuration of the superconducting Maglev and positioning of the ground coil are described. In addition, the problems concerning the ground coil caused by special operational circumstances and the purpose of this study based on these problems will be described.

The mechanical, electrical and environmental loads considered as degradation factors of the ground coil for extended period of time under the outdoor use are described in Chapter 2 "Operational environments of the ground coil". These factors are important elements in considering the determination of the specifications of the ground coil, durability verification of the product and various degradation diagnosis methods for commercial operation.

The development results concerning the two types of coils for the purpose of cost reduction are described in Chapter 3 "Cost reduction of the ground coils". One is a mass production-oriented coil that targets the levitation coil system primarily aimed at reducing the manufacturing cost of mass-produced products by reviewing the production material and method. Another is a function and configuration combined ground coil aimed at cost reduction by reducing the required number of coils.

The reliability research results aimed at improving cable connected and bolt fastening portions, which are weak points of the ground coil in the operational environment described in Chapter 2, are described in Chapter 4 "High functionality of the ground coil". The study shows how to achieve balance between reduction of the system running cost and stabilized performance by applying a compression molding to the winding coils attained by low eddy current as one of the reduction measures of eddy current loss that occurs in the ground coil wire. In addition, the ground coil individual information management method using IC tag aimed at establishing appropriate and simple maintenance and management method for commercial operation are described. Furthermore, the research results on the ground coil self-diagnosis method using the abnormality detection sensor

are described.

The unique research results towards the establishment of endurance verification method are described in Chapter 5 "Durability verification of the ground coil". First, the basic structure of the durability verification is indicated. Second, the mutual utilizing method of the test purposes and results targeting the actual vehicle used surveys, material property tests and the validation test using the actual coil is described. Third, the degradation characteristics of the mold resin material with various factors based on the actual measurement results, the strength evaluation method of resin that assumes actual commercial operation and the accelerated aging conditions that assume a long-term use are described. Furthermore, verification used by the actual coil was performed after acquiring the investigation of the actual running and the results of material property tests. It is important to know how to apply the load corresponding to the purpose of the endurance verification of the actual coil. The accuracy of durability verification is influenced by developed test equipment and the jig themselves. In this chapter, the development history of the test equipment is also described in addition to verification examples of the actual coil.

The present issues for the insulation diagnosis of the propulsion coil are discussed in Chapter 6 "Effective insulation diagnostic technique for the ground coil". The new diagnostic method is applied using EM wave detection, which makes it possible to solve problems. Insulation abnormalities that may occur in the propulsion coil or the coil connecting cables are confirmed. The non-destructive inspection to locate the defect area has been studied targeting the test coil which includes the void as an artificial defect. Locating the defect position by an EM wave detection using a radio interferometer system was studied. A method for remotely detecting partial discharge (PD) generated from the defect point has been studied. In addition, running a simulation vehicle equipped with a radio interferometer system to verify the insulation abnormality of propulsion coil laid on the guide-way and the position locating of abnormal existing coil was verified.

The results acquired by this study are summarized in Chapter 7 "Conclusions".

Chapter 2 Operational Environments of the Ground Coil

2.1 Introduction

The electrical, mechanical, and environmental prolonged and multiplex loads that are applied on the resin molded ground coils are operated under an extremely exceptional environment compared with other electrical equipment. Therefore, the design specifications for the ground coil have to be considered the operating conditions and the environment.

2.2 Mechanical load

Upon actual operation, the mechanical load applied to the ground coil can be exemplified as a continuous load with continued particular stress for a long time such as the residual stress of the coil during production, fastening stress when laying on the site, thermal stress due to temperature change and fluctuating load that is repeated in a short period of time such as the EM force and train winds. However, since these loads are added as a complex load at the same time, care should be taken in the strength evaluation of molding resin material.

2.2.1 Continuous load

2.2.1.1 Residual stress

In the production of ground coils, it is necessary to integrally mold the winding coil with resin. The most quality affecting manufacturing process of the ground coil can be the integral resin molding process. Therefore, reduction of the residual stress during molding must be considered by managing the molding conditions properly. In addition, the following two points are assumed as factors of residual stress.

(1) Residual stresses caused by the curing shrinkage

Polymeric material involves shrinkage when the resin is cured in general. The insert molded product such as a ground coil has stress caused by interaction between the shrunken resin and non-shrunken inserted materials. In order to suppress this stress, measures to reduce the curing shrinkage by incorporating a filler of inorganic matter in the resin before curing or a secondary hardening above the glass transition temperature of the resin (referred to as annealing or after curing) are effective.

(2) Residual stresses caused by temperature drop

The thermosetting resin is commonly used for molding material of the

ground coil. Molding is carried out at relatively high temperatures within the metal mold. Since the linear expansion coefficient of the polymeric material is large, the resin portion will contract by the temperature drop when returning to the ambient temperature for the product to cure, and the stress will remain. It is possible to reduce the linear expansion coefficient of the whole resin by blending an inorganic filler material in order to suppress the stress. Tailoring the linear expansion coefficient of the molding material to be the winding coil will be ideal. Furthermore, slow cooling to reduce the temperature over time while keeping a uniform temperature in the entire product is also effective.

2.2.1.2 Fastening stress

The popular bolt fastening method that fastens the ground coil to the guide-way cannot prevent the stress concentration to the resin part near the fastening portion due to steps occurring on the coil mounting surface of the side wall and/or the surface accuracy error of the coil itself. Furthermore, considerable ground coil fastening axial torque is needed to keep it from a repeated EM force when the vehicle is passing. This bolt axial force will add forced deformation to the coil, and there will be a risk when continuous excessive stress is applied to the coil as a steady load. This stress depends on the pitch of the fastening portions and the elastic modulus of the resin material. Optimum condition must be considered for holding the electromagnetic force.

2.2.1.3 Thermal stress

Ground coils operated outdoors receive repeated thermal expansion and contraction due to environmental temperature change during the day and throughout the four seasons, and receive repeated thermal stress to their resin part in the vicinity of the bolt fastened portion. It is important to match the thermal expansion coefficient of the molding resin with the coil conductor the same as the residual stress mentioned above as much as possible. The ground coils in a sunbeam reached zone in particular will have large

temperature differences compared to the tunnel section. Special care should be taken on heat stress measures for environmental temperature changes. In addition, the winding coil generates heat due to various currents (i.e. propulsion, levitation and guidance currents) while the vehicle is running resulting in non-uniform temperature distribution in the mold resin portion, which produces repeated thermal expansion and contraction at the vicinity of the fastening portion resulting in repeated thermal stress. In order to reduce these thermal stresses, the coil fastening structure compensating for thermal expansion and contraction due to temperature changes must be required. However, since it is difficult to maintain the friction coefficient of the surface and the bolt tightening axial force to be constant, it is necessary to consider a new construction in the fastening portion itself. The new proposal of the bolt fastening portion will be described in detail in Chapter 4.

2.2.2 Fluctuating load

2.2.2.1 Electromagnetic force

The EM forces (propulsion, levitation, guidance forces) are repeatedly applied from the superconducting magnets on the vehicle to the ground coils as a reaction to the vehicle passing force. EM force applied as a distributed load to the winding coil tends to act as fatigue load to each part of the mold resin, which concentrates in the vicinity of the fastened parts. EM force F , acting on the ground coils, is given by the following equation. The calculation method of the magnetic field of the SCM and example of calculation of the EM force acting on the various parts of the ground coil are shown below.

$$\mathbf{F} = \mathbf{I} \times \mathbf{B} \quad (2.1)$$

where I is current of the ground coil, B is interlinked magnetic flux density.

(1) The parameter setting for the magnetic field calculation

Take the coordinate system as shown in Fig. 2.1. It is assumed that SCM are arranged at a pitch of τ in the traveling direction. SCM are arranged in a

cycle W_y in the y -direction for the convenience of calculation. Also, the arc portion of SCM is approximated by a set of coils stepwise as shown in Fig. 2.2, to converge in the infinite number of divisions ^{(1), (2)}.

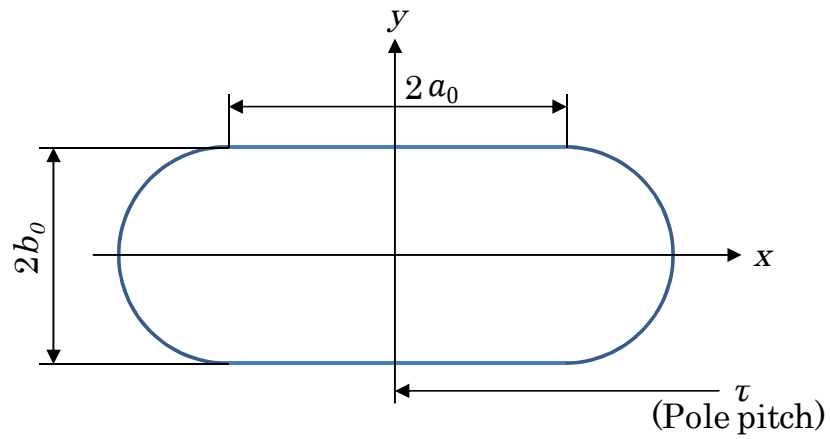


Fig. 2.1 Model of SCM and coordinate system



Fig. 2.2 Stepped approximation of the circular arc portion

(2) Calculation of the magnetic field created by SCM

If the superconducting coil [length $2a_0$, width $2b_0$, the center of the coordinates is $(x_0, 0, 0)$] has the magnetomotive force I_s , the magnetic flux density B at the specific position (x, y, z) can be expressed as follows ^{(1), (2)}:

$$\mathbf{B} = \frac{2\mu_0 I_s}{\tau W_y} \sum_{m=-\infty}^{\infty} ' \sum_{n=-\infty}^{\infty} e^{-k_{mn}z} \frac{\sin k_{xm} a_0}{k_{xm}} \frac{\sin k_{yn} b_0}{k_{yn}} \times e^{-jk_{xm}x_0} e^{j(k_{xm}x+k_{yn}y)} (-j\mathbf{k}_{mn} + k_{mn}\mathbf{e}_z) \quad (2.2)$$

where $k_{xm} = m \frac{\pi}{\tau}$ $k_{yn} = n \frac{2\pi}{W_y}$

\mathbf{e}_x , \mathbf{e}_y , \mathbf{e}_z are unit vector in each direction

$$\mathbf{k}_{mn} = k_{xm}\mathbf{e}_x + k_{yn}\mathbf{e}_y \quad k_{mn} = \sqrt{k_{xm}^2 + k_{yn}^2}$$

$\sum_{m=-\infty}^{\infty} ' : This value shall be the sum value, where m is an odd number.$

Furthermore, calculate the magnetic field in the same way as the circular arc portion of the superconducting coil. If the arc portion is divided into number L in the longitudinal direction as shown in Figure 2.2, the rectangle of the number k -th can be expressed as follow:

Length: $2a' = b_0 / k$

Width: $2b_k = 2\sqrt{b_0^2 - \{(2k-1)a'\}^2}$

Center: $a_0 \pm (2k-1)a'$

The synthesized magnetic flux density B of SCM is as follows:

$$\mathbf{B} = C_0 \sum_{m=-\infty}^{\infty} ' \sum_{n=-\infty}^{\infty} e^{-k_{mn}z} \left\{ \frac{\sin k_{xm} a_0}{k_{xm}} \frac{\sin k_{yn} b_0}{k_{yn}} + 2 \frac{\sin k_{xm} a'}{k_{xm}} S_L(m, n) \right\} \times e^{j(k_{xm}x+k_{yn}y)} (-j\mathbf{k}_{mn} + k_{mn}\mathbf{e}_z) \quad (2.3)$$

where $C_0 = \frac{2\mu_0 I_s}{\tau W_y}$

$$S_L(m, n) = \sum_{k=1}^{-L} \frac{\sin k_{yn} b_k}{k_{yn}} \cos k_{xm} \{a_0 + (2k - 1)a'\}$$

Each x, y and z directional component of the magnetic flux density B can be expressed as follows:

$$B_x = C_0 \sum_{m=-\infty}^{\infty} ' \sum_{n=-\infty}^{\infty} e^{-k_{mn}z} \left\{ \frac{\sin k_{xm} a_0}{k_{xm}} \frac{\sin k_{yn} b_0}{k_{yn}} + 2 \frac{\sin k_{xm} a'}{k_{xm}} S_L(m, n) \right\} \\ \times e^{j(k_{xm}x + k_{yn}y)} (-jk_{xm}) \quad (2.4)$$

$$B_y = C_0 \sum_{m=-\infty}^{\infty} ' \sum_{n=-\infty}^{\infty} e^{-k_{mn}z} \left\{ \frac{\sin k_{xm} a_0}{k_{xm}} \frac{\sin k_{yn} b_0}{k_{yn}} + 2 \frac{\sin k_{xm} a'}{k_{xm}} S_L(m, n) \right\} \\ \times e^{j(k_{xm}x + k_{yn}y)} (-jk_{yn}) \quad (2.5)$$

$$B_z = C_0 \sum_{m=-\infty}^{\infty} ' \sum_{n=-\infty}^{\infty} e^{-k_{mn}z} \left\{ \frac{\sin k_{xm} a_0}{k_{xm}} \frac{\sin k_{yn} b_0}{k_{yn}} + 2 \frac{\sin k_{xm} a'}{k_{xm}} S_L(m, n) \right\} \\ \times e^{j(k_{xm}x + k_{yn}y)} (k_{mn}) \quad (2.6)$$

(3) Electromagnetic force acting on the each portion of the ground coils

Based on the magnetic field created by SCM, the EM forces acting on each portion of the ground coils are calculated and are shown below. The calculation result assumes that the most severe load condition on the design acting on the ground coil was applied.

① Propulsion coil

The phase of the LSM (Linear Synchronous Motor) current providing the propulsive force to the vehicle is normally controlled so that the propulsive force of SCM is maximized. However, if the train has a long configuration, the phase shift occurs between the leading and trailing vehicles due to thermal expansion and contraction of the seasonal temperature changes. In

addition, this phase shift gives unnecessary lateral (the guide direction) force to the propulsion coil, and this phase shift causes excessive load on the flat ground coils. In this study, the EM forces acting on each side of the propulsion coil shown in Fig. 2.3 are calculated as three directional components described in Table 2.1.

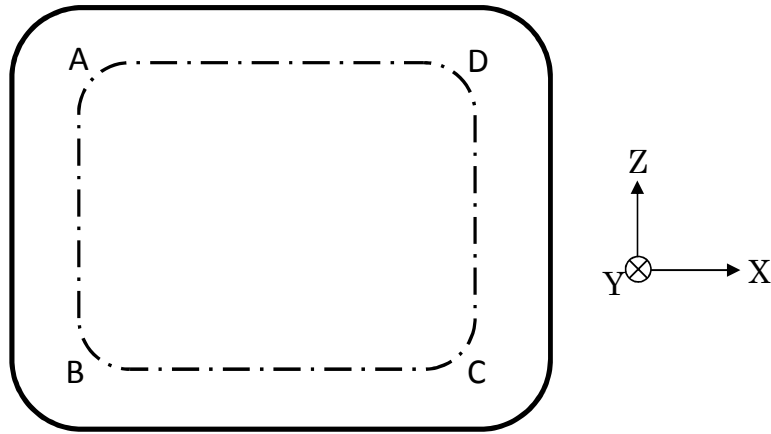


Fig. 2.3 Center position of conductor of propulsion coil

Table 2.1 EM force act on each side of propulsion coil

Coil side	F_x (kN)	F_y (kN)	F_z (kN)
AB	1.28	3.01	0
BC	-0.06	3.53	1.30
CD	-3.72	1.39	0
DA	-0.06	3.53	-1.30

② Levitation and guidance coil

The repeated lateral directional load largely affects the durability of the mold resin of the flat levitation and guidance coil. In particular, if an excessive guidance force is superimposed while levitation running, it will be the most severe load condition. In this study, running at a levitation speed of 100 km/h is assumed. The EM forces acting on each unit coil of the levitation and guidance coil shown in Fig. 2.4 are calculated as three directional components described in Table 2.2.

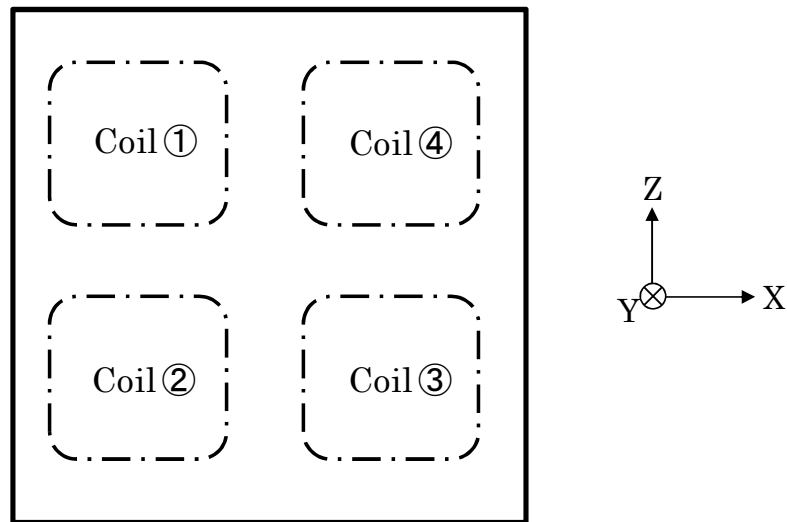


Fig. 2.4 Center position of conductor of levitation and guidance coil

Table 2.2 EM force act on each unit coil of levitation and guidance coil

Unit coil	F_x (kN)	F_y (kN)	F_z (kN)
Coil ①	-0.13	-0.91	-9.99
Coil ②	0.27	12.1	-10.5
Coil ③	6.69	22.3	-17.4
Coil ④	-2.74	-2.06	-13.2

2.2.2.2 Train winds

The pressure fluctuations associated with the train passing and train winds generated by the train passing act as a wind pressure on the surface of the ground coil resulting in a repeated stress at the vicinity of the fastened parts. However, as the mechanical load caused by train wind is much smaller compared with the load of the EM force, it is negligible in the strength design of the mold resin. On the other hand, care must be taken for the surface unevenness of the coil and the gap between the installed coils, because it may cause noise intrusion into the vehicle due to train running wind.

2.3 Electrical load

Ground coil can be classified into propulsion coil and levitation and guidance coil according to their purpose. The former receives power from the substation and gives motive power to the vehicle. The latter generates levitation and guidance forces without external power supply and without control from the outside. The electrical load corresponding to special high-voltage equipment is applied intermittently to the propulsion coils.

2.3.1 Power-frequency withstand voltage

Voltage applied to the propulsion coil is determined by the system section length, speed and required propulsion power for the target system. The propulsion coil is considered the power apparatus of the three-phase alternating current. The ultra-fast system for mass transport requires an insulated design for a nominal voltage of 33kV considering the efficiency of the motor.

2.3.2 Impact withstand voltage

The switching surge at the time of opening and closing of the power feeding section switch and the lightning surges under outdoor operation can be considered to be an impact voltage applied to the propulsion coil. However, if very large and steep voltage such as lightning surge is applied, the counter electromotive force of the inductance becomes greatly increased. As a result, it is clear that only the leading coil accepts most of the voltage through analysis and by the results of the experiment. That is, in order to design a lightning allowable insulation, it is necessary for each layer of the coil to have a similar dielectric strength equivalent to the withstand voltage. This will give significant influence to the system design. Therefore, in order to secure from lightning surges exceeding dielectric strength, overhead ground wire, lightning arrester, etc. are used.

2.4 Environmental load

It is assumed that the integrally formed ground coils with molding resin of polymeric material will be used outdoors for a long period of time. Therefore a decrease in strength of the material due to environmental factors will be inevitable. It is important to examine the specification considering the expected degradation to the end of operation life for the design of the ground coil. It is necessary to grasp the accurate environmental load.

2.4.1 Deterioration due to water absorption

The hydrolysis of polymeric material to a low molecular weight in general is caused by the existence of moisture in the oxygen-containing air (rainfall, condensation in the tunnel, humidity). Hydrolysis with cleavage of molecular chains develops from the surface to the depth of the material resulting in reduced strength of the material. Because the degree of influence is different depending on the molecular structure of the material and the operating conditions, design study that takes into account the operating environment is important.

2.4.2 Ultraviolet degradation

The main components of the ultraviolet rays in sunlight reaching the ground that passes through the ozone layer have a wavelength of 300 to 400nm. Ultraviolet rays exert chemical reactions on irradiated objects to promote oxidative degradation and accelerate aforementioned hydrolysis on polymeric material. Therefore, level of ultraviolet rays and weather resistance treatment against ultraviolet radiation are important for long term outdoor use.

2.4.3 Others

It is necessary to consider other environmental degradation factors such as alkaline water that is generated through the tunnel and guide-way structures, salt damage due to sea breeze near the coast, blowing dust caused by train wind of ultra-high-speed train passing on the ground coils.

2.5 Summary

The ground coils used as an EM guide-way are forced to be exposed to electrical, mechanical, and environmental complex load. Therefore, when designing the ground coil, it is necessary to scrutinize the operating and environmental conditions over a long time and set appropriate specifications.

Mechanical loads can be classified into the continuous load receiving a specific stress for a long time and the fluctuating load intermittently applied for a short time. The continuous load consists of residual stress of the coil manufacturing and on-site installation stresses, thermal stress due to temperature change, etc. The fluctuating load consists of EM force and vibration during the vehicle passing, train wind, etc. These loads will cause a decrease in strength specific to the polymer material of the molding resin. On the other hand, as the EM force applied coil is dependent on the system specification and vehicle running conditions, it is necessary to grasp and devise the load distribution to each part of the coil, the structure of the coil itself and the on-site support configuration.

For electrical load, it is necessary to consider the operation of the propulsion system coil, where power is supplied from the substation, as special high-voltage equipment. Therefore, the insulation design as power apparatus of a three-phase alternating current is required for the propulsion coil and coil connection cables. Operational environment of these coils and cables that are constantly exposed to the electromagnetic vibrating environment is extremely severe condition as power equipment, and it is necessary to increase reliability and be maintained by a careful monitoring.

Decrease in strength of the material of the resin molded ground coil due to environmental impact is inevitable. Therefore, it is necessary to grasp the accurate environmental load. The polymeric material is hydrolyzed by the presence of oxygen and moisture in general resulting in low molecular weight. In particular, ultraviolet rays in sunlight promote chemical reaction on the irradiation object to accelerate degradation. Therefore, it is important to grasp the kinds and extent of the environmental impacts for a long-term outdoor use of ground coils, and perform weather resistant measures as needed.

Chapter 3 Cost Reduction of Ground Coils

3.1 Introduction

Two types of methods were tackled from different aspects for the study to reduce the cost of the ground coil ⁽¹⁾. The first is intended to review the construction materials and manufacturing method of the coil to reduce manufacturing cost as mass-produced items. The second is intended to review the function and structure of the ground coils to reduce the cost by reducing the required number of coils.

3.2 RIM system coil

The integral molding process of the winding coil with resin is essential, which is the most important process in the production of ground coils. Therefore, the selection of molding material and manufacturing method give significant impact on the reliability of the coil. And it is also the key to cost reduction as to how this process can be efficiently completed in a minimum time. In this study, the reaction injection molding method (hereinafter referred to as RIM system) using DCPD (dicyclopentadiene) resin, which can be expected to reduce the cost by simplifying the winding coil structure and by shortening the molding cycle, is studied and developed through the prototype production of practical levitation coils.

3.2.1 Characteristics of the RIM method

RIM is defined as "a particular molding method in which two or more types of low molecular weight and low viscous liquid monomers is blended in a mixing chamber, injected into a sealed mold and is hardened by reaction in a short period of time." Figure 3.1 shows an outline of the molding system ⁽²⁻⁴⁾. This method of pouring low viscous liquid raw materials directly into a mold differs from the general injection molding of thermoplastic resin or from the SMC (Sheet Molding Compound) has shown the best result of molding ground coils so far. Since short-time molding is possible under normal temperatures and normal pressure, this method has a number of advantages for mass production ⁽⁵⁻¹⁰⁾. The typical features of DCPD RIM that has been applied to the molding of the ground coil is shown below.

(1) Unlike SMC or epoxy molding, as it is possible to obtain a polymer (molded article) directly from the monomers, the molding process will be simple (Fig. 3.2).

(2) Because it is possible to arbitrarily control the speed and timing of the polymerization reaction, it is possible to suppress the increase of viscosity of the liquid mixture until the injection is completed. It facilitates the wide

selection of cycle time of molding.

(3) Molding is possible at normal temperatures and at normal pressure. Because it will be thermally cured by self-reaction heat, it is possible to reduce the molding costs (molding equipment, number of molds, saving energy).

(4) Since load to the insert material is light during molding, simplification is possible for winding the coil, assembling operation and insulating structure.

(5) Since DCPD is discharged in large quantities as a by-product during the cracking of petroleum, the raw material can be easily secured and can expect reduction of refining cost due to the expansion of the market.

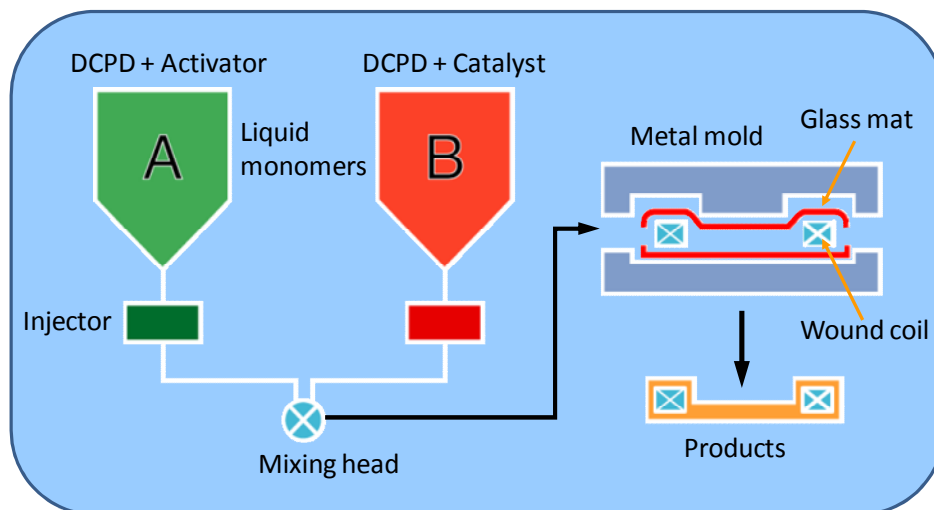


Fig. 3.1 Outline of the molding system

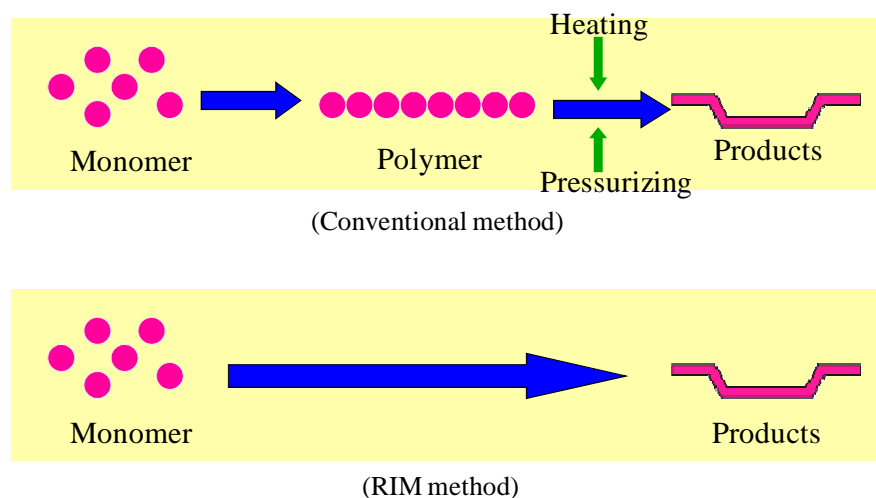


Fig. 3.2 Difference in the molding process

3.2.2 Development history

DCPD material used by RIM is a new concept of molding method that has a lot of potential as described above. Therefore, although this molding material appeared less than 30 years ago in the world, it has been applied to many products due to its various superiorities and its rapid expansion of applications. However, most of the applications so far are on the assumption of a standard composition of neat resin (non-reinforced) molded products. This is the first time to use integral mold to seal a large metal such as a ground coil. The development history of the ground coil system by RIM is described below.

3.2.2.1 First Stage: Preliminary study

Primary trial on the Miyazaki Test Line

(1) Basic properties of DCPD resin

Basic properties of the resin, influence on the aluminum conductor and compatibility with the insulation coating material of the wire were investigated to confirm suitability as a mold for resin of the ground coil.

(2) Neat forming coil prototype experiment

The prototypes of the sidewall levitation coil using neat resin for the Miyazaki Test Line were molded in the Railway Technical Research Institute. Their performance was confirmed by various bench tests before installing to the actual site. Twelve coils (1 cell length of the propulsion coil) were installed to the site and their performance was confirmed.

3.3.2.2 Second Stage: Improvement of molding quality

Second prototype for the Miyazaki Test Line

(1) Improvement of the molding parameters

Molding quality (strength of the resin, residual stress, dimensional accuracy) was improved by the improvements of the molding conditions (the application of glass mat, pre-heating of the winding coil, uniformity of

reaction, etc.)

(2) Confirmation of durability

One hundred forty four levitation and guidance coils were laid (approximately 1 section length of the propulsion coils) to the site according to the extension of the sidewall levitation area of the Miyazaki Test Line to confirm function and durability. Inexpensive PCW (Powder of epoxy resin Coating Wire) was used for wire.

3.3.2.3 Third Stage: Improvement of the critical strength of the resin

Trial manufacturing of practical coil

(1) Examination of flame retardant

Flame retardant of the resin by adding red phosphorus powder.

(2) Improvement of the mechanical strength

Improvement of adhesion on the boundary surface between the resin and glass mat and/or phosphorus powder by applying surface treatment (silane treatment), as well as improvement of the mechanical strength and water absorption resistance.

(3) Detailed stress analysis

Implementation of the detailed strength evaluation by FEM (Finite Element Method) analysis in parallel with the durability evaluation by the bench testing

3.2.3 Development of the practical levitation and guidance coil

3.2.3.1 Coil specifications

An outline of the practical levitation and guidance coil specifications based on the operating conditions is shown in Table 3.1. The external view of the coil is shown in Fig. 3.3. This trial incorporated new ideas of safety

based on flame-retardant resin, stability based on the preformed glass mat and labor reduction based on the application of metal bushes.

Table 3.1 Specifications of the practical coil

Items	Specification
Magnet wire	EP. powder coated
Shape of the wire	Low type of eddy current loss
Molding method	RIM method
Resin of molding	DCPD (Dicyclo-pentadiene)
Thickness of molding	7mm
Blend of the resin	Flame-retardant resin
Reinforcement fiber	Continuous strand glass mat
Fixing point to the guide-way	Use of the metal bushes
Withstand voltage (to ground)	2,800V / for one minute
Withstand voltage (interlayer)	4,000Vp

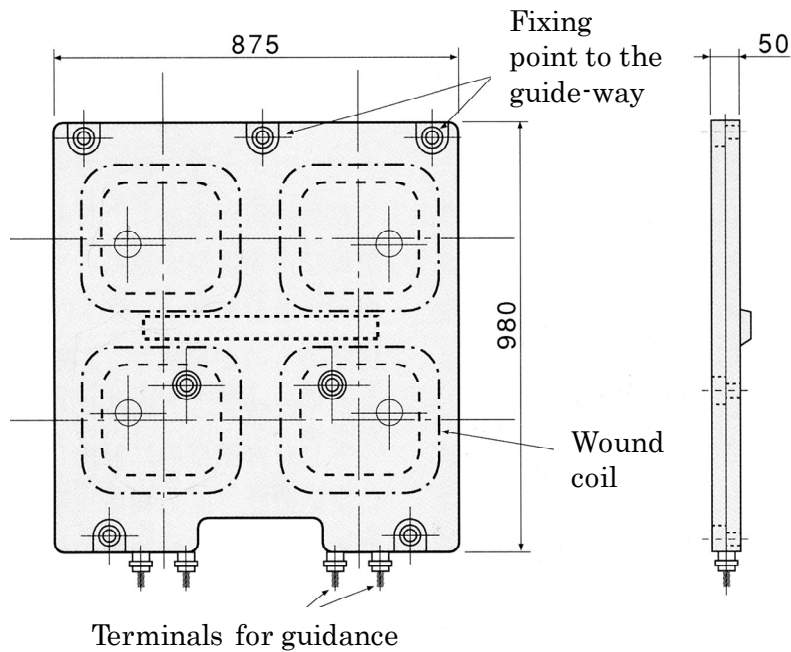


Fig. 3.3 Exterior of the trial coil

3.2.3.2 Flame retardant of the resin

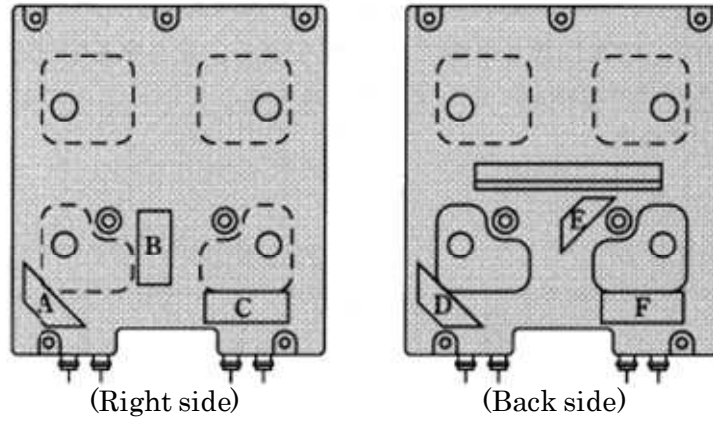
Over 80% of the total length of the track is tunnel section in the Yamanashi Test Line. It is assumed that significant percentage of tunnel and underground sections will be required in the future commercial lines. Therefore, fire protection of the ground equipment is an important development theme to ensure safety. The flame-retardant resin is achieved in the practical coil by blending red phosphorus powder compound to DCPD solution. A test specimen was sampled from the article for confirming the flame-retardant effect, and a combustion test based on JIS K 7201 (a combustion test method for the polymer material by the oxygen index method) was performed. As a result, the oxygen index^{※3.1} improved from 21.0 (before compounding flame retardant) to 31.5 (after compounding flame retardant). This data shows increased flame-retardant effect.

※3.1: Oxygen concentration calculated from the oxygen and nitrogen flow rates required for either continuous burning time for more than 3 minutes or continuous combustion length for more than 50mm.

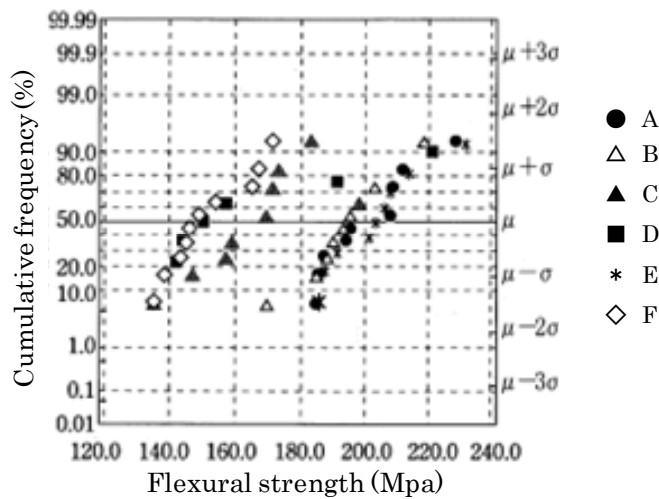
3.2.3.3 Preform of glass mat

Concerning the glass fiber reinforced resin, previously prepared glass mats of various shapes were manually inserted around the winding coil before molding. However, this work not only consumes a number of steps but also decreases the uniform molding quality. It is not suitable as a mass production method for the ground coil that requires stable performance. In a practical ground coil, preform of glass mat was applied with the aim of stabilizing molding quality and cost reduction by reducing molding process numbers. The preform method used in this study is to soften the mat binder by heating the glass mat of predetermined thickness and to form into the integral three-dimensional shape using a resin mold. It is also used to position the winding coil when molding it in a mold. Test pieces were cut out from the each part of the formed coil and the glass content percentage and bending strength were measured. As a result of measurement, stabilization of the physical properties and normal impregnation of compound solution into the preform mat were confirmed. Figure 3.4 shows the improvement of

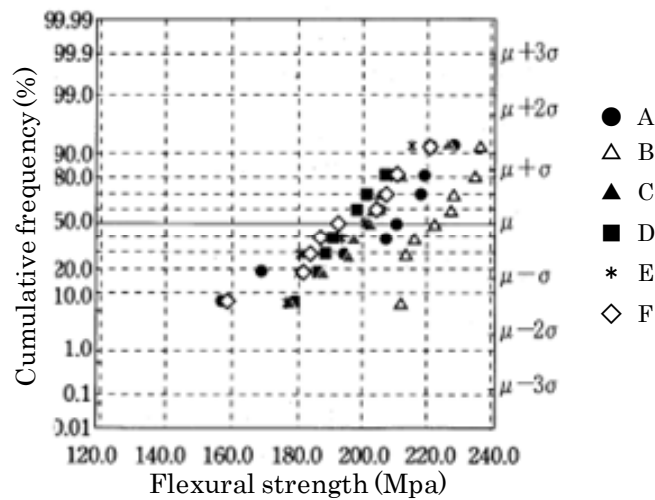
bending strength distribution of the preform applied prototype comparing with the conventional preform unapplied product.



Sampling point of the trial coil



Before the pre-forming process was applied



After the pre-forming process was applied

Fig. 3.4 Distribution of the flexural strength

3.2.3.4 Application of metal bush

Normally, the EM force generated in the ground coil is supported by the frictional force with the attached object acquired by the bolt axial force. The thermal expansion and contraction due to temperature change are allowed by sliding the bolt fastening of the ground coil. However, the initial axial force of the bolt fastening cannot be kept constant and the axial force gradually decreases due to creep deformation of the resin and finally the coil loses its functions. Therefore, an axial force management by the periodical bolt fastening is also required. And it will be a problem of reliability and maintainability of the ground equipment. The coil of the actual type aims for stable performance and simplified maintainability. The fastening part configuration using a metal bush that can neglect creep deformation is applied to the bolt fastening part in order not to reduce the axial force after bolt fastening. In this case, the strength of the resin which holds the metal bush is the target of the evaluation using the model coil fabricated by various conditions. The push-out strength test of the metal bush was performed. Two types of cylindrical metal bush with cross-knurling finished on the outer periphery were tested as shown in Fig. 3.5. According to the test results of experiment, the push-out strength of the simple cylindrical shape that corresponds to the coil on the top and middle fastening portions was 56.8 kN on average for the target value 19.6 kN, the strength that corresponds to the coil on the bottom fastening portions was 155 kN on average for the target value 73.5 kN. It was confirmed that the metal bush has a sufficient strength to the aimed safety factor value 4.0.

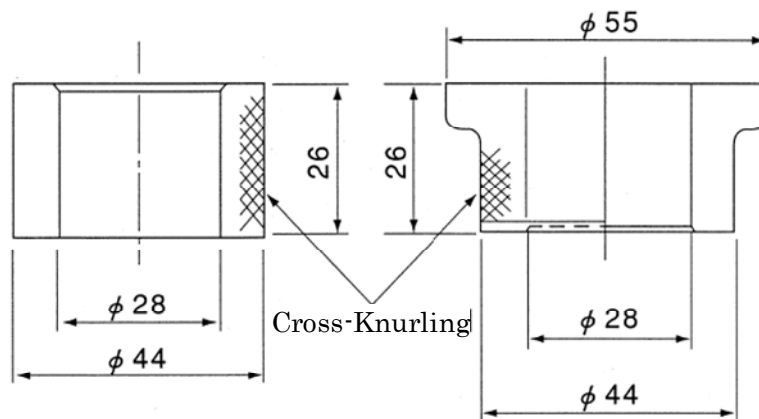


Fig. 3.5 Exterior of metal bushes

3.2.4 Durability evaluation

3.2.4.1 Preliminary verification by the bench testing

Prior to the on-site installation of the practical coil, various performance and durability were confirmed in the Institute. The preliminary validation test results for the mechanical strength properties are described as a typical example.

(1) Step fastening test

At the time of the coil fastening to the structure, the simulation step of +3 to -3mm at specific portion of the bolt fixing part was set and the coil was fastened with 20 kN axial force. The generated stress was measured. As a result, the generated stress can be seen to concentrate at the bolt fixed part. The maximum stress is approximately 10 MPa for the step of +2 mm, which is the worst case for on-site installation. Sufficient durability for long-term operation was confirmed.

(2) Static load test

While a coil was fixed with the simulated sidewall, uniform static load (0 to 200 kN) simulating the electromagnetic force in the guide direction was applied to the four sides of the terminal side of the levitation unit coil and the generated stress and deformation in each part of the coil were measured. As a result, no abnormality including crack was confirmed with a load of 200 kN, which was the maximum capacity load of the loading equipment. When the load equivalent to the maximum lateral force for normal traveling was applied, the generated stress was maximum 4.5MPa around the metal bush. High durability for practical use was confirmed. The test condition of the static load is shown in Fig. 3.6.

(3) Environmental fatigue test

The test coil was installed in the thermostatic chamber used for durability experiment with the same test configuration described above. Mechanical and environmental loads shown in Fig. 3.7 were applied simultaneously to confirm the abnormality after completion of experiment.



Fig. 3.6 Test condition of the static load

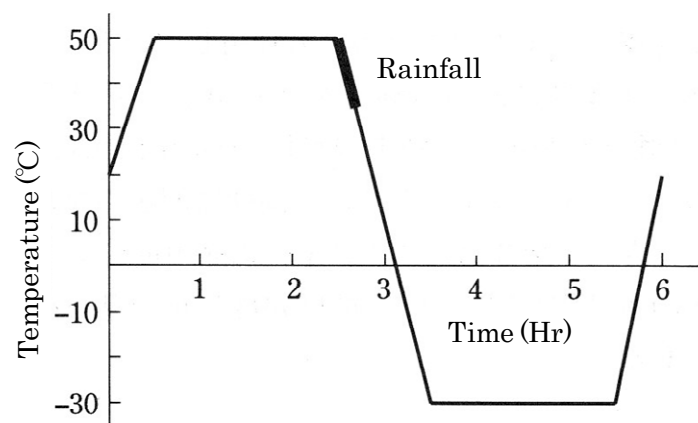


Fig. 3.7 Environmental load conditions

- ① Mechanical load conditions
 - i Bolt fastening axial force 30 kN
 - ii Applied load 45 kN (max)
 - iii Loading times 10^7 times
 - iv Excitation frequency 10 Hz

- ② Environmental load conditions
 - i Composite heat cycle
-30 to 50°C / 6 hours

- ii Rainfall
10 minutes descending from 50 to -30°C
- iii number of additional times
46 times (Mechanical fatigue period)

(4) Preliminary examination result

After completion of the preliminary validation experiments and the aforementioned environmental fatigue experiments by the composite loads, the following items were researched and measured. Complete validity was confirmed for on-site operation.

① Appearance investigation

A result of the investigation of color check on the coil surface by staining liquid penetrating agent, no abnormality such as a crack was observed.

② Interlayer insulation

The impact voltage of 4.0 kV_p was applied to the coil lead terminals, and the damping voltage oscillation waveform was measured. No abnormality was observed in the waveform, the same as the initial interlayer insulation test result. The sufficient interlayer insulation was confirmed.

③ Push-out intensity of the metal bush

The push-out intensity measuring results of the metal bushes for each bolt fixing portion were on the average 60 kN for simple cylindrical shape and 170 kN for single flange with cylindrical shape. It was confirmed that the metal bush had a sufficient securing force for the intended target value. The measured values were approximately the same level as the measurement results of the specimen that was not performed in the environmental fatigue experiment. A sufficient durability around the bush was confirmed.

3.2.4.2 On-site durability evaluation

This practical prototype coils are installed to the part of the Yamanashi

Test Line in May 1999 as improved ground coils after confirming a variety of bench test results ⁽¹¹⁻¹⁴⁾. The durability test with high speed levitation running of the vehicles was performed. At that time, two types of prototype coils (with and without surface coating) were installed in order to evaluate the differences in the environmental degradation of the mold resin due to the presence or absence of weather-resistant paint. As a result of the field endurance test over a long period of time, oxidation degradation which is considered to be affected by the ultraviolet rays was observed for the coils with no weather-resistant coating. Exposure of glass fibers were observed in the same way as conventional coils. Requirement of the weather-resistant coating for sunbeam reached area was suggested. On the other hand, no particular problem has occurred in the long-term operation concerning the functions as a levitation and guidance coil and durability of the bolt fastening portion similar to the weather-resistant coating coils. Figure 3.8 shows the status of the prototype coils installation in Yamanashi Test Line.



Fig. 3.8 State of the prototype coils laid on the Yamanashi Test Line

3.2.5 Cost reduction effect

As mentioned at the beginning of this chapter, the main aim in the development of this RIM system coil is to reduce the costs. The RIM system was compared and verified with the SMC system which was popular as the conventional mass-produced molding system by considering the production cost of levitation coils for practical specifications. As a result, the prospect of cost reduction of about 40% in the molding cost and about 30% in total cost was obtained.

3.2.5.1 Reduction efficiency for molding costs

The molding cost was included into the material costs, equipment costs and processing costs. The RIM system was compared with SMC as the standard. The comparison example is shown in Fig. 3.9.

3.2.5.2 Other cost reduction effect

As mentioned in “Characteristics of the RIM method” we aimed at not only the simplification of the molding process but also lightening the burden to the wound coils. As a result, we found that various incidental efficiencies are expected.

(1) Material

It is possible to reduce the wire cost by using an inexpensive epoxy powder coating wire instead of prepreg insulating wire used by the SMC system.

(2) Coil construction

The RIM system can omit the coil assembly and baked-solidification processes that are the essential requirement of the SMC system for molding in high temperature and high pressure environment. Therefore the winding and assembling process can be greatly reduced.

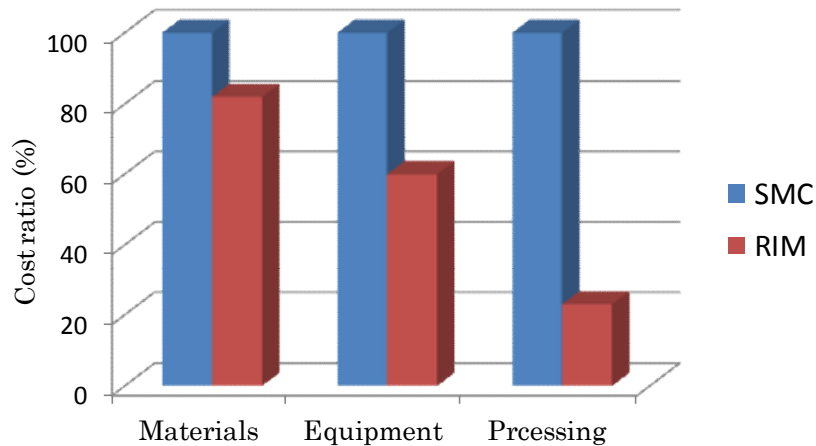


Fig. 3.9 Comparative example of molding costs

(3) Coil installation

Since the elastic modulus of the resin is about half of SMC, it is possible to reduce the generated stress of the coil when it is mounted. This results in successful lowering of installation costs.

3.2.6 Application study of the propulsion system coil

We studied further decrease of the cost of the ground coil based on the low-voltage system. By decreasing the power feeder line voltage to 6.35kV (Nominal 11kV) which is equivalent to the Miyazaki Test Line, the insulation structure of the coil body and cable connections can be simplified resulting in cost reduction and reliability improvement. In this case, the RIM system application to the propulsion system coil can be also considered. We investigated the suitability of applying the RIM system whether it satisfactory resulted as the low voltage levitation coil system.

3.2.6.1 Examination items

(1) Check the suitability and performance when DCPD resin is used as the insulating material.

(2) The mica was used as the main insulation to the earth. The mica as the electric insulator and DCPD resin as the mechanical strength material were checked for functional integration.

(3) Confirm the formability by vacuum injection of the blended solution.

3.2.6.2 Prototype test by the bar model

As shown in Fig. 3.10, the epoxy powder coated aluminum flat wire was used as a conductor. The two types of prototype bar models (one was inside shielded and the other was not shielded) were used for various experiments. As a result, the following performance was confirmed.

(1) Model with internal shield layer (with mica insulation)

Forming a mica insulating layer equivalent to the phase voltage 6.35kV (line voltage: 11kV) around the conductor, providing a conductive shield layer around the mica layer, placing a glass mat to the outer layer, and vacuum injecting the DCPD blend solution into the RIM mold, various experiments were performed to the bars.

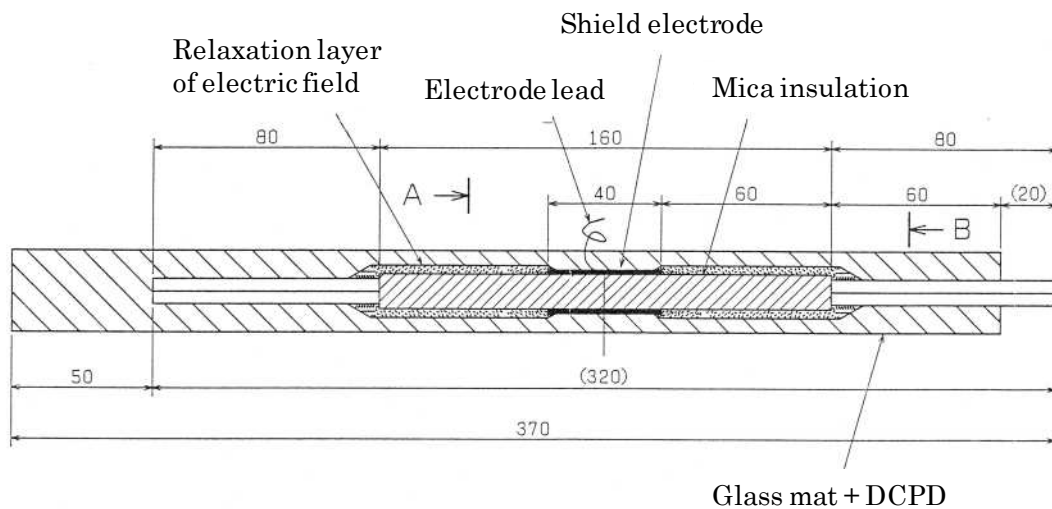


Fig. 3.10 The outer shape of the bar model

As a result, sufficient performances were confirmed to the electrical properties and withstand voltage. However, PD was confirmed at low voltage of 3kV between layers because the mica flakes were used. However, because the PD resistance life of mica is longer by several orders than that of the polymer material such as epoxy resin and mica has an operating experience as a generator and other equipment successfully, mica as an electrical insulating material can be integrally used with DCPD resin as a mechanical strength member.

(2) Model without internal shield layer (without mica insulation)

The bar was manufactured by arranging glass mats around the conductor and injecting DCPD blended solution. Its breakdown voltage to the ground was 40 to 50 kV and the PD start voltage was about 11kV. These characteristics were better than that of internal shielded ones. However, it is necessary to consider the long-term reliability of DCPD resin used as an insulating material, specifically verification of the durability of the conductor-resin interface will be required.

3.2.6.3 Prototype test of the model coil

Based on the test results of the prototype bar model, the prototype model coils shown in Fig. 3.11 was trial manufactured and performed various tests for the two types of outer shield layer with the external shielding layer (electrically conductive coating is treated on the outer layer of the formed coil) and without the external shielding layer. As a result, the following performance was confirmed.

(1) Existing the external shield

PD has occurred due to remaining voids in the mold. The $\tan\delta$ characteristics had tended to increase with the voltage due to PD. Breakdown value (to the ground) was 40 to 50 kV. The breakdown portions were all air flashover or the base part of the rear terminal. It may have caused the electric field concentration to the bar welded terminal portion to be affected.

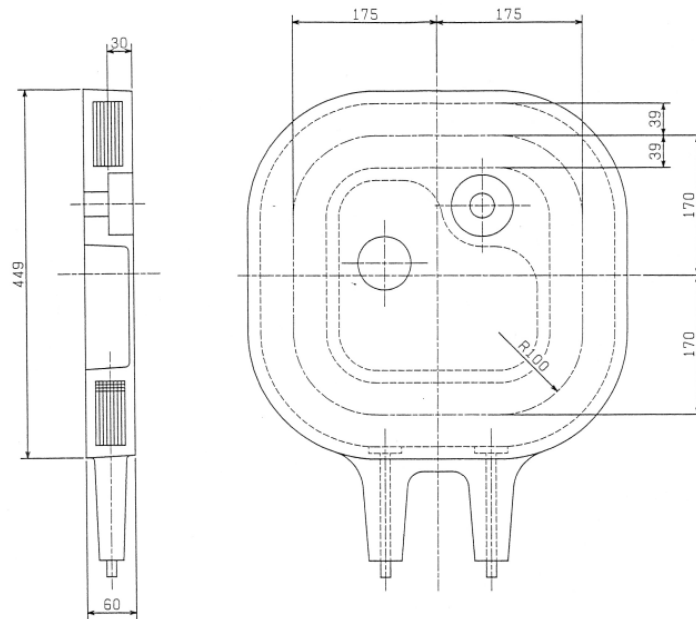


Fig. 3.11 The outer shape of the propulsion model coil for low-voltage system

(2) No external shielding layer

The insulation properties and insulation breakdown (to the ground) value results were almost the same as that of the model coil with the external shielding layer. However, Q_{\max} was larger by about one order of magnitude although the PD start voltage was increased slightly as compared to the outer shield layer existing model in the mount simulated electrical test. It was confirmed that the shielding layer was effective for field relaxation. Either coil satisfied the electrical properties of the voltage corresponding to the phase voltage 6.35kV (line-to-line 11kV) substantially. However, it is necessary to further investigate the omission of the shield layer for its mounting conditions and contamination on the coil surface because it shall be used for the long-term outdoors without having the internal insulating shield.

3.3 PLG system coil

Another effort toward cost reduction is the reduction of the required number of coils by simplifying the ground coil configuration. The purpose of ground coil can be classified into levitation guidance coil and propulsion coil. By connecting the drive power supply to the levitation guide coil, the propulsion power is supplied to a vehicle. That is, the coil can be used with three functions: propulsion, levitation and guidance. Consequently, it is possible to halve the total number of ground coils. We have developed this propulsion, levitation and guidance combined system named the PLG system.

3.3.1 Principle of PLG system

PLG system uses the circuit configuration of a conventional levitation guidance coils (hereinafter, referred to as LG coils). The PLG system is available by connecting the drive power supply to each guidance cable (referred to as null flux cables) which is connected with the LG coils facing in the opposite sides of the vehicle and its connection terminals (Fig. 3.12). However, as the PLG system has to connect the drive power supply to the LG coil, which is completely isolated and formed as a closed circuit, it is necessary to strengthen the insulation configuration of the coil.

I will explain the principle of the PLG system here briefly. First, because the cable is connected the same as the conventional LG coil for the levitation and guidance function, the reverse induced current flows to the upper and lower coils for the levitation force, and the reverse induced current flows to the each of the facing left and right coils across the vehicle for the guidance force. Therefore, the necessary levitation and guidance electromagnetic force will be provided to the vehicle without external control. The propulsion force will be supplied to the vehicle by connecting each PLG coil that is arranged in the traveling direction to each phase of the drive power supply in order and flow a three-phase current, which is synchronized with the vehicle speed similar to the linear synchronous motor ⁽¹⁵⁾.

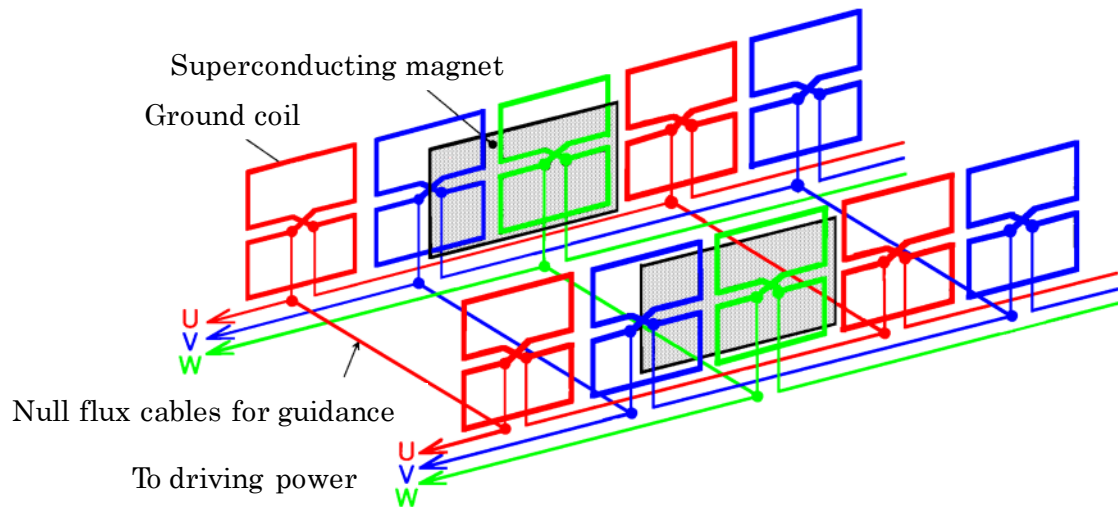


Fig. 3.12 Configuration of the PLG system

3.3.2 Development of PLG coil for practical use

3.3.2.1 Specifications of the coil

Table 3.2 shows the basic specifications of practical PLG coil based on the actual operating conditions. Figure 3.13 shows the external view. This coil configuration was changed to the eight shape from the conventional double eight shape aimed at doubling the coil pitch resulting in an improvement of lift to drag ratio (lift force/resistance). Furthermore, reduction of the vibration force to the SCM was performed by reducing the upper unit coil height and asymmetrically shaping the lower unit coil. Figure 3.14 shows the improved characteristic of the PLG coil according to the application of eight shape and asymmetric configuration. The figure shows the expected increase of the lift to drag ratio of about 30% at a speed 500km/h by the eight shape and the contribution to the reduction of the burden to the SCM by the vertical asymmetry ⁽¹⁶⁾. Furthermore, a series of prototype ground coils were manufactured with the aim of increasing reliability. Small and high reliability of the cable connection part, application of FRP bush, low eddy current loss, application of the IC tag and application of the abnormality self-diagnosis detection device were promoted. Elements of these developments will be described in detail in Chapter 4.

Table 3.2 Specifications of the practical PLG coil

Items	Specifications
Conductor material	Aluminum for electricity
Conductor cross-section	100mm(W)×40mm(D)
Conductor space factor	More than 80%
Coil shape	Rectangle (Upper and lower coil asymmetry)
Coil turns	36 times
Molding method	Epoxy resin casting method
Insulation to the earth	12mm (standard)
Nominal voltage	33kV
Bolt fastening portion	Laminated FRP bush
Lead-out terminals	Inter-phase 2, guidance 1

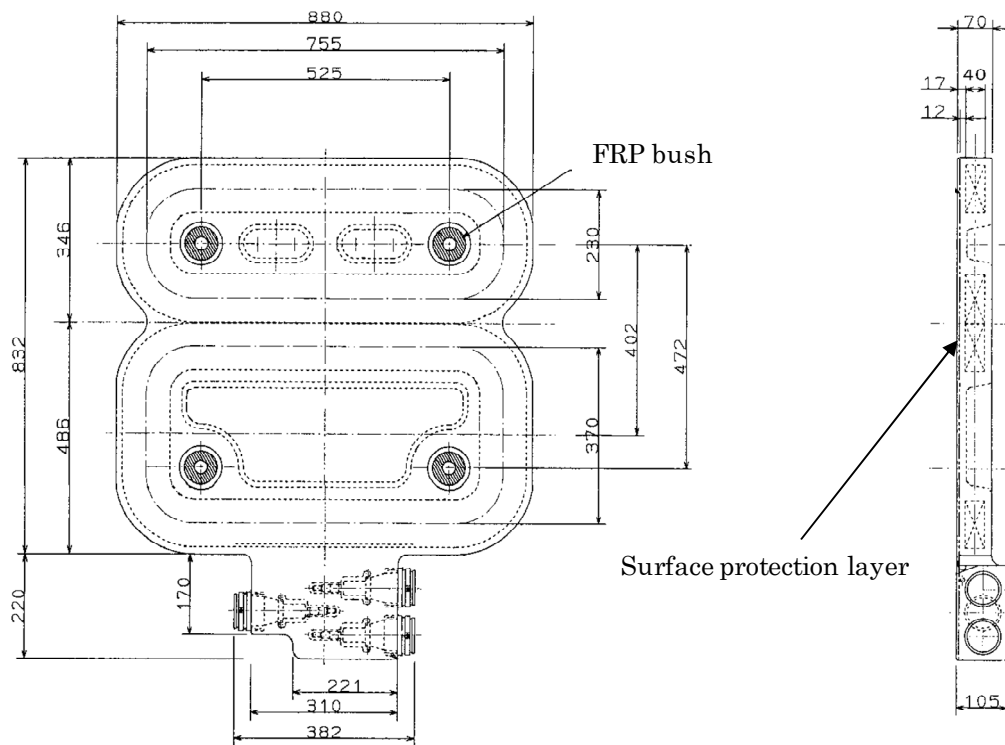
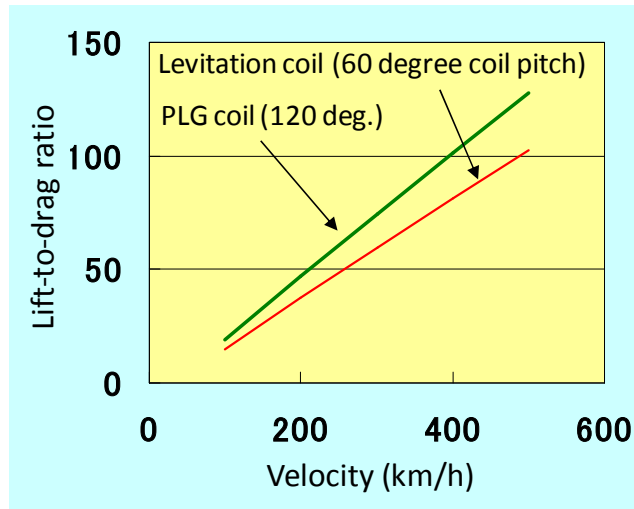
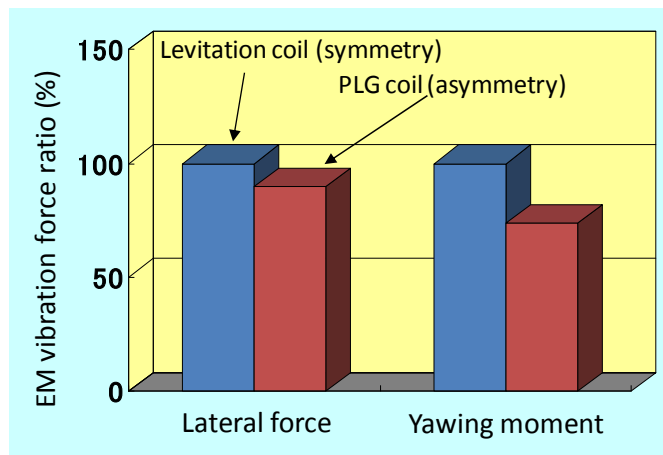


Fig. 3.13 Exterior of the PLG coil



(1) Improvement of the lift-to-drag ratio



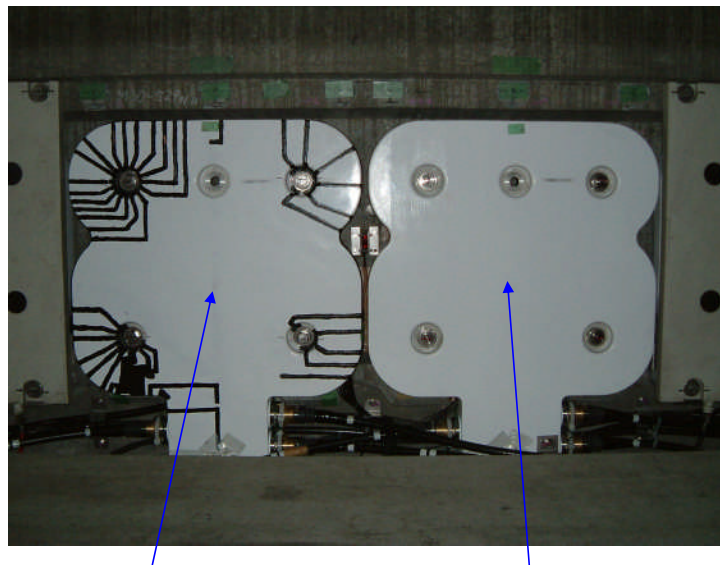
(2) Reduction of vibration force to the SCM

Fig. 3.14 Improved characteristics of the PLG coil

3.3.2.2 Durability evaluation

Because the PLG system includes these three functions, it is necessary to fulfill required specifications of all functions. Careful durability verification in addition to the performance evaluation is required to confirm the reliability. After various performance verifications for the PLG system were confirmed with the prototype coil, the four units were laid as an experimental purpose on the Yamanashi Test Line and the electromagnetic

forces and strains generated during the vehicle passing, the effectiveness of the three functions were examined . The on-site test situation is shown in Fig. 3.15. Furthermore, various stationary durability tests that assumed 35 years of commercial operation were implemented and the soundness of the prototype coil was confirmed ⁽¹⁷⁾. The enforcement examples of the durability experiment are also discussed in Chapter 5.



Stress measurement coil EM force measurement coil

Fig. 3.15 Test situation on-site

3.3.3 Development of the surface protection layer

The low voltage levitation and guidance coils are arranged at the outside (vehicle side) of the propulsion coils, which is a special high-voltage equipment, in the current configuration of the guide way of the superconducting Maglev. On the other hand, the PLG system can use three ground coil features in the same coil. The ground coil is a single layer configuration as shown in Fig. 3.16. Any protection measures must be required because the special high-voltage equipment of PLG coil is exposed to the vehicle surface.

3.3.3.1 Aim of the surface protection

The surface protection was applied to the PLG coil of the special high-voltage equipment. The purposes of protection from exposure of the charging portion are described below ⁽¹⁸⁾.

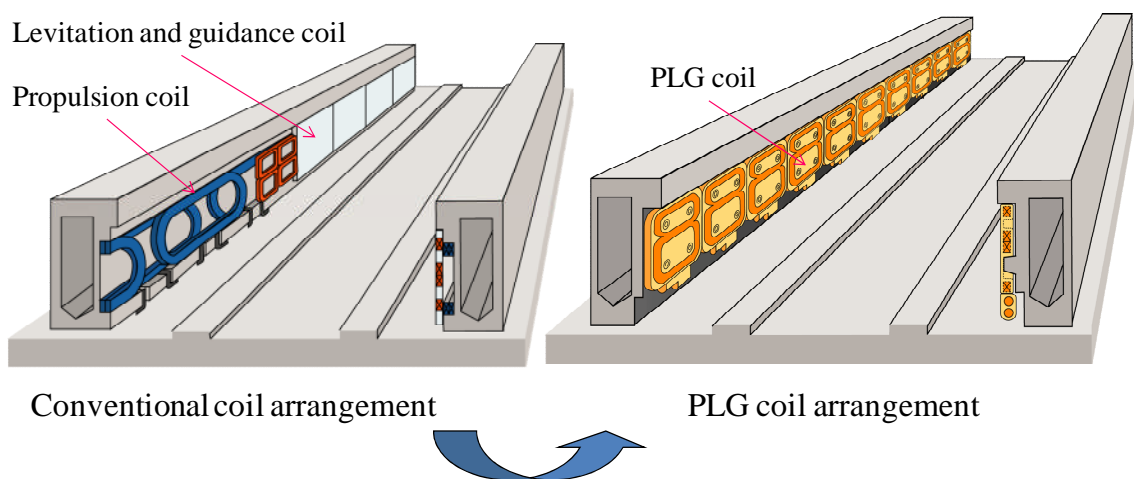


Fig. 3.16 Comparison of the guide-way configuration

(1) Securing safety inside the guide way

The propulsion ground coils to be used in the future commercial line will be operated in the nominal voltage 22 to 33 kV as the special high-voltage device. Because the high voltage is applied to the power supply from the substation, the electric field relaxation shielding was applied to the outermost layer of the coil. However, the propulsion coil of the superconducting Maglev system forms with a high-resistance shield surface layer in order to minimize the eddy current loss while the SCM on the vehicle passes through at high speed. Therefore, as the surface potential of the coil is increased in spite of the shield layer being grounded, it is necessary to secure safety inside the guide-way from the viewpoint of prevention from electric shock.

(2) Protection of the coil itself

The ground coils installed in the guide-way face a constant risk of flying objects by repeated traveling at ultra high-speed of 500km/h. Therefore, the possibility of damage received by the fine dust in the guide way or small parts falling off from the vehicle may not be insignificant. In particular, the special high-voltage coil (epoxy resin molded in general) exposed to the vehicle surface has a possibility of cracking or breakdown caused by the collision energy of small flying objects. Therefore, it is necessary to protect the surface from the viewpoint of the mechanical protection of the coil itself.

3.3.3.2 Configuration of the surface protection layer

The conventional examination method is to adhere the protection plate (thickness: 5 to 7 mm) onto the coil surface or attach it with bolts. However, later attachment measure increases the installation cost and decreases reliability. This study examined various configurations assuming the unification of the protection layer to the coil during the resin molding. The main feature of this configuration was installation of the ground layer at the conductor side of the protective layer to electrically insulate the internal high voltage charging unit from the protective layer of the vehicle side and further protect the coil surface mechanically. The conductive coating applied FRP

(Fiber Reinforced Plastic) and the reinforcing glass cloth sheet facing the vehicle side were combined while considering the positioning accuracy of the protective layer, resin impregnation characteristics and other parameters. The cross-sectional structure of the prototype coil is shown in Fig. 3.17.

3.3.3.3 Prototype test results ⁽¹⁹⁾

(1) Partial discharge characteristics

The PD characteristics at the time of commercial frequency AC voltage application between the conductor and the ground measured via the test cable are shown in Figure 3.18. The discharged charge amount was about 10pC (measured ambient noise level) at applied voltage of 50kV. The sufficient initial performance as the special high-voltage equipment of nominal 33 kV was obtained.

(2) Thermal shock test

The liquid phase heat shock load (test coil was immersed for 60 minutes alternately in hot water of 80°C and cold water of 10°C, and repeated three times) and the refrigeration load (in a thermostatic chamber of -30°C for 48 hours) were applied to the test coil and the external degradation and the dielectric breakdown strength were investigated. As a result, no visible heat shock degradation was confirmed and twice the breakdown strength against the initial value for the withstand voltage (AC70kV for 1 minute) was maintained.

(3) Temperature rise characteristic test

The influence of the existence of the surface protective layer to the temperature rise characteristics was investigated by supplying power to the sample coil. As a result, the values of temperature rise of each part of the coil was approximately proportional to the square of the applied current, and no significant difference was observed between existence of protective layer.

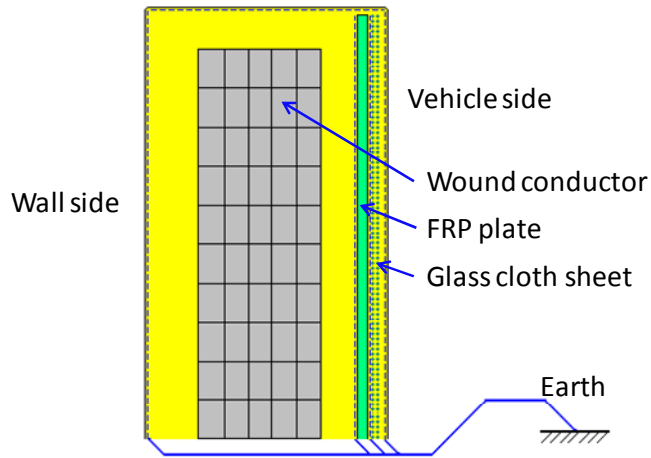


Fig. 3.17 Cross-sectional structure of the prototype coil

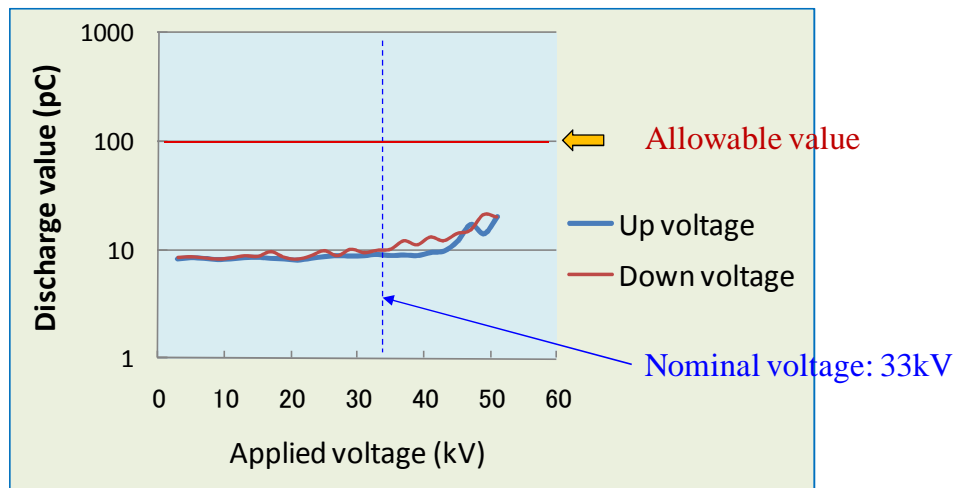


Fig. 3.18 Initial characteristic of PD

3.3.3.4 Impact strength evaluation ^(20, 21)

(1) Test method

The impact strength of the surface of the ground coil using an air pressure gun was evaluated by simulating situations in which flying small objects hit the ground coil while the vehicle passes by the ground coil. (Fig. 3.19) The evaluation was made by gradually increasing the speed of the steel ball to fire from the air cannon to target the winding conductor of the PLG coil. The

critical strength was set as the breakdown point immediately after collision while the high voltage load (33kV/minute) was applied between the winding conductor and the surface protective layer.

(2) Test result

The impact strength was compared and evaluated by targeting the PLG coils of the same specification with or without surface protective layer. As a result, the specimens with the protective layer at the surface of the vehicle side had impact strength of about twice that of the specimen which did not have a protective layer. It was confirmed that the impact absorption by the protective layer was functionally effectively.

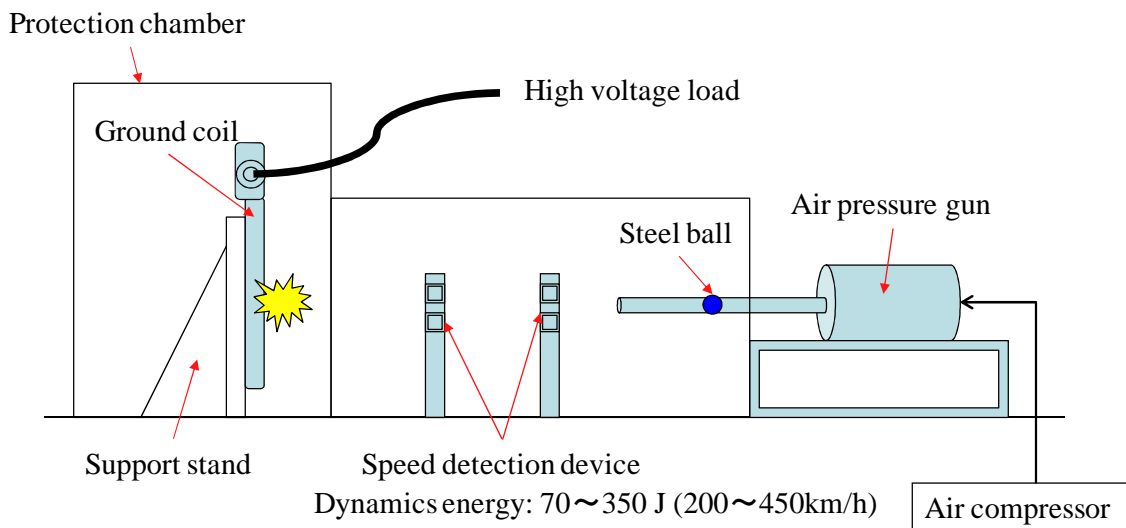


Fig. 3.19 Test configuration of impact resistance strength evaluation

3.4 Summary

The cost reduction is an important proposition for a vast number of ground coils. In this chapter, we have made advanced research and development for the two systems, which is expected to reduce the cost. The manufacturing costs can be reduced by reviewing the material and process by applying the RIM system. The overall cost can be reduced by half of the required number of coils by applying the PLG system.

3.4.1 RIM system coil

The RIM system by molding with DCPD is a molding method of a new concept that has many possibilities. This self-reaction heat cured molding method promotes not only short molding time but also have the following advantages when applied to the ground coil.

(1) While having strength equal to or greater than the conventional SMC method, it can reduce the elastic modulus of the resin in half. Consequently, it is possible to reduce the continuous loads such as residual stress, bolt tightening stress, thermal stress significantly.

(2) This coil has a significant advantage to the impact strength compared with the mold for other resins owing to the elastomer component contained in the raw material.

The practical RIM system levitation coil was newly developed that incorporates flame retardant resin, a pre-formed glass mat and an application of the metal bush. As a result, the intended functions and durability were confirmed from various stationary test and on-site durability test by installing to the Yamanashi Test Line assuming a long-term outdoor use.

The manufacturing cost comparison between the RIM system and conventional SMC system was performed targeting the practical specification of the levitation coils. The total reduction by about 30% was estimated.

Furthermore, it was confirmed that the electrical insulation and the mechanical strength both functioned successfully by using mica for ground

isolation and by installing the inside shield layer to the RIM method propulsion coils. It is considered effective for the low voltage PLG system because the charging part is not exposed to the coil surface. However, it is necessary to verify the long-term reliability concerning the DCPD resin used as an insulating material and the insulation configuration of the internal coil.

3.4.2 PLG system coil

The PLG system where the same coil has the three functions (propulsion, levitation and guidance) has an advantage of reducing the total number of ground coils to half, and thus a cost reduction will be expected.

In the development of practical type PLG coil, the coil configuration was changed from conventional double eight shape to the eight shape and the upper and lower unit coils were configured asymmetrically with the aim of improving characteristics of the lift-to-drag ratio and reduction of the vibration force to SCM. In addition, intended functions and integrity were confirmed by the characteristics of the three functions of the prototype coils tested at the Yamanashi Test Line and various stationary durability tests.

Furthermore, the surface protection layer was developed for the purpose of the surface protection of the vehicle side of the PLG coil that the monolayer arrangement was assumed. The reliability and maintenance costs were taken into account for construction of the protection layer. The impact absorption layer with ground layer was integrally molded. As a result of evaluation tests using the prototype coils, it was confirmed that the intended function was acquired without particularly affecting the characteristics of the coil.

Chapter 4 High Functionality of the Ground Coil

4.1 Introduction

For the commercial operation of the ground coils, it is important to increase the performance and reliability within the limited cost and design conditions. In this chapter, high functionality of the ground coil applied to the PLG system coil is described as a typical example.

4.2 Small cable joint with high-reliability

The propulsion system coil requires the coil connection cables be in proportion to the required number of coils and the connecting parts of the special high-voltage becomes a huge number. On the other hand, when considering the limited on-site work space, miniaturization of the connection part is an essential requirement. Maintaining the reliability of the operating environment where repeated electromagnetic force being applied must be considered.

4.2.1 Development point of linear connecting part

4.2.1.1 Improvement of the dynamic durability

By changing the connecting portion from the conventional L-shape to the linear type and by providing with a stopper mechanism to the fastening brackets, the reliability under vibration environment was improved.

4.2.1.2 Miniaturization

The breakdown strength was increased by increasing the surface pressure of the insulation interface that is being applied to the spring structure of the cable-side connecting portion. Furthermore, electrical reliability was increased by changing the material of the conical insulator of the cable-side connecting part from conventional EP rubber to silicon rubber that increases adhesion of the interface ⁽¹⁾ (Fig. 4.1).

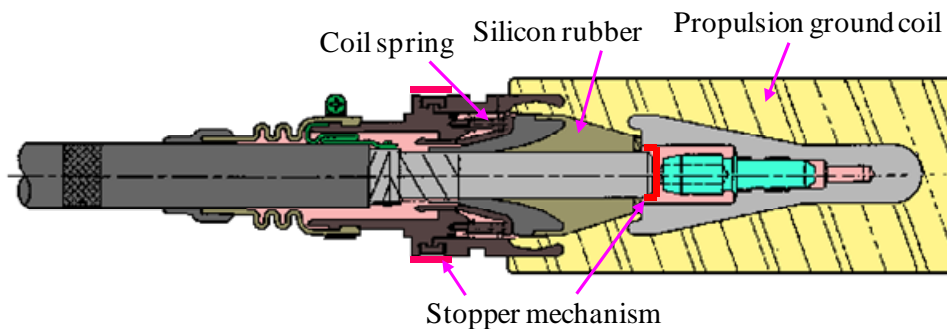


Fig. 4.1 Linear type cable joint

4.2.2 Prototype test results of PLG coil connecting portion

Connecting part of the PLG coil was manufactured as a trial product and its performance was confirmed by various tests.

4.2.2.1 Assumed operating conditions

(1) Operating environment

- ① Environmental temperature : $-30\sim+50^{\circ}\text{C}$
- ② Environmental humidity : Max. 100% with condensation
- ③ Flooding : Temporary flooding

(2) Power loading condition

- ① Nominal voltage : 33kV
- ② Peak voltage : 27kV
- ③ Accumulated power loading time : 10,000 hours

4.2.2.2 Prototype test results

The following initial characteristics tests were performed targeting the prototype connection units.

(1) Partial discharge characteristics

The PD start voltage (V_i) and the PD extinction voltage (V_e) of the test bushing connected to test specimen simulating the cable side were measured while the commercial AC voltage was applied. As a result, the PD start/extinct voltage were 38kV for all four specimens. The sufficient performance for the phase voltage 19kV was confirmed.

(2) AC breakdown characteristics

The breakdown voltage was measured by the step-up voltage of 10kV/hour following the same test configuration as above. As a result, sufficient breakdown strength of 230 to 280 kV was confirmed.

(3) Lightning impulse breakdown characteristics

The breakdown voltage was measured by applying the impact voltage of 10 kV step-up voltage from 180 kV_p following the same test configuration as above. As a result, high insulation strength was confirmed for 680 to 740 kV_p as well as for commercial AC voltage.

(4) Airtight test

After confirmation of the initial insulation characteristics, the specimens were immersed in a water tank. Compressed nitrogen of 4.9×10^4 Pa was applied for one hour from the cable end to confirm the tightness of the connection portion. As a result, no abnormality was observed in the two target specimen. Airtight was completely maintained.

4.2.3 Durability evaluation

The long-term electric applied vibration test that simulated the vibrating environment under commercial operation and the long-term outdoor electric applied test that simulated the current flowed heat cycle were performed on the developed linear type connection parts. Durability of insulation was confirmed from a mechanical and thermal standpoint.

4.2.3.1 Long-term vibration test with voltage applying

The durability of the insulating members and the conductor contact parts in the vibrating environment while the voltage was applied that simulated the actual use was verified.

(1) Test procedure

As shown in Fig. 4.2, the test specimen was connected to the test bushing which simulates the coil side. It was connected to the vibration tester through the test fixture. The vibration test under voltage being applied was performed for 30 days by the following test conditions. The vibration frequency was selected as the peak frequency acquired by the frequency sweep test.

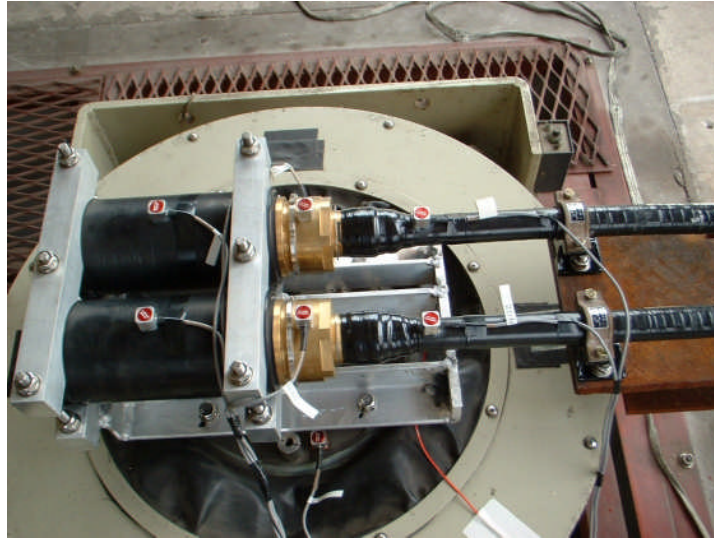


Fig. 4.2 Test situation of long-term vibration with voltage applying

- ① Vibration frequency: 106 Hz
- ② Vibration acceleration: 400m/s^2 (0-p) Fixed
- ③ Applied voltage: AC 36.8kV ^{*4.1}

(2) Test result

The insulation characteristic test and the dissection test were performed for the specimen after completion of the 30-day vibration test under high voltage. As a result, the same performance was maintained in the PD, and the AC breakdown characteristics were almost equal to the initial performance. Furthermore, scratches were observed on the conductive contact portion by the dismantling survey, but no deformation of the insulator or the abnormality of the surface was confirmed. It was confirmed that the specified durability was maintained.

4.2.3.2 Long-term outdoor power supply test

By applying the heat cycle while supplying high voltage and power supply to the specimen simultaneously, electrical and thermal durability was verified which is expected in the actual use.

(1) Test procedure

According to the "High voltage test method of the connection part and special high voltage (11kV to 275kV) with cross-linked polyethylene cable", JEC-3408-1997 Electrical Standards Committee Standards, the heat cycle of 8 hours on and 16 hours off was applied to the specimen (Fig. 4.3).

① Applied voltage: AC 27.9kV ※4.2

② Conductor temperature: When energized, the conductor temperature of the temperature control dummy cable was set to 90 °C.

③ Test period: 30 days

(2) Test result

The insulation characteristic test and dismantling survey were performed on the specimens that were exposed for 30 days of high voltage and power supply experiment. As a result, V_i and V_e of one of the two specimens were low (7 to 8 kV) and they were significantly lower than the phase voltage 19kV. However, the two specimens maintained the initial performance of the AC breakdown characteristics substantially equal to the initial value. Furthermore, relative displacement of the pre-molded insulator and the cable was confirmed from the dismantling investigation. These findings were fed back to the stopper mechanism as shown in Fig. 4.1 to improve the reliability of the connection part.



Fig. 4.3 Test situation of long-term outdoor power supply

※4.1: The applied voltage was set by referring to Clause 6 "Power frequency withstand voltage test for the type test", "High voltage test method of the connection part and special high voltage (11kV to 275kV) with cross-linked polyethylene cable", JEC-3408.

$$V_t = \frac{E_0}{\sqrt{3}} \times K_1 \times K_2 \times K_3 \cong 36.8 \quad (4.1)$$

where V_t : Test voltage value

E_0 : Cable highest voltage (36kV)

K_1 : Degradation coefficient = $\{10,000 \text{ hours} / (24 \text{ hours} \times 30 \text{ days})\}^{1/n}$

Assuming that $n = 9$, $K_1 \cong 1.34$

K_2 : Temperature coefficient = 1.2

K_3 : Margin = 1.1

※4.2: The following applied voltage was set by referring to Clause 6 "Power frequency withstand voltage test for the type test", "High voltage test method of the connection part and special high voltage (11kV to 275kV) with cross-linked polyethylene cable", JEC-3408.

$$V_t = \frac{E_0}{\sqrt{3}} \times K_1 \cong 27.9 \quad (4.2)$$

4.3 High reliability of the coil fastening portion

The quality of the fastening structure in the ground coil to be used for a long period of time in the vibration existing outdoor environments is an essential element that affects the reliability of the system itself significantly in addition to the maintenance cost of commercial operation. On the other hand, the bolt tightening system that is a popular system in tightening the ground coils may be easily damaged at the fastening portions caused by the compression creep due to fastening axial force to the resin parts and stress concentration to the vicinity of the fastening portion. The selection of the fastening configuration becomes a problem of reliability.

4.3.1 Background of the development

4.3.1.1 Fastening method of the ground coil

For the fastening of the ground coil, various methods were verified (e.g. ① providing fastening holes to tighten a coil directly with bolts, ② coil was indirectly tightened via fastening material such as FRP, ③ tighten the coil via FRP member to the reinforced concrete and fasten the coil by burying it with concrete). These methods had advantages and disadvantages and presently the bolting system has become dominant at the moment due to better workability including easy coil replacement.

4.3.1.2 Issues of the bolting system

If an integrally molded coil by the resin is directly tightened with bolts, the following points must be considered.

(1) Axial force reduction due to compressive creep

If a molded coil is bolted directly, a mold resin will produce compression creep (compressive deformation) by the fastening axial force of the bolt. It will cause a loosening problem due to decline of the axial force. This will increase not only the daily maintenance and inspection costs but also

decrease the reliability of the fastening structure itself.

(2) Loosening of the metal bush

Therefore, metal bush was applied because the compression creeping was practically negligible at the fastening portion. However, as metal bush was intentionally set as a non-adhesive with molding resin (if the contacting surface was adhered, stress concentration in the molding resin is likely to be produced at the bolt fastening part), the relative displacement gradually increased due to excitation of the EM vibration when a vehicle was passed. It may be the same problem as (1).

4.3.2 Development of the vibration resistance fastening portion

4.3.2.1 Application of laminated FRP bush

In order to solve the aforementioned problem comprehensively, an application of laminated FRP bush manufactured by the sheet winding process (Fig. 4.4) to the bolt fastening portion was examined ⁽²⁻⁴⁾. By arranging the reinforcing fiber axially along the reinforcing laminate layer, FRP bush reduced the compressive creep to a negligible level practically. In addition, the stress relief layer that reduced elastic modulus to about 1/3 of the mold resin was placed to the outermost layer. With these measures, the stress concentration in the vicinity of the fastening was greatly relieved.

4.3.2.2 Comparison with the fastening portion models

The prototype fastening portion models including the conventional metal bush were manufactured using various bushes with different structures and materials shown in Fig. 4.5, and their performance was compared by various tests. Figure 4.6 shows the stress measurement results for each model at the neighborhood of the fastening portion while the static load was applied. Figure 4.7 shows the generated stresses at the simulated step on the coil when the coil was tightened with a specified axial force. From the test results,

considerable stress relaxation of the laminate type FRP bush was confirmed.

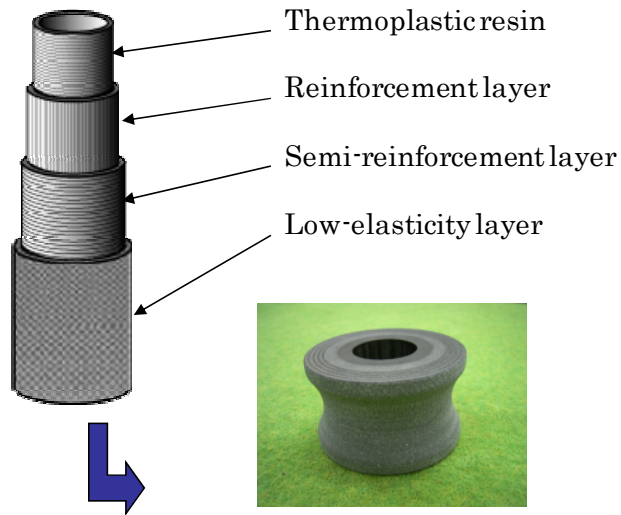


Fig. 4.4 Laminated FRP bush

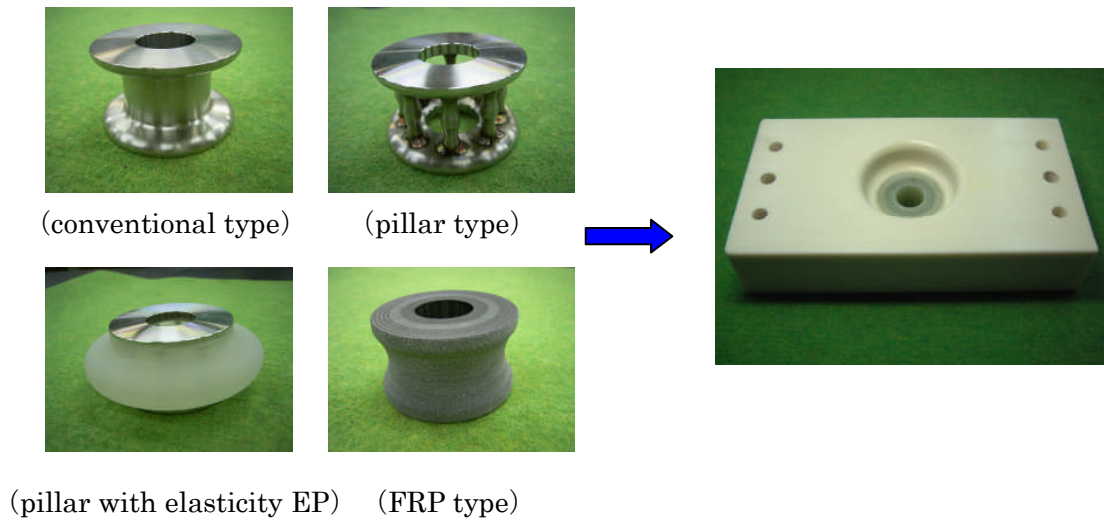


Fig.4.5 Fastening portion model

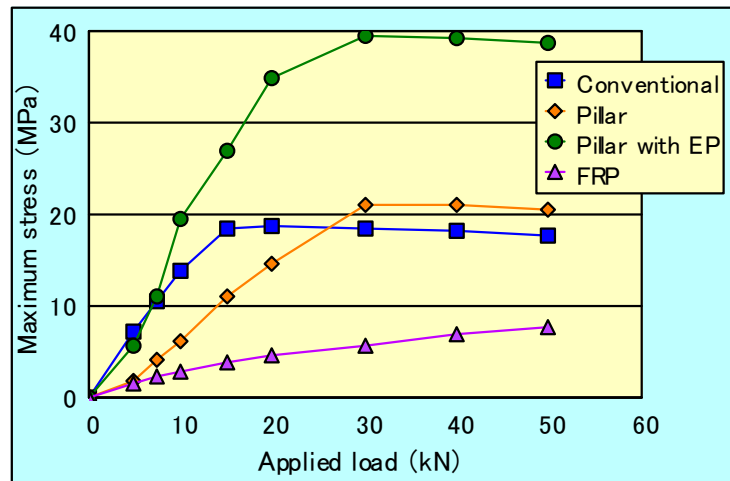


Fig.4.6 Stress characteristic in static load

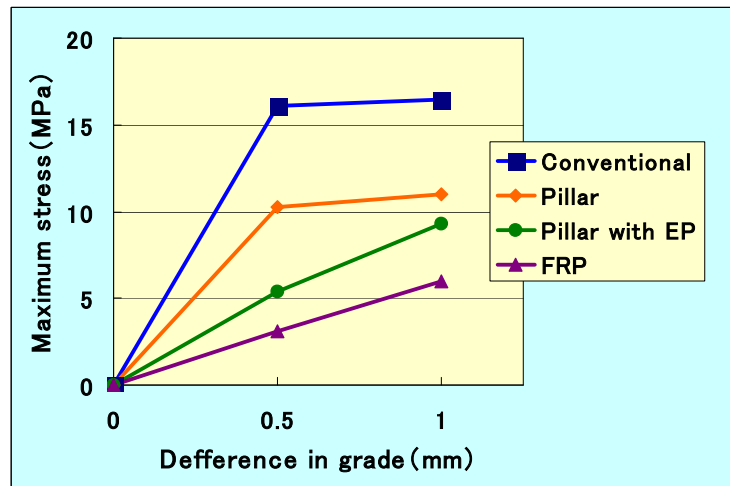


Fig.4.7 Stress in fastening a bolt

4.3.2.3 Comparative study using actual coils

The trial PLG coil was manufactured with the aforementioned bush applied to a part of the fastening portion. The trial models were compared and verified by the EM force loading. The EM vibration test equipment was used for verification that could simulate the actual traveling on the test bench. Figure 4.8 shows the comparison of the generated stress while the EM force that simulated the maximum value in actual use was loaded. From the test results, the superiority of FRP bush was also confirmed for the actual load of the EM force. The EM vibration test equipment is described in detail

in Chapter 5.

4.3.3 Durability evaluation

The durability test was performed by EM excitation using the EM vibration test equipment to compare the vibration durability of the fastening portion. The test conditions were as follows.

- (1) EM force: maximum design lateral force during normal traveling
- (2) Excitation times: 1.44 million times
- (3) Excitation frequency: 113 Hz (550km / h or equivalent)

As a result of the tests, looseness of the interface was confirmed in the conventional metal bush type and small cracks occurred in the pillar type. The problems were apparently the same as the prior estimation before beginning the actual test. On the other hand, obvious superiority was confirmed in the FRP bush that had no looseness, crack, or decrease of the bolting torque.

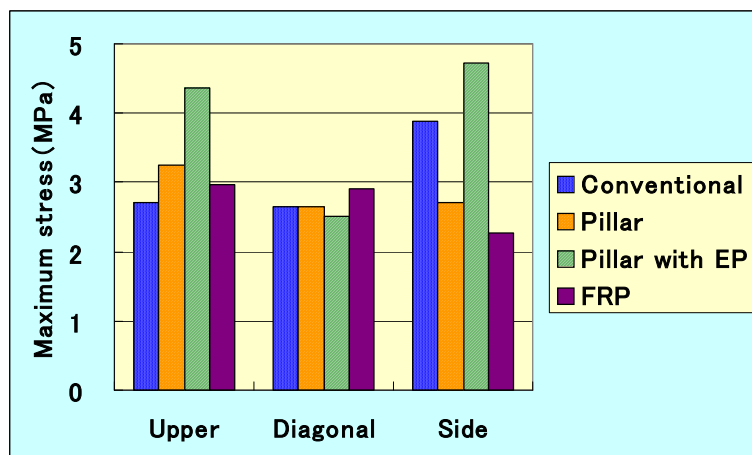


Fig.4.8 Stress in electromagnetic force

4.4 Reduction of the eddy current loss

The eddy current will be generated in the ground coils facing the SCM on the vehicle (Fig. 4.9) when the variable magnetic field occurs due to the vehicle passing. There is a loss in the generated eddy current in the coil winding conductor. The eddy current becomes not only the magnetic resistance during the vehicle running but also generates unnecessary heat in the coil conductor. Therefore reduction of the eddy current loss is extremely important from the reduction of the system running costs and suppression of the temperature rise of the ground coils. On the other hand, the subdivision of the wire cross-section is a most popular method to reduce the eddy current generated in the ground coil conductor. However, it is necessary to find the appropriate and effective subdivision by considering the rigidity of the winding coil, space factor of the conductors, impregnation of the molded resin and other parameters. Furthermore, it is necessary to twist divided wires at a constant pitch to form a uniform flux linkage from the superconducting magnet in order to eliminate losses generated from the perfusion from the divided wires. However, it is not easy to maintain the requirement for the winding wire and dimensional accuracy of the winding coil leading to a conflicting result of the purpose of the cost reduction of ground coils. In this development, we studied the technique to reduce the eddy current losses while improving the dimensional accuracy of the winding coil for the PLG system.

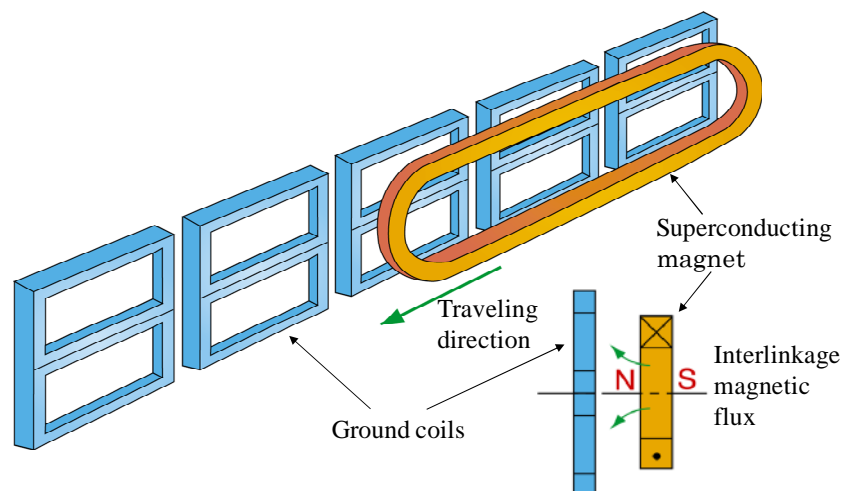


Fig. 4.9 Relative position of SCM and ground coils

4.4.1 Magnetic drag due to eddy currents

We investigated the average magnetic drag of a vehicle that received the eddy current generated in the ground coil conductor when the ground coils were arranged continuously with a constant pitch ⁽⁵⁾. The vehicle traveling resistance by the magnetic drag is obtained as a reaction of the sum of the magnetic drag acting on the ground coils calculated by the impulse method. It is necessary for determining the magnetic drag of the vehicle to sum the forces occurring from the multiple ground coils. This is calculated by taking the average of the forces generated by the ground coils during the specified time and multiplying the number of corresponding coils. Here, it is assumed that $f(t)$ is the force acting on the ground coil at time t , and $F(t)$ is a half (left or right side) of the forces acting on the vehicle. Assuming that Δt is the time required for the vehicle to travel by laying the pitch of the ground coils, the force generated in the n -th coil of interest is $f(t + n\Delta t)$. Therefore, the instantaneous magnetic drag value $F(t)$ the vehicle receives at time t is shown below.

$$F(t) = \sum_{n=-\infty}^{\infty} f(t + n\Delta t) \quad (4.3)$$

n : number of ground coils

The average value of the force F_a for time Δt is as follows.

$$F_a = \frac{1}{\Delta t} \int_t^{t+\Delta t} F(t) dt \quad (4.4)$$

Substitute (4.3) for (4.4)

$$F_a = \frac{1}{\Delta t} \int_t^{t+\Delta t} \sum_{n=-\infty}^{\infty} f(t + n\Delta t) dt \quad (4.5)$$

Where $\int_t^{t+\Delta t} \sum_{n=-\infty}^{\infty} f(t + n\Delta t) dt$ is $\int_{-\infty}^{\infty} f(t) dt$

That is, the sum of the forces generated on the number of n ground coils is

equivalent to the impulse exerted on the one ground coil generated by the vehicle passage at time Δt .

Thus, equation (4.5) is shown below.

$$F_a = \frac{1}{\Delta t} \int_{-\infty}^{\infty} f(t) dt \quad (4.6)$$

This means that the impulse acting on the one ground coil is divided by Δt .

4.4.2 Quantitative evaluation of eddy current loss

Prior to the development of ground coils with the low eddy current loss, quantitative evaluation of eddy current loss generated in the wire was performed to select the wire.

4.4.2.1 Development of the evaluation test equipment for eddy current loss

Until now, in order to quantitatively evaluate the eddy current loss generated in the ground coil and fastening members (metal), it is unavoidable to measure the magnetic drag acting on the specimen by an actual vehicle traveling in the test line. However, there were problems not only because of the large field test site but also the insufficient test measurement accuracy. Therefore, the test equipment that can evaluate the eddy current loss in the stationary equipment has been desired. The stationary test system capable of quantitatively evaluating the eddy current loss for the wire samples was studied prior to the selection of the coil wire. After various studies concerning the system for simulating the variable magnetic field generated during the SCM being passing at a high speed, we have developed an evaluation test instrument of the eddy current loss having a high speed rotational mechanism that rotates a disk to which sample wires are secured in a strong magnetic field (Fig. 4.10). This instrument was configured so that the mechanism that generates eddy current loss was the same as the actual vehicle traveling. The eddy current was generated by the relative movement of the two-pole electromagnet simulating the SCM and

the ground coil wire. The magnetic drag was taken into account so that it was easily separated from the eddy current by monitoring the rotational resistance using a torque meter while the electromagnet was excited and non-excited. Figure 4.11 shows the measured results of the magnetic flux density distribution during excitation (rated current: 60A) at the center plane ($Z=0$) of the magnetic poles of the electromagnet. It was confirmed that the magnetic flux density exceeded 1T in a circle of about 27mm radius at origin ($X = 0, Y = 0$) of the pole center, and was greater than 0.8T in a circle of 55mm. Further, since the maximum magnetic flux density of the ground coils exposed to the passage of a SCM is about 1T, it was confirmed that this test equipment was effective in the quantitative evaluation of eddy current loss for the sample wire. Table 4.1 shows the main specifications of the test equipment.

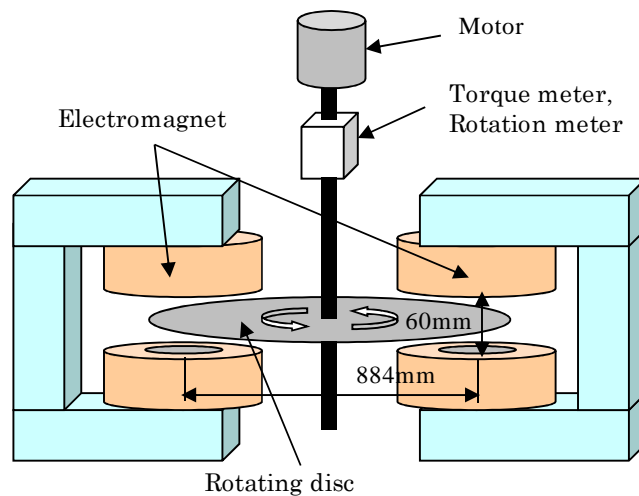


Fig. 4.10 Construction of the test equipment

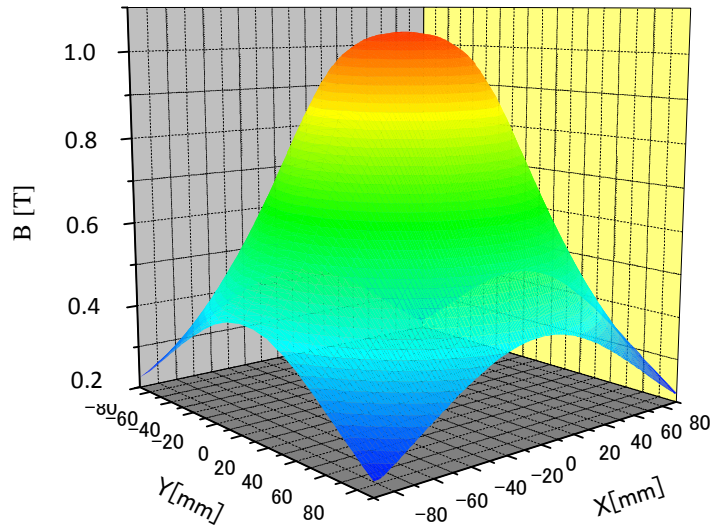


Fig. 4.11 Distribution of magnetic field

Table 4.1 Specifications of the test equipment

Number of electromagnet	2
Between the center of the magnet(mm)	884
Pole gap (mm)	60
Maximum magnetic field (T)	1.0 (at 60A)
Disc diameter (mm)	1000
Disc material	CFRP
Attachment point of the specimen	16
Maximum speed (rpm)	3000

4.4.2.2 The quantitative assessment using the wire samples

The eddy current loss Pe generated by the Joule losses in the conductor wires, of which dimensions were shown in Fig. 4.12, can be expressed by the following equation as far as the alternating magnetic flux density is constant and the magnetic field frequency is within the negligible range of the skin effect⁽⁶⁾.

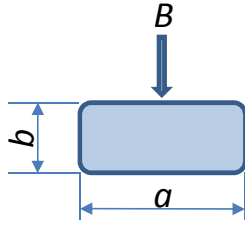


Fig. 4.12 Cross section of conductor

$$Pe \propto a^3 b f^2 B \quad (4.7)$$

- where
- a : Conductor width perpendicular to the magnetic field
 - b : Conductor thickness in the direction of the magnetic field
 - f : Magnetic field frequency
 - B : Alternating magnetic flux density

As shown in equation (4.7), the eddy current loss (Joule loss) is proportional to the square of the speed (alternating frequency f) and the magnetic drag by eddy current is proportional to the speed. The former leads to an unnecessary increase in the coil temperature and the latter leads to the running resistance of the vehicle. To reduce the eddy current loss generated in the conductive wire, it is effective to divide the conductor plane perpendicular to the magnetic field as shown in equation (4.7) and decrease the conductor width a .

Upon selection of the wire, three types of conductor having the same cross-sectional area were used for the sample wires (rectangular wire: $5.3 \times 6.1 \times 3$ wires, dislocation wire: $1.2 \times 4.7 \times 15$ wires and round twisted wires: $\phi 2.5 \times 19$ wires) (Fig. 4.13). The quantitative comparison of magnetic drag was performed by the eddy current loss evaluation test equipment ⁽⁷⁾. The sample wire was installed to the test equipment shown in Fig. 4.14. The 32 samples were sandwiched with the FRP bolts and FRP plates with pitch 22.5 degrees at both sides of the circumferential direction of the rotary disk and then they were secured. Furthermore, since the cross-sectional shape is asymmetric with respect to the interlinked field direction except for the round twisted wire, two directions of the eddy current, the edge and flat directions, were compared. The sample secured disk was rotated at high

speed and the eddy current loss was measured by the rotational torque as the difference of presence or absence of excitation of the disk interlinked DC magnetic field generator. Approximately half of the reduction in eddy current loss can be expected to be attributed to the dislocation wire for the flat direction, and 1/5 around the round twisted as compared with the conventional flat wire (3-parallel) (Fig. 4.15). It was confirmed that the reduction by narrowing the conductor wire width perpendicular to the magnetic field was significant from the measurement results as shown in equation (4.7). However, since the magnetic field direction of the SCM interlinked with the ground coils is not uniform, it was confirmed that reduction of the cross-sectional area of the no-directional wire such as a round twisted was the most effective in order to reduce the eddy current loss of the ground coils.

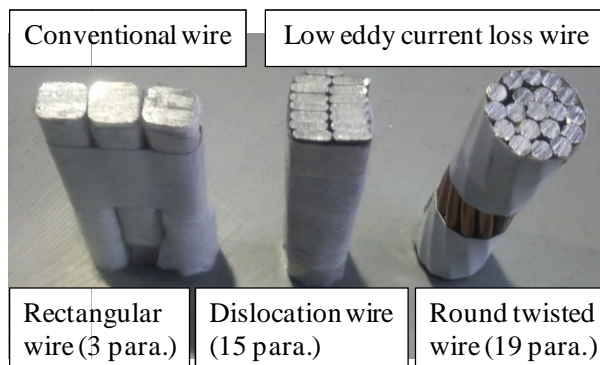


Fig. 4.13 Wire samples for quantitative comparison

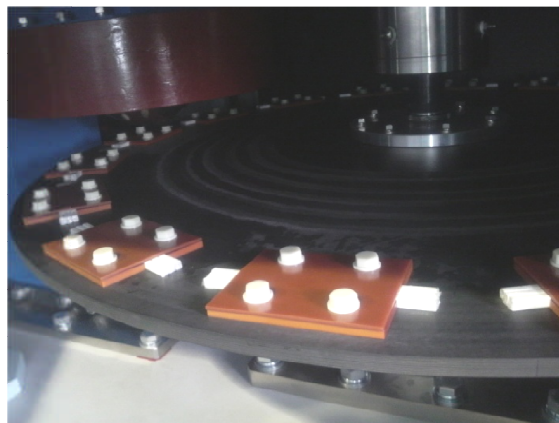


Fig. 4.14 Mounting conditions of the samples

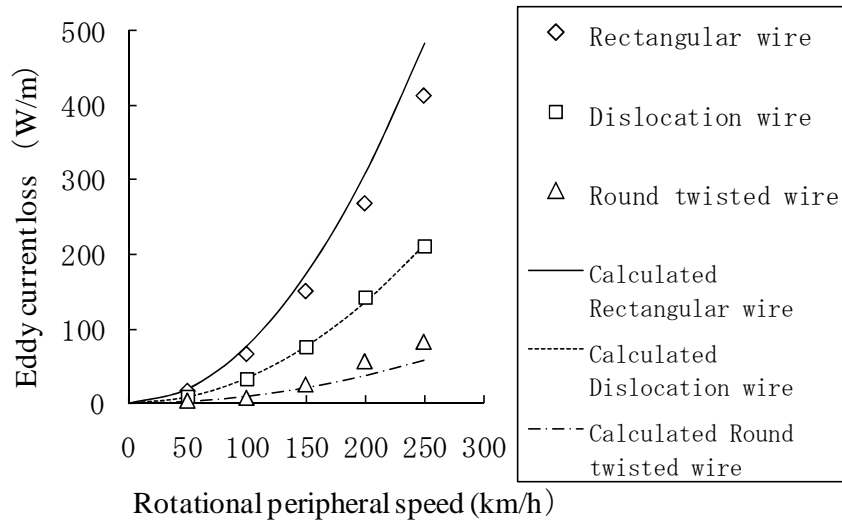


Fig. 4.15 Measurement results of eddy current loss

4.4.3 Application of compression molding to the winding coil

The levitated railway ground coil has an important role in providing propulsion, levitation and guiding the vehicle by an EM interaction with the SCM on the vehicle. In particular, the power of the propulsion coils is assumed to be supplied from the outside and it is necessary to ensure the electrical insulation function as special high-voltage equipment in addition to maintaining the mechanical strength of the resin molded air-core coil. Therefore, the resin molding is the most important step for manufacturing the ground coils. Furthermore, application of the rectangular divided wire strands, dislocation wire, twisted rectangular mold and other types have been studied for reducing the eddy current loss of the ground coil assuming subdivision of the conductor wires⁽⁸⁾. However, it was difficult to ensure the dimensional accuracy of the winding coil because twisting imbalance was left in the wire itself due to the increase in the number of parallel conductors and dislocation of the divided wire. It emerged as a mold thickness deviation (non-uniformity of the ground insulation thickness) at the time when it was integrally molded with the resin. This would affect the results in the electrical insulation performance to the ground.

Therefore, the measure was verified to control the predetermined shape by

compressing the coil after winding the round wire for improving the dimensional accuracy of the winding coil while suppressing as much as possible the wire cost and reducing the eddy current loss of ground coils. The concept of compression molding seen from the sectional direction of the winding coil is shown in Fig. 4.16. The assembly machine was aimed to improve the dimensional accuracy and improve the space factor by compression molding into a predetermined shape by a hydraulic press. It also can be diverted as a compression molding tool without removing the bobbin winding coils. It improved the work efficiency.

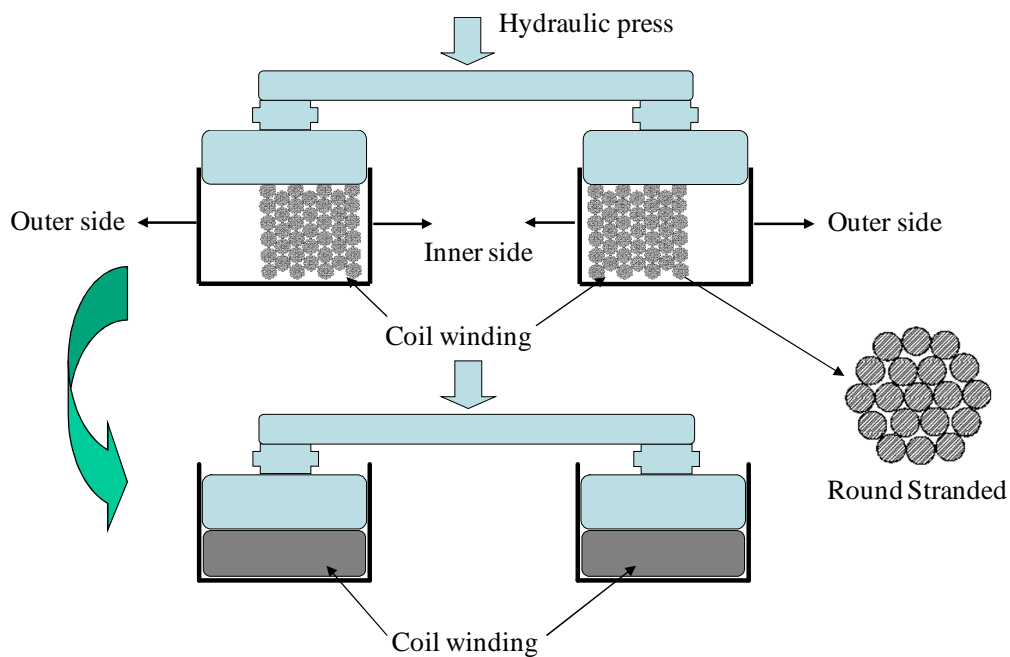


Fig. 4.16 Concept of compression molding

4.4.4 Development of the real-scale ground coil

We developed a ground coil with low eddy current loss for the actual scale based on the trial experimental results ⁽⁹⁾ of the 1/2 scale model of the winding coil assuming its application to the PLG coil ⁽¹⁰⁾.

4.4.4.1 Winding and compression molding conditions

The twisted round wire with heat insulation formal (diameter 2.5mm ×19 wires) was for winding wire. As the winding coil after compression molding became the predetermined dimensions of the resin before molding, winding conditions and compression molding conditions were pre-examined. The wire winding was designed so that the coil of each layer turns alternating odd and even in the winding process prior to the compression molding as shown in Fig. 4.17. The depressing of the lower layer guides the wire on the above layer. It decreases the spaces and facilitates the winding work. This method is the same as the wire winding of the crane. It is considered to be superior for automating the winding process of the winding coils. The compression loads (the standard upper unit coils: 12MN, the lower unit coils: 14MN) were set in consideration of the asymmetry of the upper and lower unit coil. The dimensions and reproducibility were confirmed by manufacturing trial coils. Table 4.3 shows the winding coil specification. Figure 4.18 shows the work situation of each of the processes.

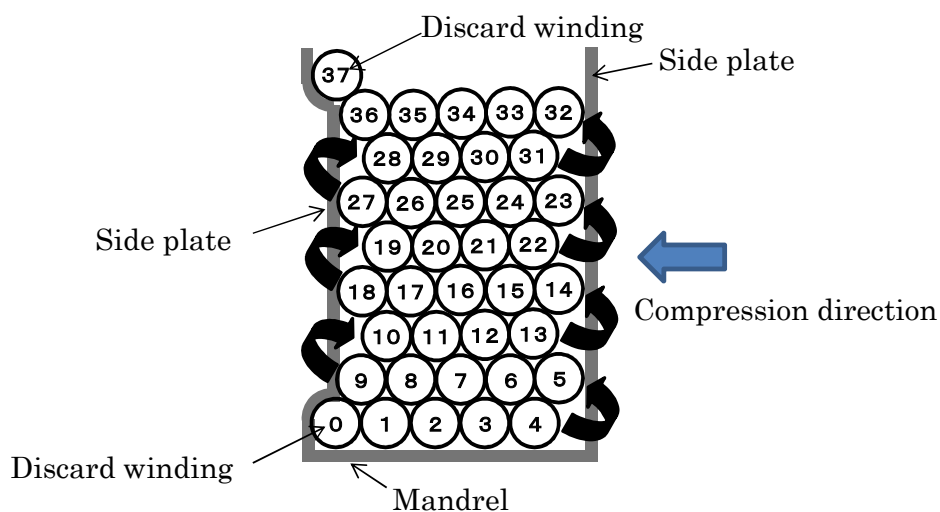


Fig. 4.17 Winding steps

Table 4.3 Specifications of real scale coil

Dimension between the upper coil center	755mm × 230mm
Dimension between the lower coil center	755mm × 370mm
Conductor cross-section dimension	100mm × 40mm
Bend radius of corners	100
Number of winding	36



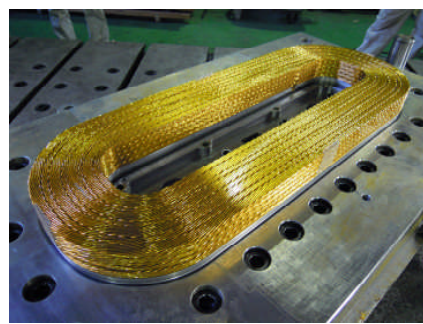
① Winding work



② Before compression molding



③ Compression molding state



④ After compression molding

Fig. 4.18 Trial of the coil compression molding process

4.4.4.2 Performance evaluation of the winding coil

Various tests were performed before and after the compression molding of the winding coil to investigate the compression effect to the winding coil.

(1) Dimensional precision

The winding coils after compression becomes the finished size by plastic deformation which depends on the compression mold dimensions. The dimensional design accuracy was improved to about $\pm 0.5\text{mm}$ compared with ± 1 to 2 mm of the non compressed conventional winding coil. However, the thickness is dependent on the strand density by the compression load. It depends on the space factor of the coil. The prototype of this coil compression molding shows the achievement of roughly 80% of space factor of the coil conductor of the initial target value. Figure 4.19 shows each unit dimension ratio by the compression load to the upper unit coils before and after compression molding. Figure 4.20 shows the change of the conductor space factor calculated from the conductor cross-sectional dimensions under the same conditions. It shows about 83% was achieved by applying a load of 12MN or higher.

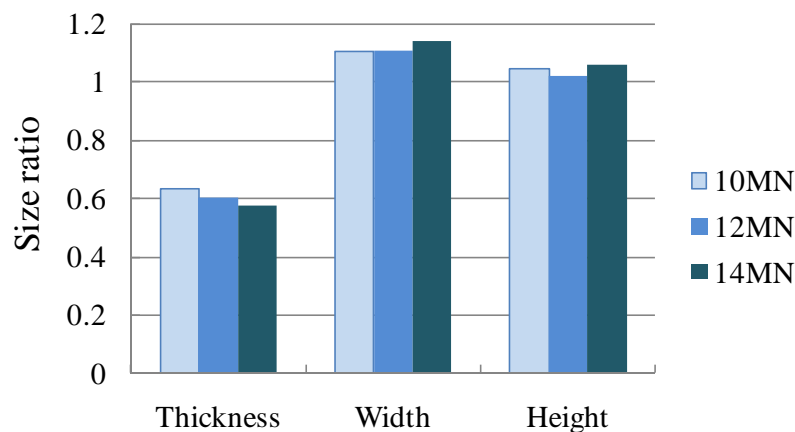


Fig. 4.19 Relationship between press load and size ratio

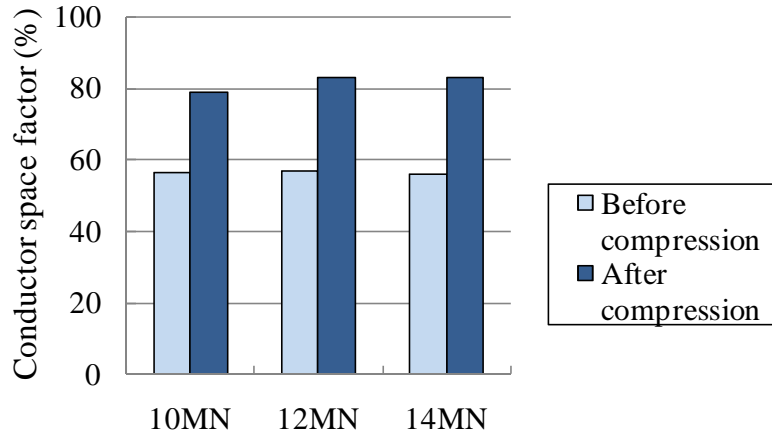


Fig. 4.20 Conductor space factor before and after compression molding

(2) Winding coil integrity

To confirm the damage to the winding coil by compression molding, the integrity survey was performed to the winding coils before and after compression molding. The failure such as short circuit or break was examined by stripping the insulation of both ends of the twisted wire (19 wires) and checking the electrical continuity between coils and of inter-layer winding coils. As a result, no damage was confirmed except for partial short circuit or break at the early stage of selecting the compression conditions of the coil molding. The cause of the damage at the early stage was located, and it was due to the outermost coil lead excessively pressing at the edge of the outer circumferential groove processing section (the spool discarded part of the 37th turn) contacting the side plate of the coil reel (pressing the jig for compression molding). After improvement of R-processing to the edge of the pressurization side plate, no short circuit or break was observed in the similar compression molding. The change in electrical resistance of the winding coil after compression molding was about 5% showing stable performance. The interlayer dielectric breakdown strength was measured by applying the impact voltage between the winding coils after compression molding. As a result, the average values of multiple coil measurements of 7.5 kV_p (the upper unit coil) and 5.3 kV_p (the lower unit coil) were obtained. These values were estimated as the discharge while voltage was applied or discharge generated from the surface layer. It was determined that it was

sealable by a resin molding in the next step.

4.4.4.3 Performance evaluation of the molded coil

The most important matter for the performance of the molded coil where the compression molding is applied to the winding coils is the interlayer insulation as a propulsion ground coil. In this evaluation, the cross-sectional study by cutting was performed after measuring the breakdown strength between the layers of the molded coils and to the ground.

(1) Inter-layer breakdown strength

The inter-layer breakdown test of the test coil was performed in compliance with JEC-0202 "Impulse voltage and current test general", Institute of Electrical Engineers of Electrical Standards Committee Standards. The multistage impulse voltage generator is often used for the impulse voltage generator. The equivalent circuit of this study is shown in Fig. 4.21. G in the figure refers to the discharge gap, R_s refers to the sum of the damping resistors inserted in each stage of the generator, C refers to the overall equivalent series electrostatic capacitance of each stage capacitor, R_o refers to the discharge resistor, L refers to the wave front adjustment inductance, C_o refers to the wave front adjustment electrostatic capacitance. In this test circuit, the lightning impulse voltage e (negative polarity) was applied three times to the coil terminals by 5kV step increment from 20kV to 50kV peak value, and by 10kV step increment above 50kV peak value to measure the breakdown value. As a result of the test using two samples, no damage was confirmed in the interlayer dielectric strength where they had 2 to 3 times ($90kV_P$, $130kV_P$) the withstand voltage reference value ($35kV_P$). Figure 4.22 shows the health waveform example before the breakdown.

(2) Ground breakdown strength

After the specified withstand voltage test, the ground breakdown strength test was performed conforming to the voltage increment procedure of JEC-0201 "AC voltage insulation test". The breakdown value was measured by incrementing the voltage by a speed of 1kV/s from 0kV by applying

commercial frequency AC voltage (effective value) between the conductor and coil shield layers through the test cables. The aforementioned interlayer breakdown test used two samples for this test. As a result, the samples were destroyed at 99.2kV and 122.4kV respectively. The breakdown portions were at the side wall surface of the upper unit coils. One was at the coil outer periphery, another at the coil inner circumferential side. The short term withstand voltage standard value of the PLG coil designed by the nominal voltage 33kV specification was to withstand for 1 minute at an applied voltage of 70kV. A satisfactory test result was acquired.

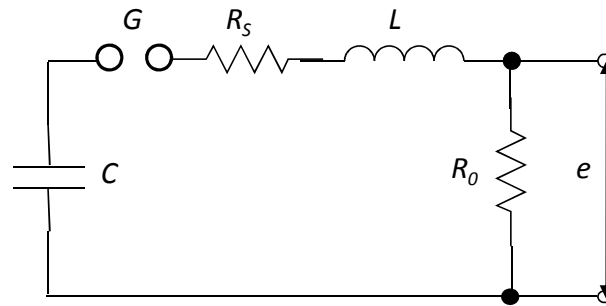


Fig. 4.21 Interlayer dielectric strength test circuit

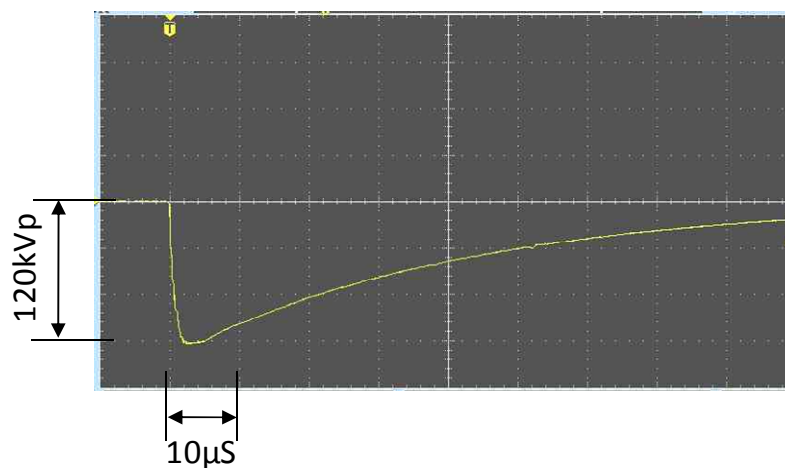


Fig. 4.22 Soundness voltage wave example at 120 kV_P

(3) Coil cross-sectional study

After completion of the series of evaluations, coils were dismantled and their cross-sectional surfaces were observed. For compression status, it was confirmed that the wire was compressed substantially uniformly and epoxy resin was filled in the small gaps although density imbalance was slightly observed on the inner periphery and the outer periphery in the curved portion of the winding coil. The cause of density imbalance generated on the curved section was assumed due to the twisted wire that was deformed at this portion due to the tension of the wire during winding and it was formed in a high density as compared to the straight wire portion. As for the thickness of the molding resin, a minimum thickness is desirable for maintaining the mechanical strength of the air-core coil and breakdown strength against the ground to take into account the EM force characteristics with the SCM and the cost of the coils. However, because the breakdown strength against the ground depends on the resin thickness, if uneven thickness exists locally even though the resin thickness is secured as the coil section design thickness, the insulation reliability will be significantly impaired. The test compression molding coil had an excellent forming condition with small uneven thickness due to excellent dimensional accuracy of the winding coil after compression. Figure 4.23 shows the appearance of the cut surface of the upper unit coil (straight and corner portions).

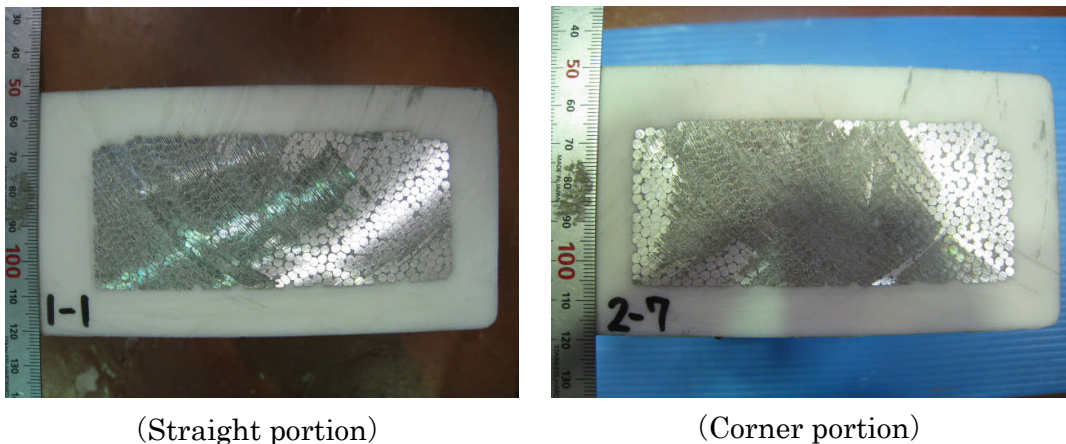


Fig. 4.23 Cutting surface of coil winding

4.5 Labor saving on the maintenance management of the ground coil applying IT

It is necessary to ensure the safety by the maintenance work on a regular basis for stable operation of the ground coil. Therefore, it is considered that establishment of appropriate and simple maintenance and management procedure is extremely important in order to reduce maintenance cost and ensure the reliability of the system. This study developed the ground coil self-diagnosis method using IC tags for the purpose of ground coils individual information management method as well as preventing troubles ⁽¹¹⁾.

4.5.1 Ground coils individual information management method using IC tags

The ground coil installed to the site is forced to be used outdoors for a long period of time. Therefore, a high degree of quality control will be required from the production to the actual commercial operation. However, it is not easy to manage various coils appropriately throughout the entire lines installed by the multiple manufacturers, installation specifications and contractors. Furthermore, periodical maintenance data update based on the work records requires not only huge labor consumption but also has a potential to reduce the reliability of the database itself due to access difficulty to the actual coils. Therefore, the built-in IC (Integrated Circuit) tag used ID (Identification) maintenance management approach for the ground coils data including production, storage, installation and maintenance was verified with the aim of doing integrated management with correct and latest database.

4.5.1.1 Selection of the IC tag

The IC tag is a small device that consists of memory IC chip, a wireless unit and antenna. It is also called as a "wireless tag" or "RFID (Radio Frequency Identification)" tag. The IC tag cannot only handle comparably

big data unlike the QR (Quick Response) code or bar code but also the tag data can be updated if necessary. The rapid spread and development of the IC tag for various fields are now progressing. Because the data read/write using electromagnetic induction or the radio wave can be performed without contacting the object, the IC tag was embedded into the ground coil to facilitate constant performance without worrying about the weather resistance.

(1) Operating environment of the IC tags

Upon application to the ground coil, the special environment must be taken into account (long-term outdoor use, vibration, magnetic field, high-voltage, low-cost, etc.). Therefore, the heat-resistant resin molded coin type IC tag was selected. Table 4.4 shows the operating condition ⁽¹¹⁾ of the IC tag for the ground coil.

(2) Confirmation of basic performance

The environmental factor that is of most concern for the ground coil installation is the effect of the magnetic field variation when the SCM on the vehicle passing on the ground coil with high speed. Therefore, the stationary test for confirming the basic performance of the IC tag simulating the magnetic field transition caused by passing the SCM was performed.

Table 4.4 Operating condition of the IC tag

Items	Conditions
1. Maximum temperature during manufacturing	120 °C
2. Environmental temperature	-30~50 °C
3. Surface potential of the IC tag	Tens of volts
4. Magnetic environment	1 T (maximum)
5. Vibration environment	300 m/sec ² (maximum)
6. Target life span	35 years

① Influence of the varying magnetic field

The magnetic field transition was simulated by turning the IC tag mounted disk on the high speed rotation test equipment in high speed described in the quantitative evaluation of the eddy current in Section 4.4.2. As a result, no abnormality was confirmed in the IC tag read data at the speed of 1200T/sec (magnetic field variation rate of approximately 1.5 times that of the actual passing time).

② Withstand voltage characteristics of the IC chip

The influence of the magnetic field variation induced voltage on the wireless communication antenna to the IC chip when the SCM is passing was verified. A part of the antenna was cut so that the voltage can be applied to the IC chip from the cut terminals. The stepwise impact voltage was applied to the antenna terminals through the variable resistor until the tag data cannot be read. The value immediately before the tag data could not be read was measured. As a result, it was confirmed that the withstand voltage was about 2.5 times the induced voltage (max. 14V), the voltage equivalent to the magnet passing at 500km/h. Figure 4.24 shows the equivalent test circuit diagram and the applied voltage waveforms.

4.5.1.2 Prototype test of the IC tag embedded ground coils

(1) Application to the PLG coil

The IC tag was embedded to the actual ground coil when the coil was molded with resin in order to avoid falling off from the coil due to environmental degradation or vibration. Because the PLG coil is special high-voltage equipment, the protective layer of about 3mm in thickness is provided on the vehicle side. In this trial coil, the IC tag was embedded by inserting it in the space of the protective layer. Since both sides of the FRP plate constituting the protective layer were electrically grounded, it was impossible for the IC tag to be exposed to high voltage.

(2) Read data evaluation

No influence to the IC tag information was confirmed by the

manufacturing temperature (120 °C) and the withstand voltage (AC 70kV/1 min.) test.

(3) Durability evaluation

From the results of the long-term durability test equivalent to 35 years commercial operation for the IC tag embedded coil (electromagnetic vibration test, accelerated weathering test), stable data transmission was confirmed. Effectiveness for the simplified on-site information management and high reliability were also confirmed.

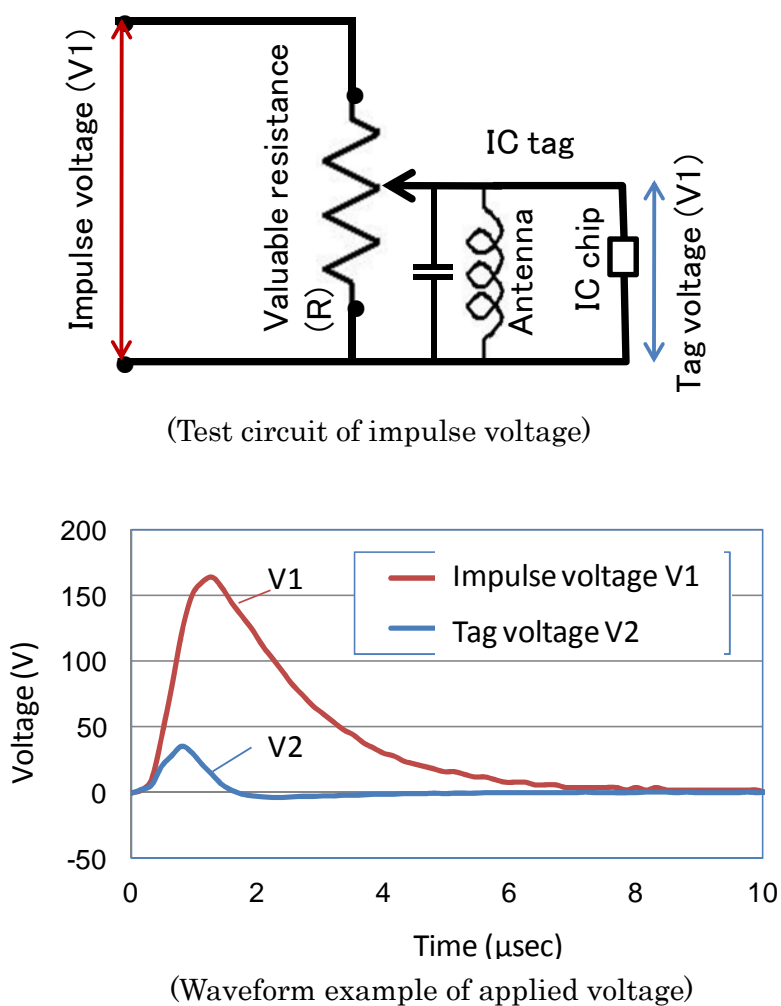


Fig. 4.24 Withstand voltage characteristics of the IC tag

4.5.1.3 Development of ground coils ID information management method

(1) The ground coil ID information and the data format

Since the capacity of the IC tag memory is limited, necessary information such as production, storage, installation, operation, maintenance and other information are all coded as much as possible to secure a wider user area as possible to deal with the various information that may be encountered in the commercial operation. Each data was blocked as a unit by providing a header to facilitate instant search and read/write.

(2) Configuration of the ID information management device ⁽¹²⁾

The ID information control system consists of the ground coil built-in IC tag, the ground coil ID read/write device having data transfer function via a wireless LAN and the data processing device that updates the database by the acquired data automatically and can search the arbitrary data (Fig. 4.25). The data processing device can be used not only for the information management but also for the "work instruction device" for on-site maintenance and inspection work by including the actual maintenance operation.

(3) Running test results of continuous data read

The RF tags set on the ground were continuously read by the traveling vehicle to assume that the maintenance vehicle collects individual information from the ground coils. As a result, 16-byte data of the individual information were collected by a traveling test vehicle moving approximately 60km per hour. With this feature, the product ID could be distinguished from the vehicle and the work history could be confirmed and a prospect to establish a ground coil maintenance and management method was obtained ⁽¹³⁾.

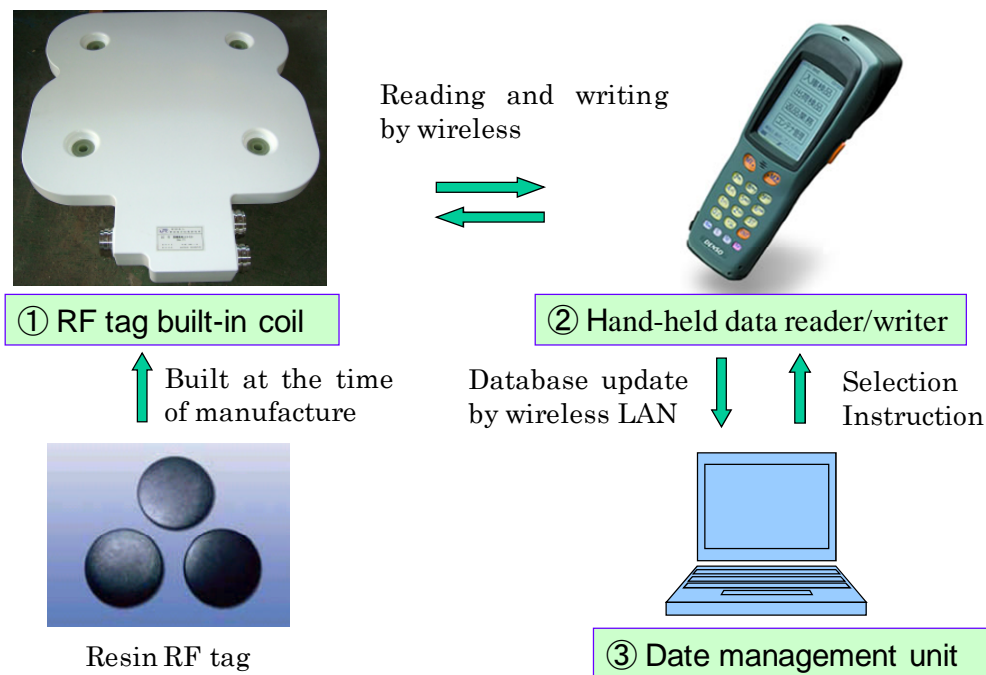


Fig. 4.25 Configuration of ground coil ID information management device

4.5.2 Ground coil self-diagnostic method

Currently the visual inspection on foot patrol has been performed as the ground coil maintenance work. However, the worker requires the expertise and experience for each inspecting point and judged abnormal. In addition, considerable efforts are required because a coil is much to be checked after its disassembly and a huge number of coils must be maintained. Therefore, currently the inspections rely on the periodical coil inspection result at the limited partial area with respect to the observation of the coils. It is an issue from the viewpoint of preventing problems. On the other hand, commercial lines do not allow trains to be inactive for maintenance. The maintenance must be done within late night hours after end of the daily commercial operation. Therefore, it is necessary to establish effective measures to predict the precursors leading to the problems based on the stationary acquired durability test results and other information for the maintenance of the huge number of the ground coils. Thus, the ground coil self-diagnostic method

having high reliability without relying on human as much as possible was studied that the coil automatically sensed its condition and transmitted the state of the problem by itself.

4.5.2.1 Concept of the ground coil self diagnosis

From various accelerated aging test results concerning the ground coil, the change of strain of the mold resin, increased vibration, abnormal temperature rise and the like were observed as predictors of a fault. Therefore, a newly developed miniature sensors integrated single chip data processor was developed. It was embedded into the coil in the coil molding process. It enabled the coil to transmit various information from the coil itself. It will be enhanced the prevention of problems by receiving the coil transmitted failure information so that the workers on foot patrol can judge by visual inspection. However, the monitoring conditions of the ground coil self-diagnostic system are different from the health monitoring system used for verifying structures in the following points.

(1) The health monitoring of the structure is a static state monitoring in general. On the other hand, the ground coil self diagnostic monitors the dynamic behavior when the vehicle is passing.

(2) The abnormality detection sensor (referred to as error sensor) installation is subject to special high voltage equipment.

(3) The error sensor is exposed to the varying magnetic field the same as the IC tag when the SCM is passing.

Figure 4.26 indicates the conceptual monitoring of the dynamic behavior when a vehicle passes through. The outline of the data acquisition procedure is described below. For example, (i) a ground coil built-in error sensor detects the vibration acceleration caused by vibration of the EM exciting vehicle during a vehicle passing and the acquired peak value will be saved to memory. (ii) After the vehicle has passed, the data will be transmitted to the data acquisition post provided at regular intervals in the guide-way. (iii) It enables not only to reduce the inspection time of ground coils significantly but also remove the troubles due to workers' skill difference or oversight resulting in improving reliability dramatically. It should be noted that the

development of small-sized, high-performance error sensor is the key to realize the ground coil self diagnosis.

4.5.2.2 Object of the ground coil self diagnosis

As the ground coil used for the superconducting Maglev system is the iron-less air-core coil, the repeated EM force acting between the SCM on the vehicle and the ground coil is applied as a distributed load to the entire winding coil. Therefore, the winding coil supporting the molding resin receives mechanical and electrical stresses simultaneously in addition to the environmental loads due to outdoor installation. It is necessary to monitor the dynamic behavior in order to obtain stable operation. The EM vibrating environment for the ground coil when high-speed vehicle is passing is peculiar to the ground coil. It is necessary to avoid unexpected vibration by the resonance phenomenon due to the reduction of natural frequency of each part of the ground coil, especially the fastening portion to the excitation frequency level. Here, the priority is set to the vibration acceleration of the bolt fastening vicinity where most likely it would lead to the main cause of troubles among the various behaviors to be diagnosed, and thus it is set to the subject of the ground coils self diagnosis.

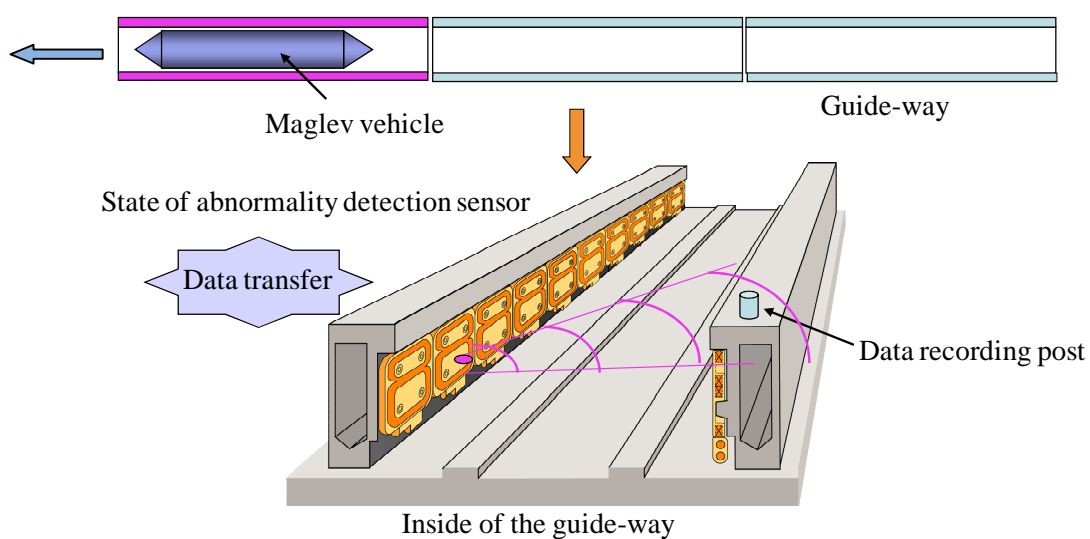


Fig. 4.26 Data transfer image of the vehicle after passing through

4.5.2.3 Basic verification of the power supply

Since outdoor use for a long period of time is assumed with the ground coils, it is necessary to minimize the error detection component as small as possible by embedding in resin molding to the winding coil due to the influence of environmental degradation ⁽¹⁴⁾. The battery life can only be expected a few months to a year at most for the error detection component, the same as the sensing and data transmission power unit. It is not suitable for long-term operation on the on-site installation. Therefore, the EM induction generator utilizing an alternating magnetic field generated to the ground coil by the LSM current (three-phase alternating current to energize a propulsive force to the vehicle) and the vibration generator were examined.

(1) Prototype of the power supply

The prototype power supplies with generators of different types to be installed to the window of the upper unit coil were examined as the first step of development. Each power supply was configured with the power generator, rectification unit and the power storage unit. It was assumed to be used for a single operation in a ground coil. Figure 4.27 shows the outline of the configuration and Fig. 4.28 shows the outside appearance of the prototypes.

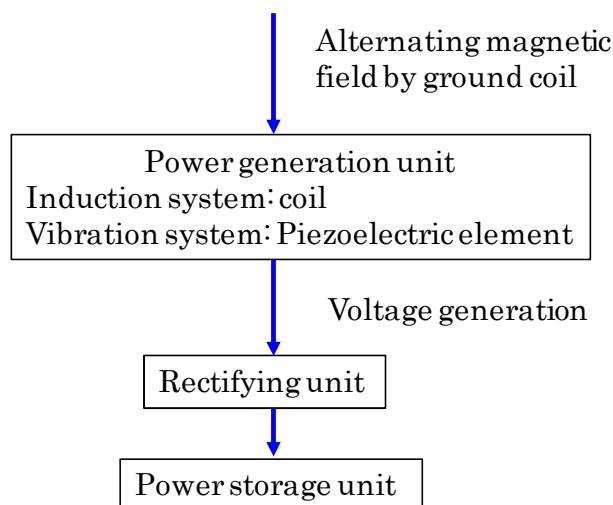


Fig. 4.27 Configuration of the power supply unit

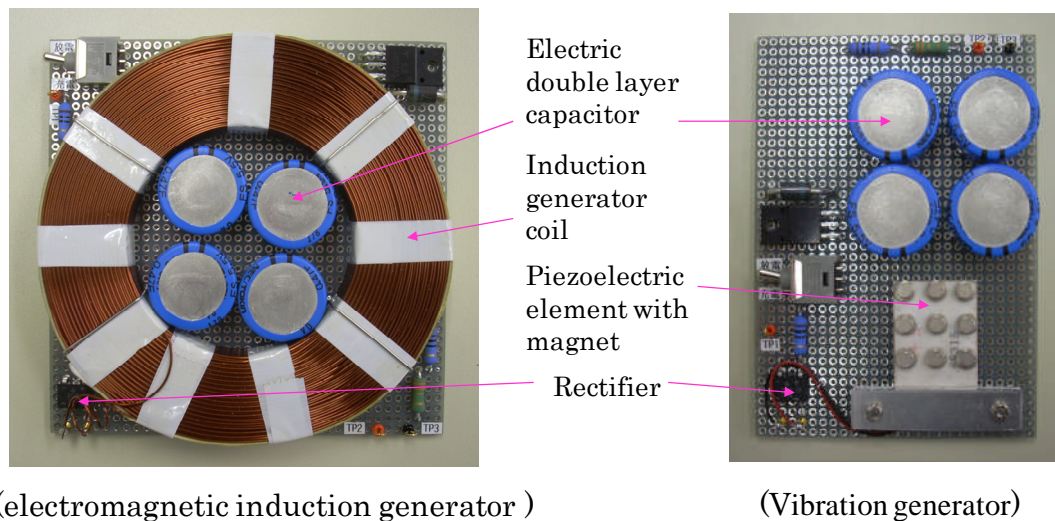


Fig. 4.28 External view of the power supplies

(2) Performance of the power supply

The EM induction generator system acquired the expected characteristics by the performance evaluation of the prototype and its charging/discharging characteristics were verified.

① Charge characteristic

The power supply unit was installed to the center of the upper coil window of the PLG coil and ratings half the alternating current (frequency 40Hz) was supplied to the PLG coil for 10 seconds, energizing every 5 minutes (simulating the actual vehicle passing), and the charging voltage of the power storage unit was measured. The charging voltage was set to 10V due to the withstand voltage of the electric double layer capacitor that was used for energy storage. From the charging characteristics, the charging voltage reached 10V by twice the energization for rated current and seven times energization for half the rated current under the magnetic field conditions (Fig. 4.29).

② Discharge characteristic

The initial voltage of power storage unit was set to 10V and the fixed voltage regulator (output voltage: 3.3V) with 250mA resistor load was

connected to discharge the electricity. The output voltage drop time under 3.3V was measured. Figure 4.30 shows the discharge characteristics of the power storage unit. The 3.3V discharge (approximately 250mA) lasted 10.3 seconds. It shows the storage capacity of about 2500mAs.

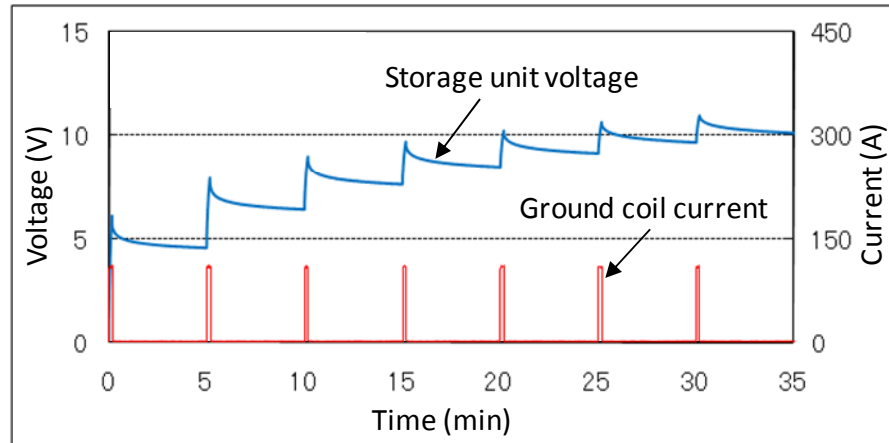


Fig. 4.29 Charge characteristic of the power storage unit

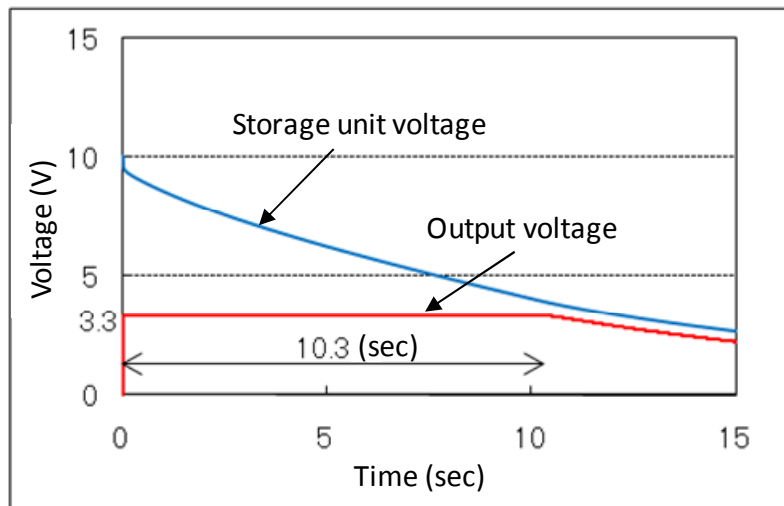


Fig. 4.30 Discharge characteristic of the power storage unit

4.5.2.4 Development of error sensor

If the concept of smart sensing is applied to the monitoring of ground coils, the development of compact and sophisticated error sensor will be essentially required. Further, in order to function for long-term at outdoor environments, it is necessary to miniaturize the components of power supply, sensor, signal processor, data storage, data transmitter and other units as an error sensor to be embedded into the mold resin. In this study, the MEMS (micro-electro-mechanical device) sensor was effectively used. We developed a prototype abnormality sensor that was intended to operate independently and embedded in a ground coil (Fig. 4.31) ^(15, 16). In addition, the sensor was embedded in the recess of the back of the PLG coil, and its performance was confirmed by the EM vibration test. As a result, it was confirmed that each component functioned properly in a high magnetic field and the integrated unit functioned as an error sensor.

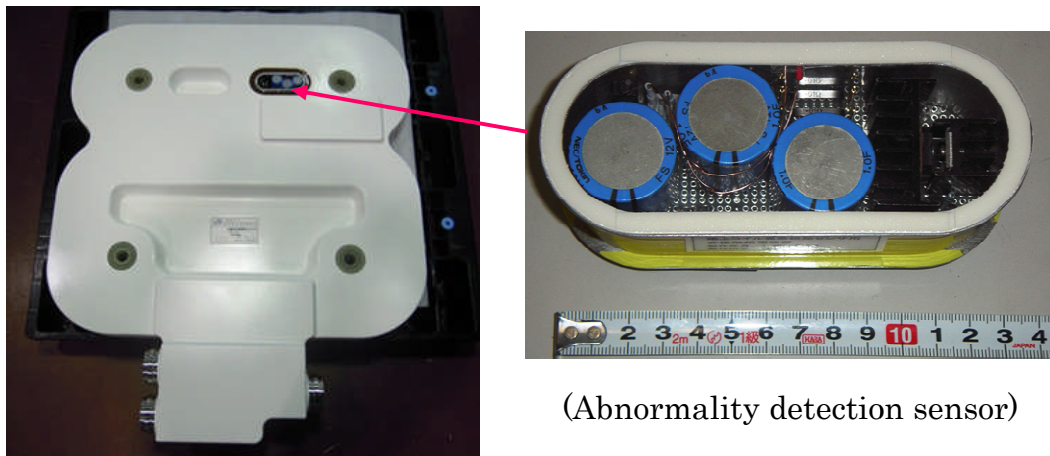


Fig. 4.31 Abnormality detection sensor embedded in a ground coil

4.6 High functioning of mold resin material

In recent years, solid insulating material has been increasing as an alternative to gas (SF₆ gas) or liquid (insulating oil) from the viewpoint of environmental impact reduction and miniaturization of equipment. The epoxy resins are widely used as a solid insulating material for power devices because it has electrical insulation properties with excellent mechanical strength. Meanwhile, large quantities of fillers in order to increase the additional functions are mixed in addition to the base resin and curing agent. Therefore the epoxy resin mold has a problem of physical properties of being hard but fragile (toughness is low). The propulsion coil requires crack resistance in addition to the electrical insulation properties. The physical improvement is demanded in terms of long-term outdoor use.

4.6.1 Functional improvement by a combination of different materials

In this study, we examined the characteristic improvement of resin in combination with thermosetting resin and thermoplastic resin.

4.6.1.1 Toughness improvement by Engineering Plastics metamorphosis

As shown in Fig. 4.32, particulate thermoplastic resin was blended with liquid epoxy resin (sea-island structure) by heating to exchange the disperse characteristics of both materials (reverse island structure). It is a technique for improving the toughness after curing.

4.6.1.2 Toughness improvement by core-shell particles

As shown in Fig. 4.33, blending core-shell particles (low elastic material) to the epoxy resin reduces elastic modulus and improves the thermal characteristics by releasing the stress concentration without impairing the mechanical strength as a molding resin material.

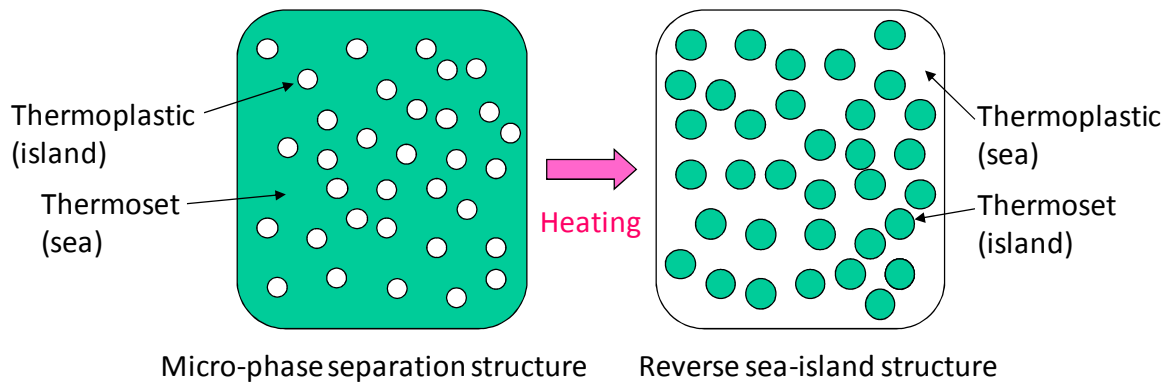


Fig. 4.32 Modified example of the engineering plastic

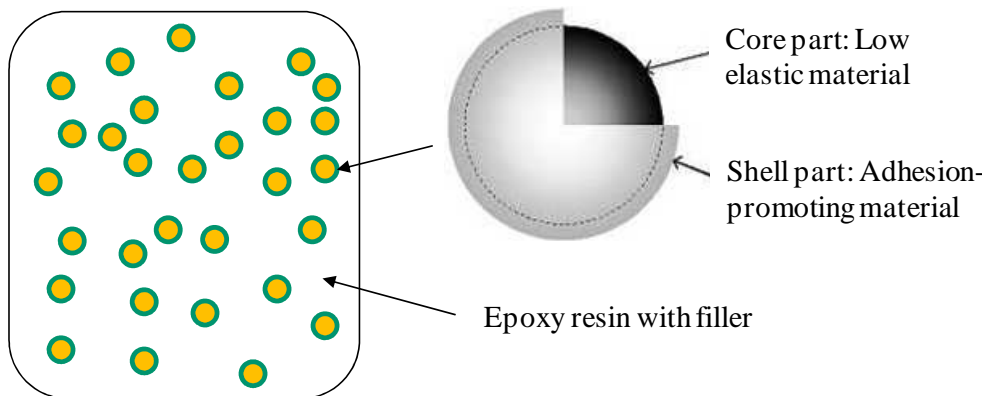


Fig. 4.33 Structural model of the core-shell particles

4.6.2 Prototype test of toughness resin material

For the improvement of toughness molding epoxy resin, toughness resin blended with core-shell particles was produced experimentally. Its effectiveness was confirmed by various tests. Improvement of the thermal characteristics by the heat cycle test results is shown as a representative example.

4.6.2.1 Heat cycle test by bolts and nuts method

Bolts and nuts (M16) were combined and secured at the center of the aluminum pipe with the inner diameter of 40mmφ. They were resin molded, vacuum degassed and cured to create the test piece (Fig. 4.34). Then the heat cycle was sequentially repeated between 130°C for one hour and -10°C for two hours, then it was repeated by expanding the low temperature (-20, -30, -40, -50 and -60°C) until cracks occur. The heat cycle load was repeated twice for each heat cycle condition.

4.6.2.2 Test results

The heat cycle test results using specimens with integrating bolts and nuts of significantly different linear expansion coefficients are shown in Table 4.4. From the test results, a significant thermal shock resistance of the core-shell compounded resin was confirmed in comparison with the usual compounded resin.

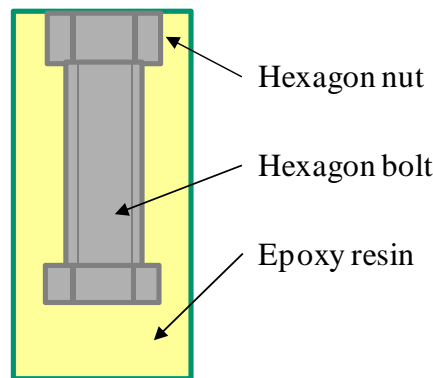


Fig. 4.34 Heat cycle test specimen

Table 4.4 Heat cycle test result

Test condition	Normal blend	Core-shell blend
130°C/1hr ⇔ -10°C/2hr 2 cycle	1	0
130°C/1hr ⇔ -20°C/2hr 2 cycle	9	0
130°C/1hr ⇔ -30°C/2hr 2 cycle	—	0
130°C/1hr ⇔ -40°C/2hr 2 cycle	—	0
130°C/1hr ⇔ -50°C/2hr 2 cycle	—	2
130°C/1hr ⇔ -60°C/2hr 2 cycle	—	8

4.7 Summary

It is important to increase the reliability and performance while considering the cost reduction for the practical installation of the ground coil.

We developed a small linear connection unit incorporating the improved dynamic durability by reviewing the conventional cable connection structure of the propulsion coil that may become a weak point in the future commercial operation. In this connection portion, the surface pressure of the insulating surface was increased by applying the spring mechanism resulting in reduction of the creepage distance. It promoted a significant success in downsizing. In addition, the dynamic and thermal reliability was further improved based on various evaluation test results.

We have developed a vibration-proof fastening unit based on the comparative evaluation of the fastening portion models that may become a weak point in the EM vibration environment. The laminated FRP bush was introduced as an alternative to the metal bush. Its superiority was confirmed that can greatly reduce the stress generated at the neighborhood of the fastening portion while avoiding bolt looseness.

The eddy currents generated in the conductor of the ground coils must be minimized as much as possible because it will lead to an unnecessary temperature rise in the coil and become the magnetic resistance of the vehicle while it is running. Quantitative evaluation results of eddy current loss using wire samples showed the superiority of a round twisted wire for the ground coil applications. Furthermore, we expect to balance the performance and stabilization of the ground coils and reduction of eddy current loss by applying a compression molding to the winding coil using the selected wire material.

It is necessary to introduce unique management techniques never before utilized in order to maintain a huge number of on-site installed ground coils stably and properly. The basic development of the IT utilizing ground coil maintenance and management system was examined. First, IC tag applied ID management system aimed at integrated and centralized management of the ground coil ID information was examined. The ID tag effectiveness was confirmed for high reliability of the information management and advanced

simplification through various validations of the IC tag and development of the ID information management system. Then, the ultimate coil self monitoring and diagnosis system to detect, forecast and transmit the abnormality prior to initiating any problems was verified. The dimensions of the power supply of the sensing unit were reduced for following the conceptual design. The outlook for functional forecast was obtained concerning the independent operation of abnormality sensor embedded into the ground coil.

The epoxy resin mold has a problem of being hard but fragile physical properties. Upon application to the ground coil with air-core structure, improvement of its characteristics is required. In this study, we examined the resin toughness improvement in combination with a thermosetting resin and a thermoplastic resin. As a result, blending the core-shell particles with a low-elasticity material in the resin core promoted a significant toughness improvement (thermal shock and mechanical impact resistance) that was a weak point of the epoxy resin.

Chapter 5 Durability Verification of the Ground Coil

5.1 Introduction

Maintaining stable performance and securing reliability are important issues in the development of ground coils because a huge number of ground coils are used outdoors for a long time. In order to solve these problems, it is necessary to organize the unique durability verification method that assumes commercial operation targeting from the materials to the completed product.

5.2 Basic configuration of durability verification

In durability verification on the ground coil, the material property test and actual product verification test have been simultaneously verified as shown in the basic configuration of Fig. 5.1 based on the actual running test results using the actual product. It is important for these tests and investigations to reflect the validity of evaluation to other studies ⁽¹⁾.

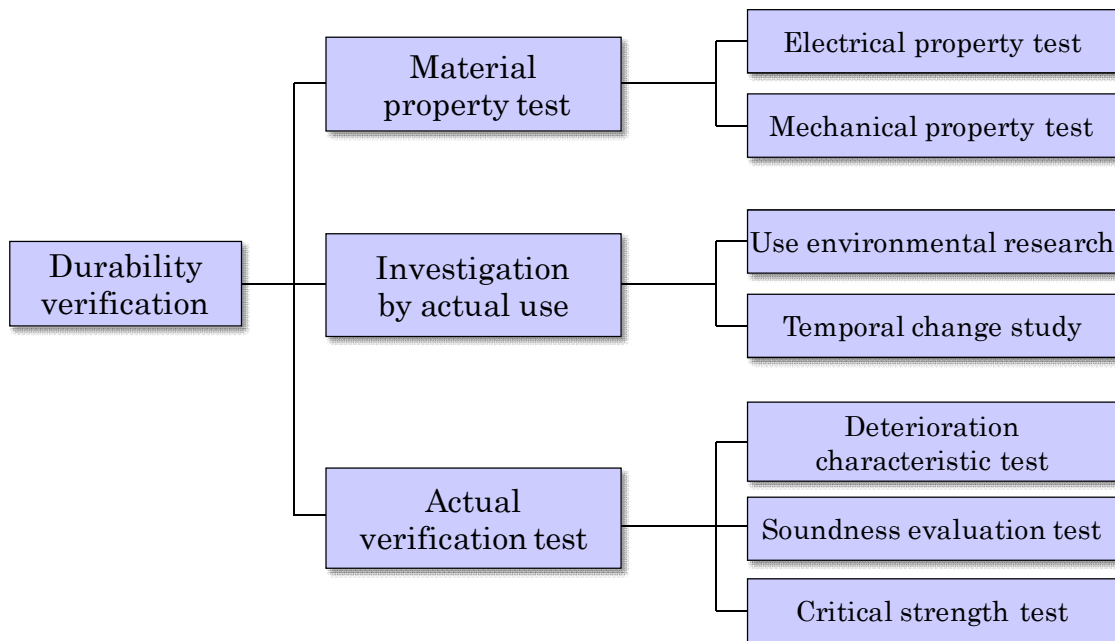


Fig. 5.1 Basic configuration of durability verification

5.2.1 Material property test

The degradation characteristics in operating environmental load was understood by the characteristics test of the material level using test pieces of the mold material. These results will be used as basic data of accelerated aging conditions for the verification test of the actual product.

5.2.2 Investigation by actual use

When the actual validation test is performed under the stationary condition, it is necessary to advance the investigation while considering the equality of the load at the time of actual use. For this purpose, it is necessary to investigate the actual on-site operating conditions in detail and acquire the data such as ambient temperature, humidity, ultraviolet irradiation level, applied voltage, temperature increase, electromagnetic force, vibration level, and generated stress.

5.2.3 Actual verification tests in stationary

The durability verification using an actual coil was classified into various degradation characteristics, soundness evaluation and limit strength tests. The accuracy of evaluation was increased by the accumulated data. Each test purpose is described below.

5.2.3.1 Various degradation characteristic test

It is a test to investigate electrical and mechanical properties of the actual coil chronologically with the accelerated aging test by applying a single load of each element of deterioration. It is possible to locate the influence of each deterioration element to the mold resin material constituting the actual coil from the test results. The test results can be used for the basis of load condition for the composite deterioration test.

5.2.3.2 Soundness evaluation test

The complex load simulating the actual operating environment as much as possible was applied to the target coil while adding the accelerated aging test equivalent to years of evaluation. It is a test to verify the presence or absence of electrical and mechanical functions of the actual coil. The durability was validated. However, issues to be considered for applying the complex load and promoting magnification of each load are considerable because of the restriction of the functions of the test facility.

5.2.3.3 Critical strength test

It is a test to find the breaking point of the actual coils at which it gets destroyed electrically and mechanically with the accelerated aging test by applying a single or complex load. The evaluation points can be classified into (1) breakdown time evaluation by applying the load with a constant condition and (2) load strength evaluation by increasing the load gradually until there is a breakdown. In the present study, it is possible to acquire valuable findings for improving the reliability of the actual coil by verifying the weak points in addition to the critical strength of the specimen.

5.3 Durability verification of the mold resin

The molding resin block that simulates the actual cross-sectional shape of the ground coil was prepared. The influence of the various degradation factors in outdoor use on the mechanical strength and insulation strength of the resin was investigated. Furthermore, the correlation between the water absorption ratio and immersion temperature of the resin block were investigated from the water absorption characteristics study of the resin block in order to examine the accelerated degradation conditions while the durability verification test was performed on the actual target coil ⁽²⁾.

5.3.1 Required functions of mold resin

Integrated resin molding has become the most important step in the preparation of the ground coils as described in this study. Selection and management of the molding materials and molding method will influence not only the performance and reliability of the coil but also give considerable impact to the construction costs of the system. The ground coils can be categorized by their applications into the propulsion system requiring external power supply, the levitation system which does not require the power supply and the multi-functional, multi-purpose system represented by the PLG system. The material and the production process are properly selected according to the requirement of each function. For example, epoxy resin is used for the insulation strength required in high voltage propulsion system, glass fiber reinforced resin is used for the mechanical strength required in levitation system, and the structurally reinforced epoxy resin is used for the multifunctional system as shown in Fig. 5.2.

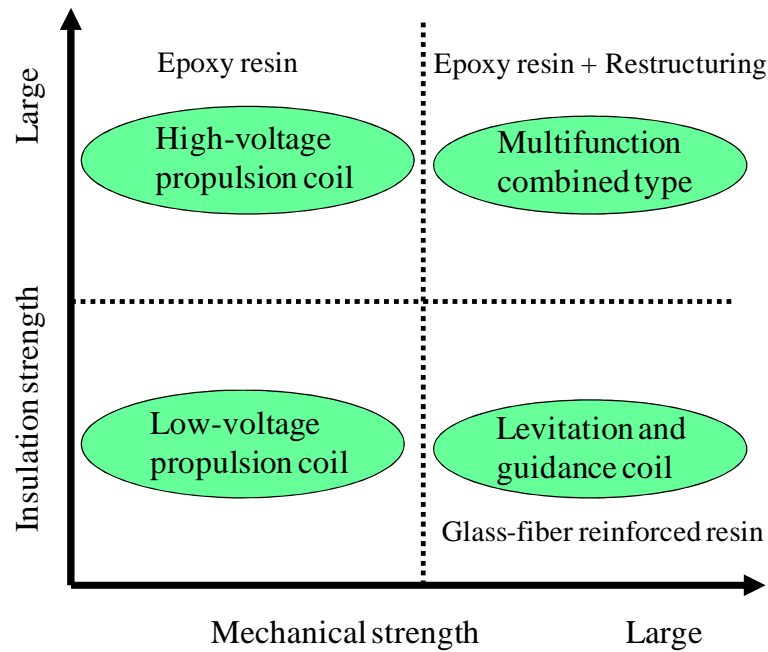


Fig. 5.2 Required functions for the ground coil

5.3.2 Environmental degradation characteristics of the epoxy resin for molding

A number of molding epoxy resin rectangular blocks that simulate the actual cross-sectional shape of the propulsion coil were prepared. Various environmental loads for the degradation characteristics were evaluated with the passage of time. In order to confirm the effects of the presence or absence of weather-resistant coating and corona shield layer of actual coil surface, similar surface treatment to the actual coil was made only to one side of the specimen.

5.3.2.1 Test method

The specimens were left in an environment that simulated the respective degradation factors. The specimens were removed after the predetermined time to inspect the degradation characteristics by the evaluation test. After that they were inspected with the specified interval. Table 5.1 shows the environmental degradation test conditions and evaluation items.

Table 5.1 Environmental degradation test conditions for epoxy resin

Degradation factor	Evaluation item	Number of samples	Temperature condition	Degradation time (Hr)	Total number
Water absorption	Flexural strength	1	60°C	0,24,100,200,500,1000,2000	7
	Insulation strength	3	60°C	0,24,100,500,2000	15
Thermal	Flexural	1	120°C	100,200,500,1000	12
	"	1	140°C	"	
	"	1	160°C	"	
	Insulation	3	160°C	200,1000	6
Alkali	Flexural	1	60°C	500,1000,2000	3
	Insulation	3	60°C	"	9
Weather resistance	Flexural	1	63°C (B.P.)	100,500,1000,2000	4
	Insulation	3	63°C (B.P.)	500,2000	6

(1) Deterioration treatment method

① Water absorption degradation

The 18 resin molding blocks were immersed into the thermostatic chamber filled with ion-exchanged water at the constant temperature (60°C) to absorb water for degradation observation (Fig. 5.3).

② Thermal degradation

The 18 resin blocks were set into the three thermostatic chamber to observe the thermal degradation at the specified temperature (120, 140, 160°C, respectively).

③ Alkaline degradation

The 12 resin blocks were immersed in a calcium hydroxide aqueous solution prepared in pH10.5 (it assumed the value of the aqueous solution flowing out from the concrete structure by condensation in the tunnel or

guide-way) to observe alkaline degradation. The two resin blocks were immersed in calcium hydroxide aqueous solution in a stainless steel container and the container was left in the thermostatic chamber, where the temperature was maintained at 60°C. Then the container was covered with a lid. However, because calcium hydroxide aqueous solution used in the degradation process became neutralized by reaction with carbon dioxide in the air, aqueous solution was replaced weekly with a newly pH prepared solution (Fig. 5.4).

④ Weather resistance degradation

The 10 resin blocks were set in a xenon weather meter to observe the weathering degradation. The resin blocks were sliced into two pieces along the thickness direction due to dimensional restriction of the sample holder. The sample was set with its non-cutting surface exposed to the xenon lamp (Fig. 5.5). The temperature of the black panel surface of the test apparatus was maintained at 63°C and pure water was sprayed for simulating the intermittent rainfall for 18 minutes at 120-minute interval.

(2) Evaluation test procedure

① Flexural strength

The 9 flexural test pieces (hereinafter referred to as TP) were mechanically excised from surfaces (front and rear sides) of each degradation processed resin molding to measure the flexural strength. The 6 pieces faced their degradation surface to the tension side, and the 3 pieces faced their non-degradation surface to the tension side in order to check the degradation influence of the resin molding block to the thickness direction. The test procedure was followed in accordance with "Flexural test method of rigid plastic" JIS K 7203.

② Insulation strength

The 6 insulation TPs were mechanically excised from surfaces (front and rear sides) of each degradation processed resin molding to measure the AC breakdown voltage by the short time measurement method. The test

procedure was followed in accordance with "Thermosetting plastic general test method" JIS K 6911.

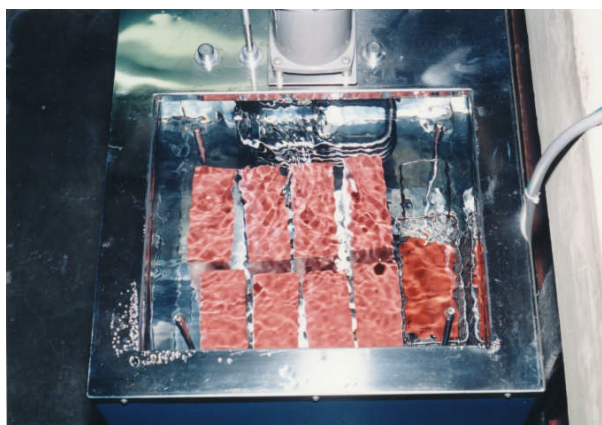


Fig. 5.3 Water absorption degradation test situation



Fig. 5.4 Alkaline degradation test situation

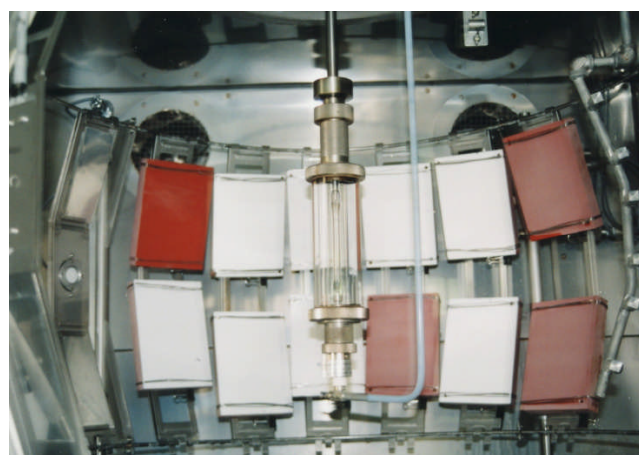


Fig. 5.5 Weather resistance degradation test situation

5.3.2.2 Test results

(1) Water absorption degradation characteristics

The water absorption degradation properties of the resin block are shown in Fig. 5.6. From the test results, the following points were confirmed.

① Flexural strength

i) The weather-resistant coating that was coated to the surface of the block exhibited no resistant effect on the water absorption degradation.

ii) Concerning the intensity of the sliced TP, a significant strength reduction was observed in the sample of the degradation side set to the tension side compared to the sample of the non-degradation side set to the tension side. It is considered that this was because the resin strength reduction by water absorption was not uniform along the resin depth direction and the effect was limited to the surface layer.

② Insulation strength

Concerning the insulation strength, it was considered that reduction of the degradation characteristics was insignificant irrespective of existence of surface coating protection.

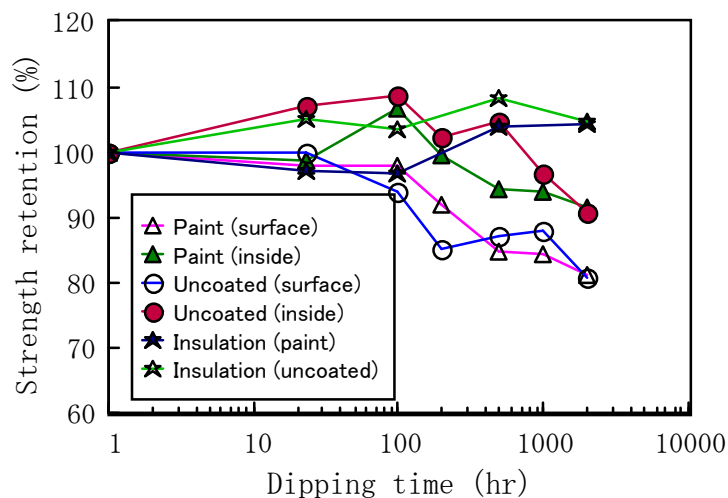


Fig. 5.6 Water absorption degradation characteristics

(2) Thermal degradation characteristics

The thermal degradation characteristics of the resin block are shown in Fig. 5.7. The following points were confirmed from the test results.

① Flexural strength

i) The weather-resistant coating on the resin surface of the block had little influence with respect to thermal degradation of the resin.

ii) The flexural strength of the surface sample was reduced due to heating. However, the flexural strength of the sample inside has risen about 5 to 10% from the initial value. It is estimated that curing of the resin constituting the blocks was promoted by heating at T_g (glass transition temperature) or higher, and the strength increased apparently. However, it was considered that oxidative degradation at the surface layer in contact with the air was accelerated by heating resulting in a reduction in strength.

② Insulation strength

With regard to the insulation strength, degradation characteristics were not observed in the same way as the water absorption degradation.

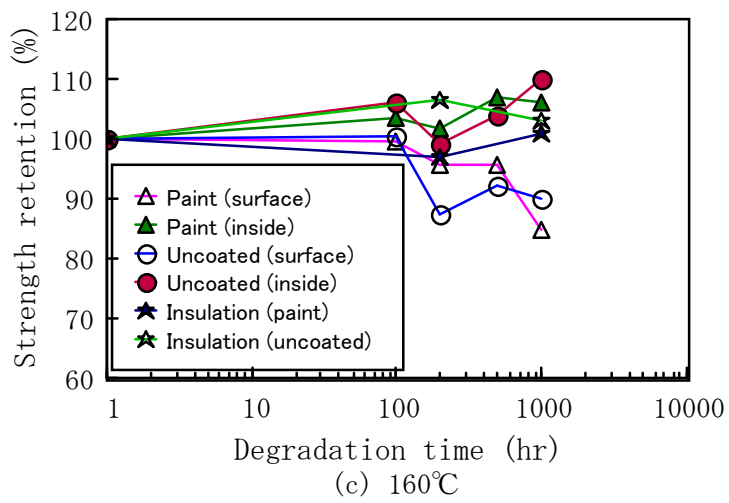
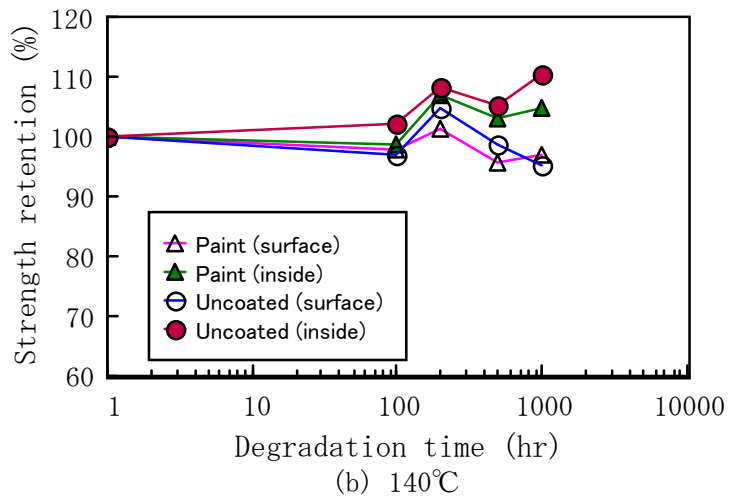
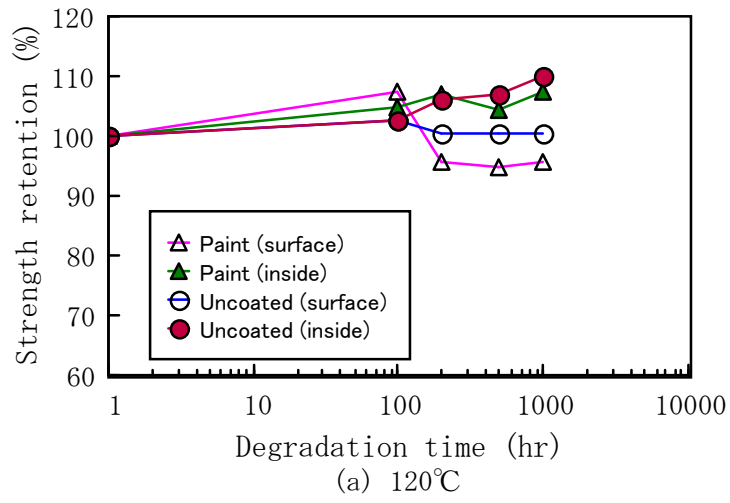


Fig. 5.7 Thermal degradation characteristics

(3) Alkaline degradation characteristics

The alkaline degradation properties of the resin block are shown in Fig. 5.8. From the test results, the following points were confirmed.

① Flexural strength

i) Concerning the flexural strength, it showed the most significant decrease among the degradation factors to be evaluated. This was considered because the alkaline component was applied to the acid anhydride curing agent in the resin and the degradation due to water absorption was further accelerated.

ii) The sample of the surface layer showed significant decrease in strength compared to the sample inside. The reason is because the degradation progress was not uniform along the thickness direction and the degradation was limited to the surface layer similar to degradation due to water absorption.

② Insulation strength

With regard to the insulation strength, no degradation characteristics were observed in the same way as the degradation due to water absorption and thermal degradation.

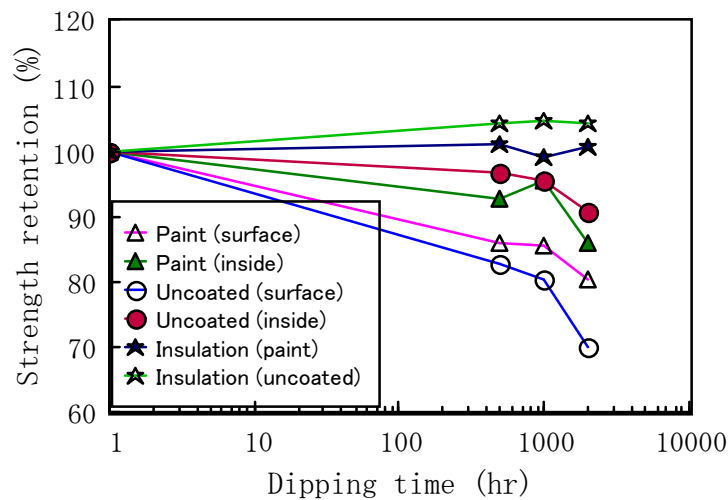


Fig. 5.8 Alkaline degradation characteristics

(4) Weather resistance degradation characteristics

The characteristics of weather resistance degradation of the resin block are shown in Fig. 5.9. From the test results, the following points were confirmed.

① Flexural strength

i) Whereas the decrease in strength of the surface layer was about 5 to 10 % due to exposure for 2,000 hours, no degradation was observed in the sample inside. This suggests that the environmental deterioration caused by ultraviolet rays was limited only to the surface layer of the resin block similar to the water absorption and alkaline degradation.

ii) When the flexural strength was compared with the presence or absence of the coating to the exposed surface, since the decrease in strength of the coated surface was half or less than the non-coated surface, it was considered that the weather resistance coating was effective for preventing deterioration of ultraviolet radiation.

② Insulation strength

With regard to the insulation strength, degradation characteristics were not observed as well as other deterioration factors.

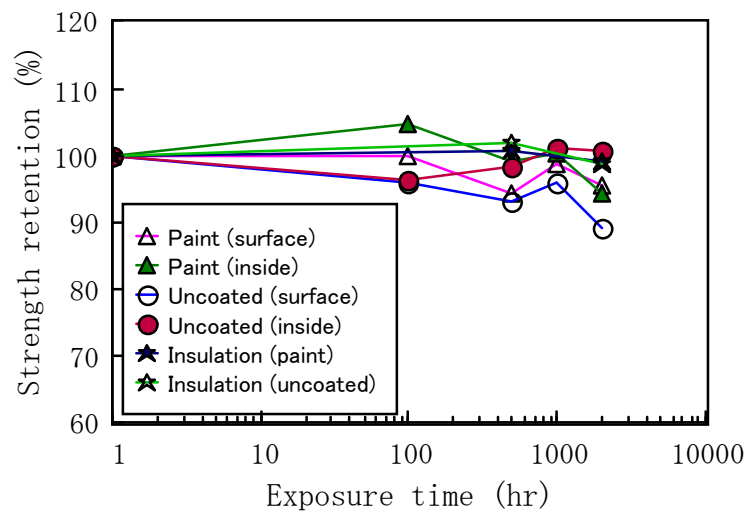


Fig. 5.9 Weather resistance degradation characteristics

5.3.3 Water absorption characteristics

We focused on the relatively large strength reduction caused by the deterioration due to water absorption as confirmed by the aforementioned environmental degradation characteristics and acquired the water absorption characteristics of the resin block (propulsion system: epoxy resin, levitation system: DCPD resin).

5.3.3.1 Test pieces (TP)

(1) Resin block

① Epoxy resin block

The resin block of the rectangular parallelepiped block simulating the cross-sectional shape of the propulsion coil was used for the test. The same specification as environmental deterioration test was used.

② DCPD Resin block

This is a rectangular parallelepiped resin block simulating the cross-sectional shape of the actual levitation coil having a main component DCPD used in the RIM system levitation and guidance coil described in Chapter 3. The specimen was manufactured that was equivalent to the actual coil molding condition and the glass content ratio. The cut surface of the block was coated with a sealant to prevent penetration of water from the glass end. The dimensions of the resin block were set to 95mm × 150mm × 50mm.

(2) Water absorption test piece

Similar to the manufacturing method described in the aforementioned resin block, the water absorption test for TP was prepared in regulation with the "Water absorption ratio of the plastic and the boiling water absorption ratio test method" JIS K 7209. The TP dimensions were set to 3(thickness) × 50 × 50 (mm). The cut surface of the DCPD was only sealed same as the resin block.

5.3.3.2 Test method

All specimens were dry-processed for 24 hours in a thermostat chamber controlled at 50 °C, and the initial weight of each specimen was measured in the precision scale. Each specimen was set in a stainless steel container filled with distilled water separated according to the types and conditions. The water absorption process was maintained at a predetermined temperature in a thermostat chamber. Furthermore, the samples were set in a constant temperature of 60°C and constant humidity chamber of 95% to perform water absorption process for reference. Then, the specimens were removed at predetermined time intervals, moisture was wiped off with clean gauze and their mass was measured. The water absorption ratio of each specimen was calculated and compared with the initial mass. The water absorption process conditions are shown in Table 5.2.

Table 5.2 Water absorption test conditions

Number of sample	Temperature conditions	Dipping time (hr)
EP block: 3	Normal	{ 0,24,48,100, 200,500,1000, 2000,5000
EP T.P.: 3	40°C	
DCPD block: 3	60°C	
DCPD T.P.: 3	80°C	
	Humidify at 60°C	

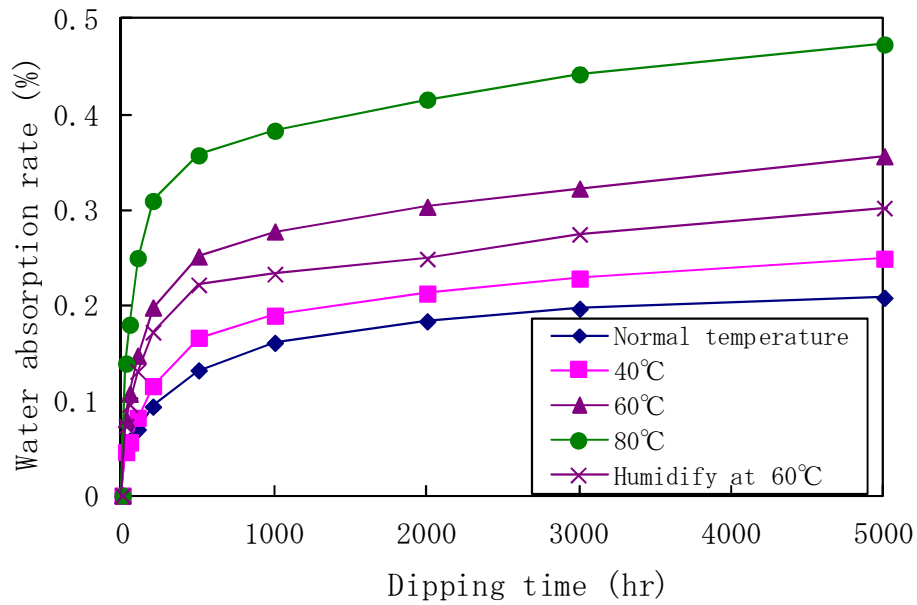
5.3.3.3 Test results

The measurement results of water absorption are shown in Fig. 5.10 for the epoxy resin, in Fig. 5.11 for the DCPD resin. From the measurement results, the following points were confirmed.

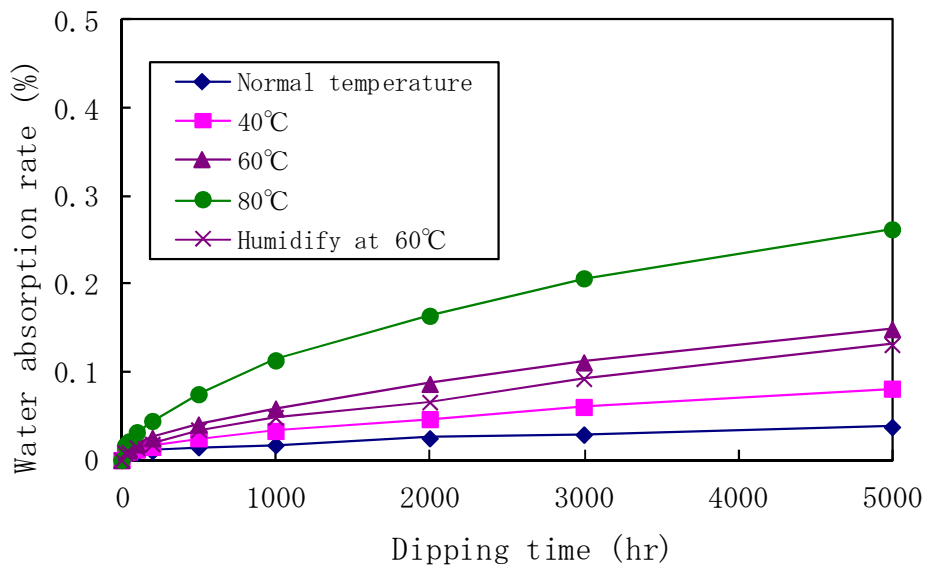
(1) In the comparison of the resin, DCPD shows a water absorption rate about an order of magnitude larger than that of the epoxy. This difference may be considered due to the void content ratio in the resin caused by the molding process (epoxy: vacuum casting, DCPD: normal pressure casting) and the configuration of the materials (presence or absence of glass fiber).

(2) Comparing the water immersion at 60°C and air humidification at the same temperature, almost the same water absorption ratio was confirmed. From this result, assuming the condensation in the tunnel in summer for example, it can be considered to be equivalent to a flooded condition.

(3) A comparison of the water absorption TP (JIS Standard) with the resin block shows higher value of TP for any resins. It is considered that the absorption of water into the resin is not uniform along the thickness direction, which is consistent with environmental degradation characteristics of 5.3.2.

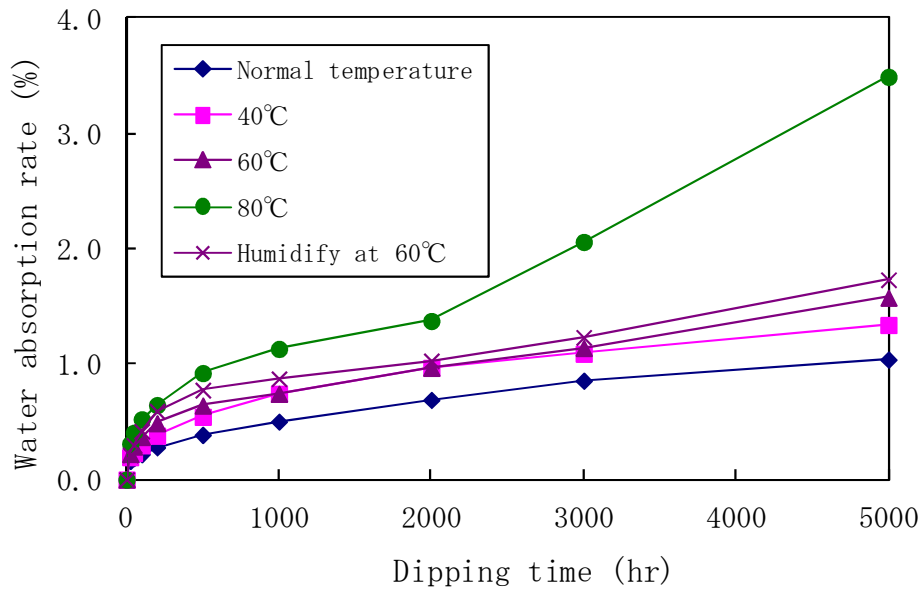


(a) Epoxy resin • JIS K 7209 Test piece

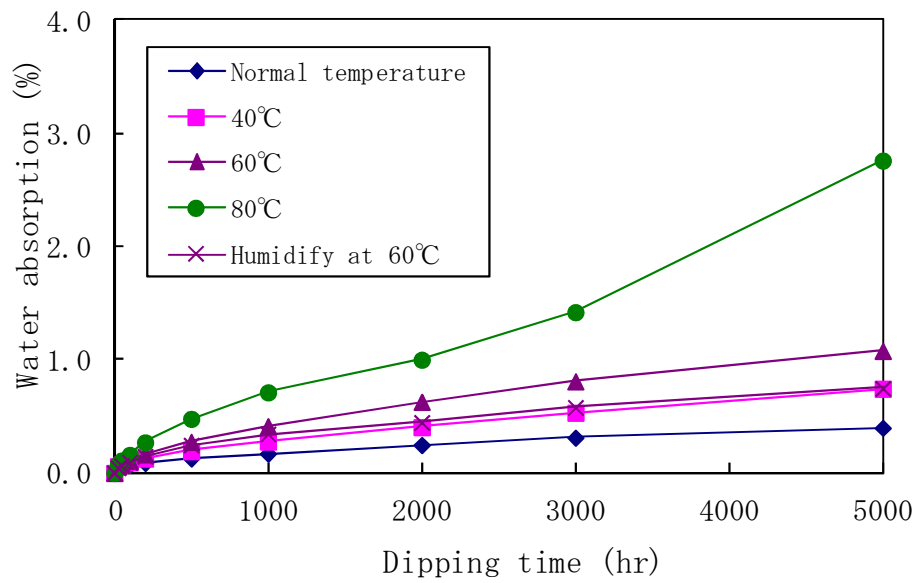


(b) Epoxy resin block

Fig. 5.10 Water absorption properties of the epoxy resin



(a) DCPD resin · JIS K 7209 Test piece



(b) DCPD resin block

Fig. 5.11 Water absorption properties of the DCPD resin

5.3.4 Verification of the reaction kinetics

Arrhenius equation: It is commonly understood that the relationship between the reaction temperature and the reaction rate of the material follows the rule of Arrhenius equation. The formula of the reaction rate related to the material degradation is:

$$\frac{dC}{dt} = Kf(C) \quad (5.1)$$

where C is characteristic values of the material, t is time, and K is the reaction rate constant. The relationship between the reaction rate constant and the temperature is given by the Arrhenius equation ⁽³⁻⁵⁾.

$$K = A \exp \left[-\frac{\Delta E}{RT} \right] \quad (5.2)$$

where A is frequency factor, ΔE is activation energy, R is gas constant, and T is absolute temperature. The following rate equation is obtained by equations (5.1) and (5.2).

$$\frac{dC}{dt} = A \exp \left[-\frac{\Delta E}{RT} \right] f(C) \quad (5.3)$$

Assuming a time elapse of t_e and the material properties changed from C_0 to C_e , integrate equation (5.3).

$$\int_{C_0}^{C_e} \frac{dC}{f(C)} = A \int_{t_0}^{t_e} \exp \left[-\frac{\Delta E}{RT} \right] dt \quad (5.4)$$

Put the $G(C)$ because left side of equation (5.4) is the function of C .

$$G(C_e) - G(C_0) = A \int_{t_0}^{t_e} \exp \left[-\frac{\Delta E}{RT} \right] dt \quad (5.5)$$

In equation (5.5), the value of the left-hand side also becomes constant by taking C_0 and C_e to be the constant. Set this value to $A\theta$.

$$A\theta = A \int_{t_0}^{t_e} \exp \left[-\frac{\Delta E}{RT} \right] dt \quad (5.6)$$

Solve equation (5.6) under the condition of a constant temperature. The following equation is obtained.

$$A\theta = A \exp \left[-\frac{\Delta E}{RT} \right] (t_e - t_0) \quad (5.7)$$

In equation (5.7), " $t_e - t_0$ " is the time required for initial characteristics reaching from C_0 to C_e . " $t_e - t_0$ " is replaced with t_L and take the logarithm of both sides. The following equation is obtained by clearing off the constant term.

$$\ln t_L = \ln \theta + \frac{\Delta E}{RT} \quad (5.8)$$

Set $\ln t_L = Y$, $\Delta E/R = a$, $1/T = X$ and $\ln \theta = b$ in equation (5.8).

$$Y = aX + b \quad (5.9)$$

Equation (5.9) shows that the logarithm of life and the reciprocal of temperature is a linear relationship. That is, it can predict the long-term life of the actual commercial operating temperature, which cannot be actually measured, by extrapolating short time and high temperature accelerated aging test results to a straight line.

The measurement results of water absorption ratio of the resin block obtained in Section 5.3.3 was verified as an example. The correlation between the time reaching the water absorption rate being constant and the temperature of the immersion water applying the aforementioned relationship was verified. Figure 5.12 shows the Arrhenius plot of the time and the temperature for each resin block from the initial state to the certain water absorption ratio (epoxy: 0.4%, DCPD: 0.04%). You can see that the relationship between the two parameters is almost in a straight line ⁽²⁾. These results can be effectively used as a basis for the accelerated aging test conditions for the endurance verification of the long-term outdoor used ground coils.

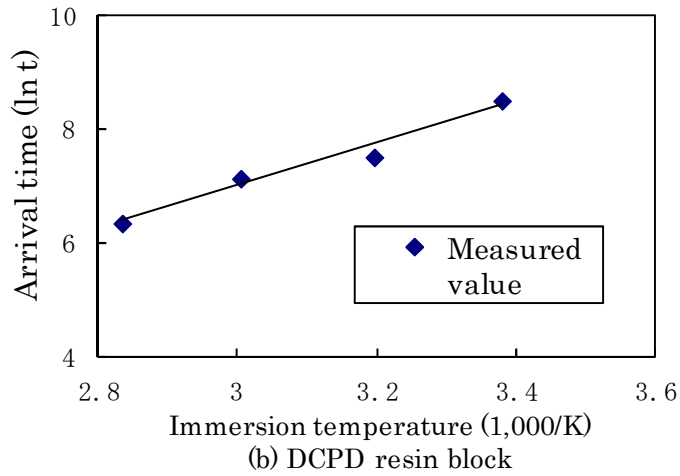
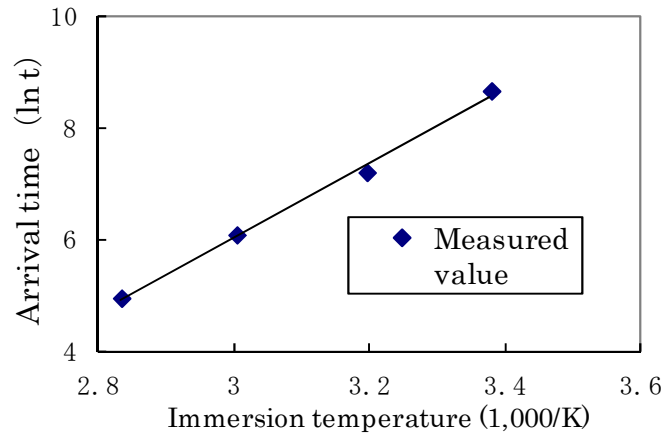


Fig. 5.12 Arrhenius plot of the time and the temperature

5.3.5 Evaluation of fatigue strength

As stated in "Operational environment of the ground coil" in Chapter 2, it is required to select materials taking into account the various operational environments and durability validation at the time of the design of the ground coils. In particular, it is necessary to consider the properties of the polymeric material for the durability evaluation of the molding resin material. The two popular fatigue strength evaluation methods of metal and other materials for the mechanical load superimposed various stresses were verified for the mold resin materials ⁽⁶⁾.

5.3.5.1 Durability evaluation using the fatigue limit diagram

The durability evaluation using the fatigue limit diagram typically used for metal materials was verified for the molding epoxy resin because the fluctuating and constant loads are simultaneously applied to the ground coil. The fatigue limit diagram of specific fatigue number of times is shown in Fig. 5.13. The straight line connecting the static breaking strength σ_b and the double swing fatigue strength σ_a is called the Goodman line. It is said that almost the metal materials shall be on this Goodman line. The Goodman line can be expressed by the following equation.

$$\sigma_a = \sigma_w \left(1 - \frac{\sigma_m}{\sigma_b}\right) \quad (5.10)$$

where σ_a is stress amplitude, σ_b is static breaking stress, σ_w is double swing fatigue strength and σ_m is mean stress.

(1) Test method

The flexural fatigue test was performed in accordance with "Fatigue test methods for flat plane flexural of the rigid plastic" JIS K 7119. The flexural fatigue strength of 10^7 times was obtained with a parameter of an average stress. Test conditions were as follows.

- ① Test equipment: hydraulic servo type material strength testing machine
- ② Test frequency: 30 Hz
- ③ Environmental temperature: 23°C
- ④ Stress ratio R: $R = \sigma_{\min} / \sigma_{\max} =$ minimum stress/maximum stress
 $R = -1, -0.4, 0, 0.4$

(2) Test results

As a result of the fatigue test, it was found that the average stress affected the fatigue strength significantly, and a decrease of double swing fatigue strength limit by 10 to 20% was obtained. The fatigue limit diagram of time intensity $N = 10^7$ based on the test results is shown in Fig. 5.14. The obtained fatigue limit diagram is located inside the Goodman line that connects the static breaking strength and the double swing fatigue strength,

and it is a downwardly convex curve.

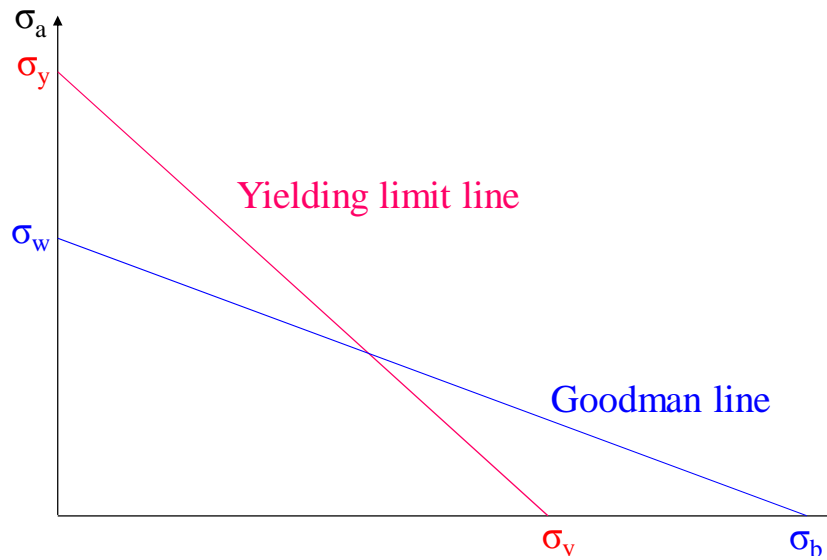


Fig. 5.13 General fatigue limit diagram

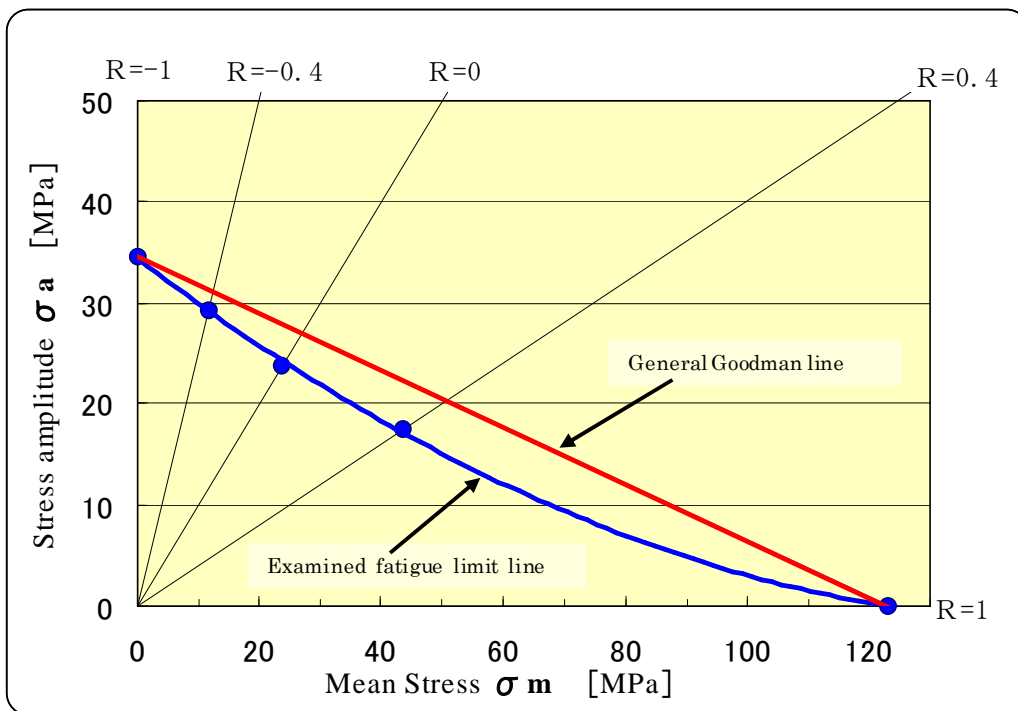


Fig. 5.14 Examined fatigue limit diagram

5.3.5.2 Durability evaluation using the cumulative damage rule

Fluctuating load affects the fatigue strength of the material. Because the repeated numbers or sizes of load factors of the ground coils are not uniform, it is necessary to consider the influence on the life span for complex loads. There is a cumulative damage law to evaluate the fatigue damage of the material not depending on the constant load. In this section, this law was verified whether this general approach for metals and other materials could be applied for life span evaluation of the mold resin material.

(1) Cumulative damage law

If each repetition number of times to the fatigue break is set to $N_1, N_2, \dots,$ and N_i respectively, the corresponding stress amplitude can be expressed by $\sigma_1, \sigma_2, \dots,$ and σ_i . Their relationship can be illustrated in Fig. 5.15 in case of $i = 2$. It was assumed that the fatigue damage accumulated linearly with the number of repetitions, and each stress amplitude was repeated n_1, n_2, \dots and n_i times respectively. n_i refers to the repeated numbers of stress σ_i . N_i refers to the number of times to break the specimen where the stress σ_i was repeated independently. If σ_1 is repeated independently, it will fail the fatigue life span when n_1 becomes N_1 . Because the fatigue damage can be expressed by the ratio of the number of repetition, the fatigue damage of each stress level can be expressed as $n_1/N_1, n_2/N_2, \dots$ and n_i/N_i . The cumulative damage rule is defined by the sum of the ratio of the number of repeated fatigue damages at any particular time. The sum of these fatigue damage is called the cumulative fatigue damage value D . When this value reaches "1", it means that the fatigue life span has arrived. This relationship can be expressed by the equation below.

$$D = \sum \frac{n_i}{N_i} = 1 \quad (5.11)$$

where n_i is number of repetitions of stress σ_i

N_i is number of time to break where the stress σ_i is repeated independently

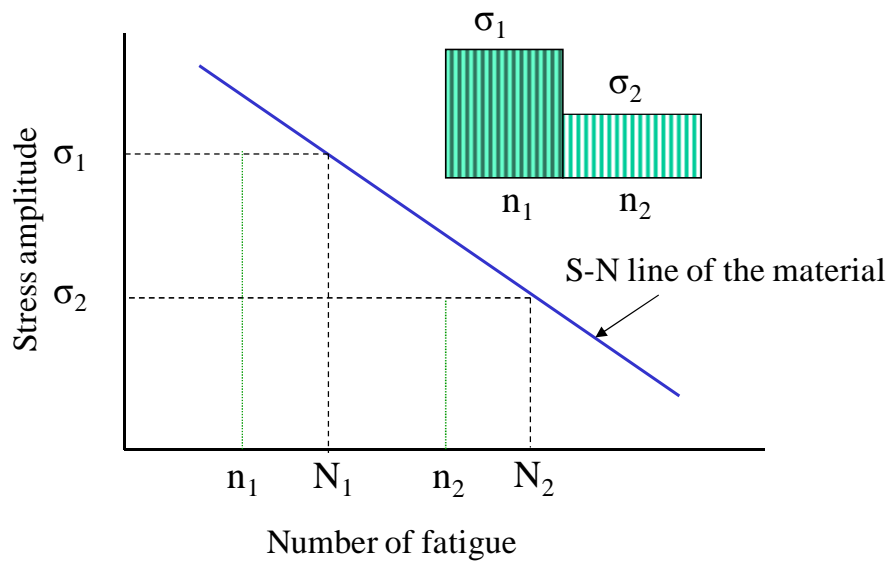


Fig. 5.15 The concept of cumulative damage

(2) Test method

The fatigue strength by the two-stage stress was measured in accordance with "Fatigue test methods for flat plane flexural of the rigid plastic" JIS K 7119. First, the S-N diagram was created in normal double swing. Then, the two-stage fluctuating stress value was created based on this result. In the two-stage fluctuating stress test, the stress increasing condition from low to high stress and the stress decreasing condition from high to low stress were performed. Thus, the rupture life of the two-stage fluctuating stress load was compared with the life expectancy from the cumulative damage law.

(3) Test results

The high stress σ_H was set to 47MPa (about 70,000 times the average breaking number) and the low stress σ_L was set to 40MPa (about 1.7 million times the average breaking number) as the two-stage stress value from the acquired S-N diagram.

① Stress ascending test

After the predetermined number of fatigue at low stress was applied, the number of times to break the specimen at high stress was measured. The test results obtained when the cumulative cycle ratio of (n_L/N_L) varied between 0.02 and 0.4 is shown in Fig. 5.16. From the test results, the

cumulative fatigue damage value D was less than 1. It showed a short life expectancy.

② Stress descending test

Similarly, the number of breaks was measured by applying the two-stage stress from high stress to low stress. The test results are shown in Fig. 5.17 obtained by varying the cumulative cycle ratio (n_H/N_H) between 0.1 and 0.7. From the test results, the cumulative fatigue damage value D was less than 1 except for the case of 0.14 of n_H/N_H . It showed a short life expectancy. From the aforementioned test results, the life evaluation method based on the cumulative damage rule may not be satisfied in the mold resin material.

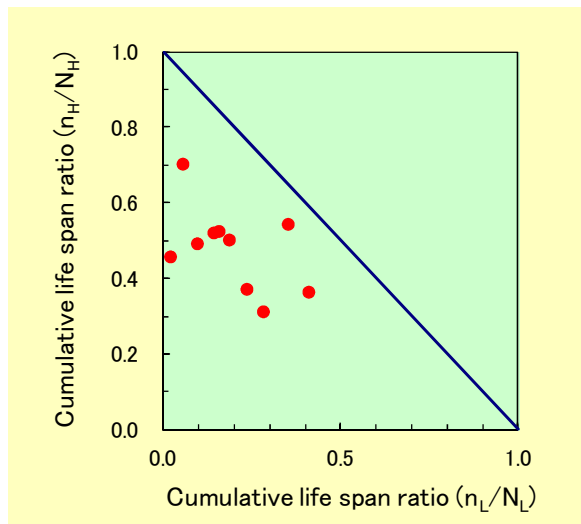


Fig. 5.16 Stress ascending test result

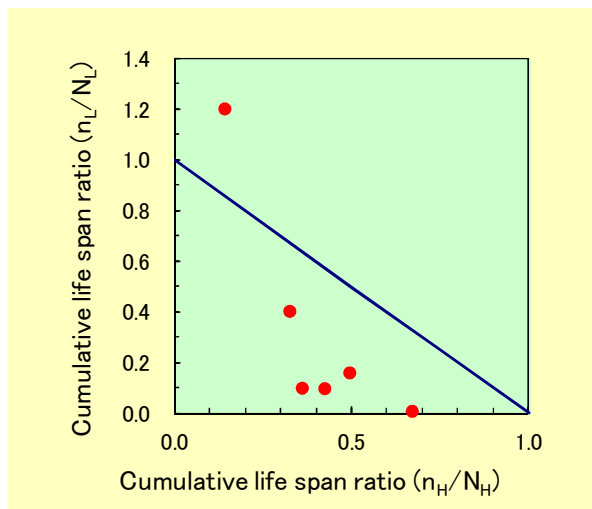


Fig. 5.17 Stress descending test result

5.4 Durability verification of actual coil

The durability verification of actual coil was performed by applying the accelerated aging load that was equivalent to the life of the commercial operation. The result was determined by the "soundness evaluation test" that estimated whether the coil maintained the specified functions. It is desirable to apply the combined loads simultaneously to the specimen at the same time. However, the combined degradation was simulated by repeatedly loading each parameter sequentially due to the limitations of the test equipment. Therefore, the development of effective test equipment itself has become important in order to systematize the verification method for the endurance verification of the coil in actual use.

5.4.1 Dynamic durability verification

As the ground coils are vibrated continuously by the EM force of the vehicle passing, it is significantly important to verify the dynamic resistance against the vibration loads to ensure the reliability of the entire system.

5.4.1.1 Development of the EM vibration test equipment for ground coil

The EM vibration test equipment for ground coils that can simulate the actual traveling at a stationary was developed (Fig. 5.18). The ground coils were installed by opposing the SCM and an arbitrary current was supplied from the inverter power supply to simulate the actual traveling conditions. Unlike the conventional mechanical loading test apparatus, it had a unique feature where the EM force could be directly applied to the winding conductors of the coil. It is possible to vibrate the coil which is almost equivalent to the actual traveling with the load distribution and excitation frequency.

In addition, another important idea has been incorporated in this test equipment. Because the traveling vehicle transfers the synchronized moving magnetic field created by the ground coils like a surfer riding on the waves, the moving magnetic field seems stationary from the traveling vehicle, and

the vibration created to the SCM will be quite small. However, since the SCM on the vehicle is also fixed in the stationary test, varying magnetic field (fundamental wave component) created by the ground coil becomes by design an unexpected excessive vibration source for the SCM. In order to avoid this effect, the aluminum plate electrically shields the ground coil shown in the configuration diagram. As shown in Figure 5.19, strong DC magnetic field penetrates through the ground coils side from the SCM. However, varying magnetic field created by the ground coils is shielded by the eddy current generated in the plate and it does not reach the SCM side. That is, this innovative filter of the shielding plate prevents excessive vibration to the SCM and enables the test over a long period of time.

The automatic measurement monitoring system was developed to incorporate this test device based on the data acquisition from sensors placed on each part of the specimen. The functions included the inverter power supply control, measurement data acquisition and state monitoring ⁽⁷⁾. The same monitoring functions were also incorporated to the superconducting magnet refrigerator, and it enabled the long-term durability test with unmanned operation.

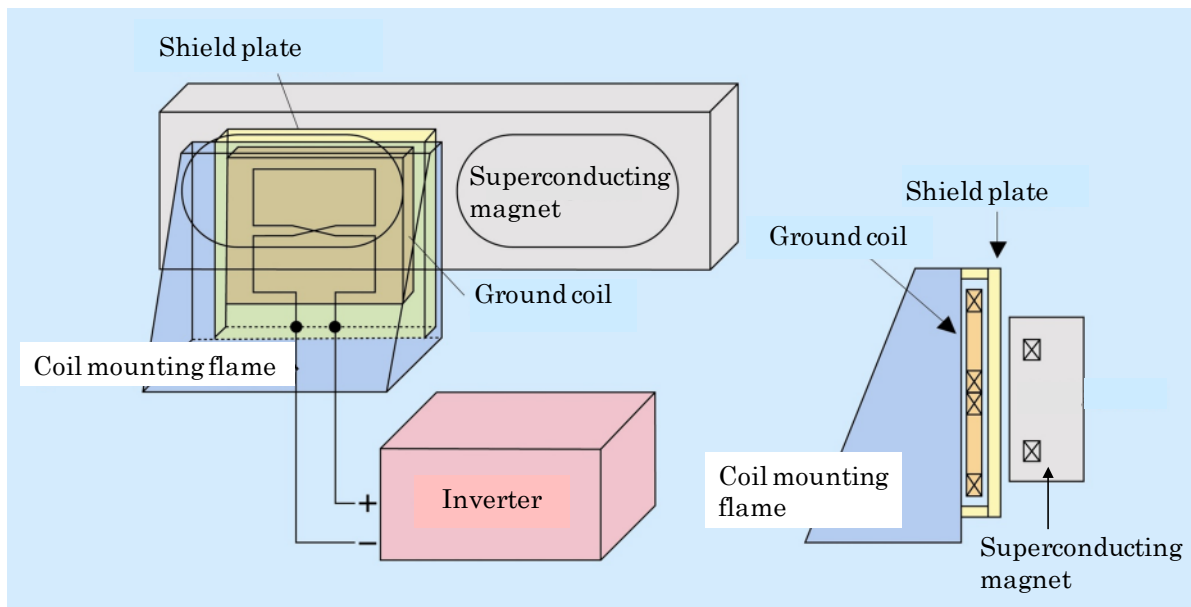


Fig. 5.18 Configuration of the EM vibration test equipment

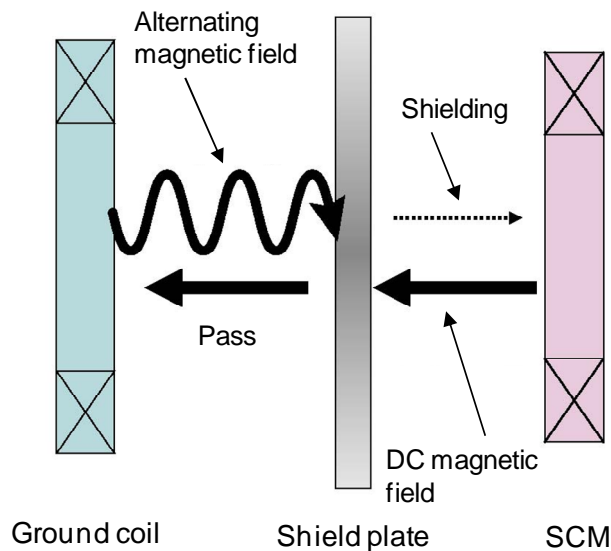


Fig. 5.19 Effect of shield plate

5.4.1.2 Dynamic durability evaluation procedure

This test equipment is capable of simulating the actual traveling up to the high-speed range and it is possible to acquire the dynamic characteristics of the fastening and cable connection parts of the ground coil that were difficult to acquire by the conventional test equipment. This equipment can be effectively used for the durability evaluation measures assuming a long-term operation. An example of the evaluation procedure for dynamic durability test of the ground coil is shown in Fig. 5.20. For various characteristic measurement in step (2), 3 component forces using a load converter (longitudinal, lateral, vertical), the frequency characteristics of the vibration acceleration, energized condition of the temperature rise characteristics of the ground coil, vibration acceleration for applied vibration, and generated stresses were measured as data for determining the vibration excitation conditions for long-term test. The validity of the design was confirmed in advance. Fig. 5.21 shows the example of the characteristics obtained by this test equipment. It shows the frequency characteristic of the vibration acceleration of the lower propulsion coil obtained by sweeping the inverter power supply vibration frequency continuously. As a result, the degree of

vibration or the presence or absence of resonance point in the operating speed range can be estimated to facilitate the feedback to the improved design ⁽⁸⁾.

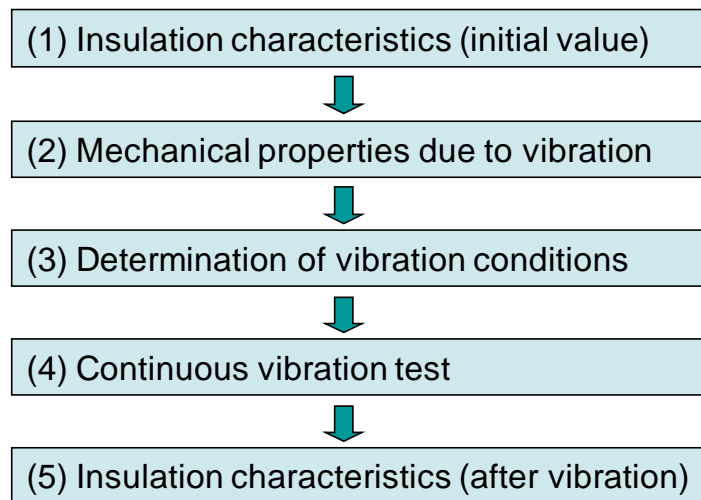


Fig. 5.20 Evaluation procedure of dynamic durability

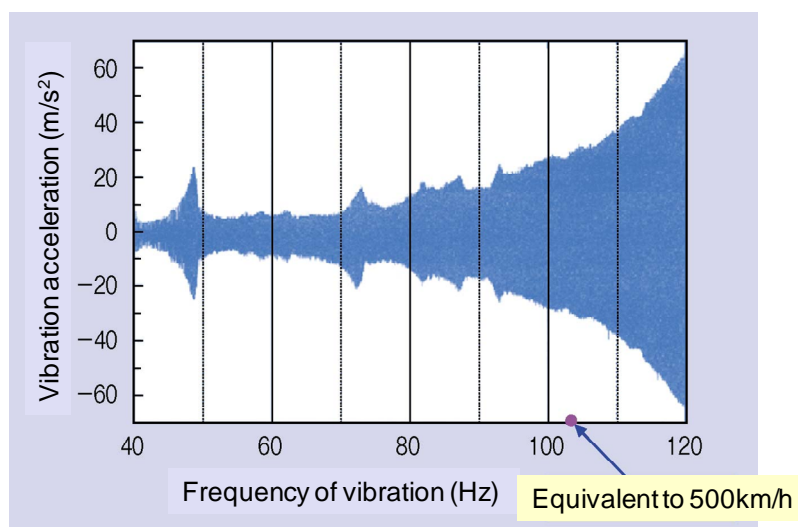


Fig. 5.21 Frequency characteristic example of vibration acceleration

5.4.1.3 Dynamic durability verification for the cable connected part

The dynamic reliability by the EM vibration environment to the cable connection and bolt fastening portions of the propulsion ground coils is concerned. Therefore, we devised a mechanical vibration equipment for estimating dynamic durability of the cable joint part, simulating the EM vibration of the vehicle when it was passing through ⁽⁹⁾.

(1) Overview of dynamic evaluation test equipment for cable connection

This test device intended for cable connections of the ground coils evaluated the dynamic properties and dynamic durability of the corresponding connection portions (Fig. 5.22). The bushing corresponding to the coil side was fixed and the specified part of the cable was optionally displaced and the test unit was forced vibrated by the specified frequency.

(2) Vibration conditions for the dynamic durability test

The dynamic characteristics of the PLG coil cable connection unit were previously acquired as parameters of the displacement and frequency at the forced vibration application. And the vibration conditions were set for the dynamic durability test (Table 5.3). The vibration acceleration of the evaluation part was set to equal the expected maximum value of the actual vehicle traveling as the test conditions.

(3) Test result

The pressure sensors were mounted on the surface of the insulator side of the cable connection portion to investigate the surface pressure changes while applying the vibration for the durability test. As a result, no significant change from the initial surface pressure (380 to 420kPa) was confirmed even after the forced vibration of five million times and normal spring mechanism of the connecting portion was confirmed (Fig. 5.23). After completion of vibration, the connection part was removed from the bushing, and the contacting surfaces were investigated visually. As a result, no abnormality such as local deformation was found on the connection surfaces and the soundness was confirmed.

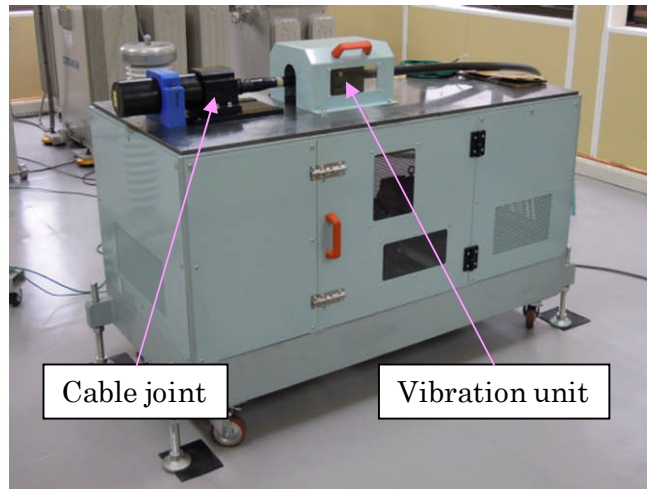


Fig. 5.22 Dynamic evaluation test equipment for cable joint

Table 5.3 Vibration conditions of dynamic durability test

Items	Test condition
Vibrating portion	300mm from the fixed portion
Amplitude	$\pm 3\text{mm}$
Frequency	30Hz
Repeat count	5 million times
Form of vibration	5 hour continuous per day
Test temperature	Normal temperature (23°C)

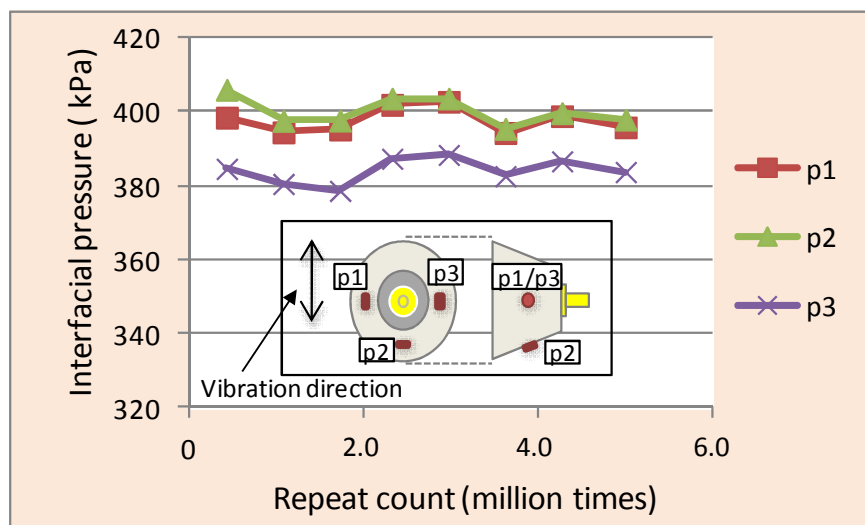


Fig. 5.23 Changes of interfacial pressure due to mechanical vibration

5.4.2 Accelerated weathering verification

The mold resin material used for the ground coil reduces its strength due to hydrolysis by ultraviolet rays or thermal energy and oxidation degradation in the presence of oxygen and moisture. Therefore, the accelerated weathering test under the actual operating conditions taking into account the environmental degradation properties of the material level is important in order to verify the validity of the coil design.

5.4.2.1 Development of ultra-accelerated weathering test equipment

The ultra-accelerated weather durability test equipment (Fig. 5.24) was developed in order to quickly evaluate weather durability of the ground coil to be used for long-term in outdoor environment ⁽¹⁰⁾. This is a large temperature and humidity chamber with ultraviolet (UV) irradiation and watering functions. The program controlled loads of temperature, humidity, water spraying (rainfall), UV can be independently or in combination be applied to the specimens. The main specification of the test equipment is shown in Table 5.4. A metal halide lamp was selected as the ultraviolet irradiation light source which enabled super-accelerated deterioration. This light source is capable of light emission efficiency of the ultraviolet region while keeping the compatibility with the combination of the wavelength cut filter to increase the magnification of the accelerated UV degradation. Because the radiation of heat ray (infrared to visible light) is small in spite of strong ultraviolet radiation, it is a feature where the light does not give unnecessary heat load to the specimen and the tank.

5.4.2.2 Standardization of promotion magnification

Prior to the weathering study for the actual coil, the accelerated weathering test of the material level was performed for a comparative evaluation with the outdoor exposed weathering test results of the same material to determine the standardization of the magnification of this test equipment. The evaluation items were set to the three-point flexural

strength based on the "Flexural test method of rigid plastic" JIS k 7203. As shown in Figure 5.25, the promotion factor of the resin determined by the standardization of the strength decrease rate was about 100 times. The expected promotion was confirmed.



Fig. 5.24 Appearance of ultra-accelerated weathering test equipment for ground coil

Table 5.4 Main specifications of ultra-accelerated weathering test equipment for ground coil

Inner dimension	W:2500mm × D:1800mm × H:1700mm
Temperature range	-40°C ~ 90°C
Humidity range	20 % ~ 95 % (4°C or more)
Watering ability	450 liters per hour (100mm per hour)
UV light source	Metal halide lamp (12kW × 4)
UV intensity	400W/m ² (irradiation distance: 600mm)

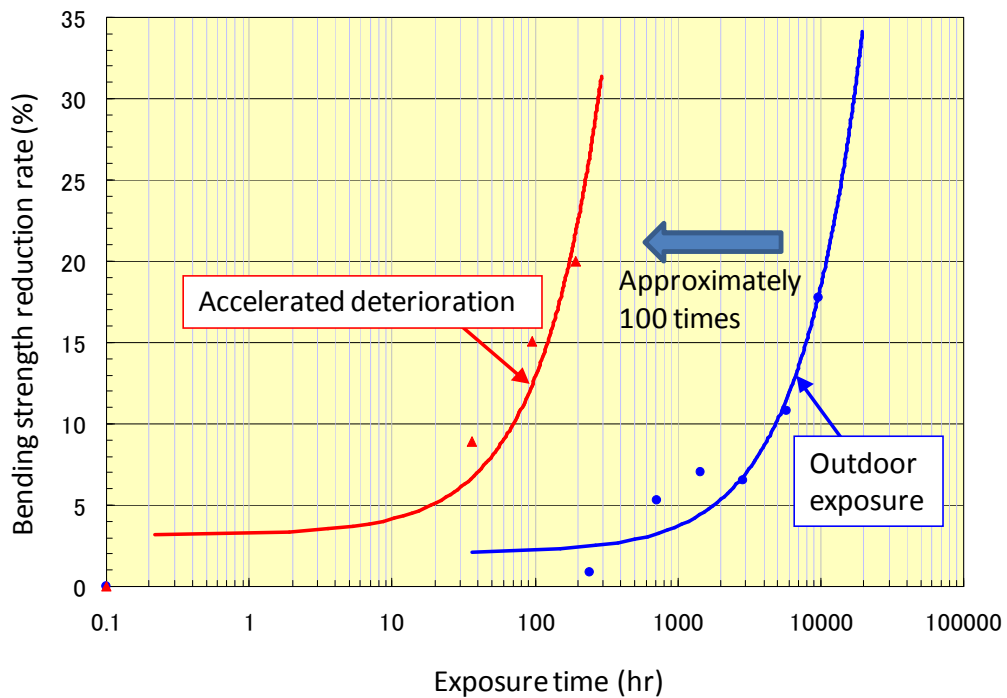


Fig. 5.25 Strength reduction characteristics by weathering test

5.4.2.3 Accelerated weathering verification of actual coil

The soundness of the actual ground coils was evaluated basically from the electrical characteristic test results performed before and after the weathering test the same as the evaluation procedure shown in Fig. 5.15. It is important for the test to keep the ultraviolet intensity constant that primarily influences the accelerated deterioration. Therefore, this test measured the uniformity and the intensity distribution in the test coil arrangement portion to determine the weather resistance test conditions based on the accelerator magnifications standardization set by the aforementioned paragraph. Also, the resin test pieces were cut out from the actual coil as needed to evaluate the flexural strength characteristics and the mechanical soundness. Figure 5.26 shows the situation of the accelerated weathering test including the cable connection targeting PLG coil. From the electrical characteristics before and after the weathering test, the soundness of the actual coil equivalent to the life of commercial line service was

confirmed.

5.4.3 Thermal durability verification

The thermal stress due to seasonal temperature alteration and switching of power supply during operation is a significant load for the ground coil of long-term outdoor use. Particularly the propulsion coil requires insulation stability that accounts for thermal stress. In this verification, the long-term outdoor power supply test for the propulsion coil and the cable connected parts as a part of the thermal durability verification was performed ⁽¹¹⁾. As stated in Section 4.2.3, this study was in compliance with the long-term power supply test in Paragraph 5, Development Test, "High voltage test method of the connection part and special high voltage (11kV to 275kV) with cross-linked polyethylene cable", JEC-3408. This heat cycle experiment was performed for about six months, and while applying a total load equivalent to the total acceleration voltage of actual years, the power was supplied on for 18 hours and off for 6 hours per day, simulating an actual commercial operation. The soundness evaluation was determined by the appearance and the aging of the insulating properties at before, middle of the stage and after the durability test. The long-term outdoor power supply test situation targeting the PLG coil is shown in Fig. 5.27. The characteristic degradation due to power supplying load was not observed for the aging of the insulation characteristics. The thermal durability of the PLG coil including the cable connection has been confirmed.



Fig. 5.26 Accelerated weathering test situation of PLG coil



Fig. 5.27 External view of thermal durability test

5.5 Summary

Durability verification of the ground coils which are forced to be operated in a severe environment, has become an important issue in ensuring the reliability of the Maglev entire system. Therefore, at the time of endurance verification, it is important to evaluate appropriately by understanding the characteristics of the materials and structures of the ground coils while considering appropriate verification measures equivalent to the actual on-site operation.

In endurance verification of ground coils, unique verification procedures have been performed for the material property tests, actual operation study and the actual coil verification test as a basic configuration. It is important to carry out the investigations and experiments while reflecting on the obtained results from both.

The environmental degradation characteristic of the molding epoxy resin for long-term outdoor use was acquired. From the test results, a significant decrease in strength due to water absorption and alkali was observed and the development of the degradation was not uniform along the thickness direction, and was limited to the surface layer. Furthermore, the resin block simulating the cross-sectional shape of the ground coil was also created and the water absorption characteristic with a parameter of the immersion temperature was acquired. Then, the reaction kinetics was verified by the time to reach to the certain water absorption ratio and the immersion temperature based on the water absorption characteristics. As a result, it was confirmed that the correlation between the two parameters followed approximately the Arrhenius law. And it was confirmed that the reaction kinetics was effective in setting the accelerated aging conditions of the actual coils. In addition, the fatigue strength evaluation method was also verified for the mold resin material that took into account the operational environment of the ground coils. As a result, the conventional fatigue limit diagram or the cumulative damage rule used for metal materials could not be applied to the evaluation method and a tendency of short life of the durability was confirmed.

The verification of dynamic durability in consideration of the actual

operational environments of the ground coil was essential. Therefore, the ground coil EM vibration equipment simulating the real traveling stationary was developed. It was confirmed that the dynamic durability of the coil fastening and cable connection portions could be verified effectively. In addition, we have developed an ultra-promotion type ground coil weathering test equipment intended to measure long-term outdoor use. It was possible to facilitate light source magnification of about 100 times that of the outdoor exposure without giving unnecessary thermal load by combining a special filter with the metal halide lamp having an excellent luminous efficiency within the ultraviolet region. It was expected from the test results of the actual coil that the weather resistance of the equivalent commercial line service life could be verified in a relatively short period of time. In addition, as a thermal durability verification, the long-term outdoor power supply test which was applied to the development test for the cable connection part was applied to the heat cycle load for the propulsion coil. This verification test assuming an electrical load of the actual commercial operation is considered as an effective verification measure considering the screening of the abnormal insulation described in the next chapter.

The need for durability confirmation is increasing along with the current development of various low-cost, high-performance ground coils for practical use. Establishment of the verification method according to the purpose and application is an urgent requirement. For this purpose, an accurate capture of the deteriorated form of the ground coil and critical strength is a point of durability verification, and accumulation of test data is important.

Chapter 6 Effective Insulation Diagnostic Technique for the Ground Coil

6.1 Introduction

Because a huge number of ground coils are used in Maglev system, a reduction in ground coil cost while keeping high reliability is required. The propulsion coil especially needs the high insulation stability as high-voltage equipment. Because the ground coil, which is made with the resin-molded winding, does not have a core in the structure, the ground coil must be exposed to the electromagnetic force directly. As a result, there is a possibility that minute defects in the molded resin of the ground coil may develop. Therefore, the development of effective insulation diagnosis techniques that can evaluate the propulsion system coils laid to the actual site without affecting the commercial operation will be expected.

6.2 Insulation abnormality that should be considered in the propulsion ground coils

Because the propulsion ground coils require the insulating function as special high-voltage equipment, inspection at shipment for all coils is mandated by the coil manufacturers and to confirm that there are no abnormalities in the insulation performance. Therefore, no abnormalities in the coils and cables at the time of shipment and stable operation are expected. However, it is necessary to take into account the temperature rise due to the power supply during operation, EM vibration caused by vehicles passing by, the material deterioration due to long-term outdoor use and other elements in addition to the on-site improper installation of the coils and cables. The actual operation will not always be stable. In the extreme case, if a product passes the shipping inspection but has a potential defect factor, this defect factor may become apparent when a continuous load is applied during operation. The insulation abnormalities ^(1, 2) to be considered in the operation of the propulsion ground coils are described below.

6.2.1 Voids and foreign substances

While a winding coil is molded with resin, voids and foreign substances within the compound ingredients need to be considered. The electric field concentrates in the voids and at foreign substances while high voltage is applied to the coil, which results in occurrence of PD. Although the coil is inspected, there is a possibility that PD cannot be observed due to some factors, e.g. the size of the voids and foreign substances, atmospheric pressure, boundary condition between the coil and resin.

6.2.2 Separation of conductor from molded resin

It is presumed that the close adhesion state is maintained between the winding coil and molded resin in the propulsion ground coil. However, it is

possible for separation to occur between the winding coil and molded resin due to repeated EM force when the trains pass by. Space is formed by the separation, where PD occurs.

6.2.3 Exfoliation of shield coating

The electric conductive shield coating of the propulsion ground coils is exposed to the EM vibration for an extended period of time. This might be the cause of local exfoliation of the shield coating, which leads to the occurrence of PD.

6.2.4 Improper on-site installation

Improper on-site installation of coils and cables might be the cause of PD occurrence. Figure 6.1 shows an example of a possible improper on-site installation for connecting the high voltage power supply cable to the propulsion ground coil. The foreign substance caught between the insulation surfaces causes electric field concentration, which leads to the occurrence of PD.

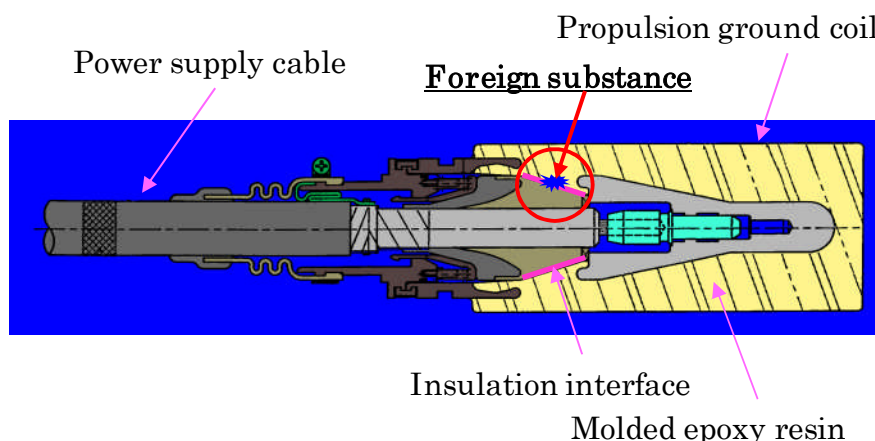


Fig. 6.1 An example of improper on-site installation for connecting the power supply cable to the propulsion ground coil

6.3 Insulation properties of the defect simulated ground coils

The defect simulated evaluation for the coil body and the cable connections concerning the insulation diagnosis of propulsion ground coil is an important step for development. We investigated insulation characteristics and aging variation of the ground coils caused by the effects of various defects mentioned above.

6.3.1 Exfoliation of shield

The defect influence on the long-term insulation performance of the coil was investigated targeting the case of the partial exfoliation of the surface shielding layer caused by mechanical stress ⁽³⁾.

6.3.1.1 Specimen

Specimens used in this study were a single-layer propulsion coil integrally molded with an epoxy resin. The coils of the partially peeled surface shielding layer were prepared as the specimen (Fig. 6.2) in addition to the integrity coil. Three defect areas were selected: 10mm x 10mm, 30mm x 30mm and 50mm x 50mm.

6.3.1.2 Electric field distribution of the defect areas

The results of the electric field distribution analysis of the test coils indicated a tendency of the electric field to concentrate at the edges of the shielding layer and coil conductor. The electric field strength where the electric field is concentrated was estimated about four to five times the integrity coil for the end surfaces and approximately two times the uniform distribution portion of the conductor corner. An example of the analysis of equipotential distribution simulating the coil model is shown in Fig. 6.3.

6.3.1.3 Test procedure

The power frequency voltage effective value of 22kV was applied both to the conductor and the shielding layer of each specimen consecutively through the test cable. ※6.1 The insulation properties of each specimen ($\tan \delta$ and the PD characteristics) were chronologically measured (initial, 200, 500, 1000, 2000 and 5000 hours). After the characteristics of the 5000 hours were acquired, the defect parts were repaired with conductive coating and the breakdown value against the ground was measured.

※6.1: The electric field strength of the integrity coil was set to approximately 10% of the material destructive value.

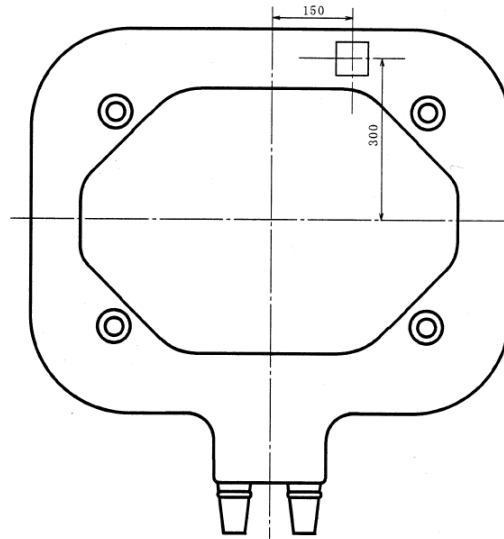


Fig. 6.2 Defect coil simulated exfoliation of shield layer

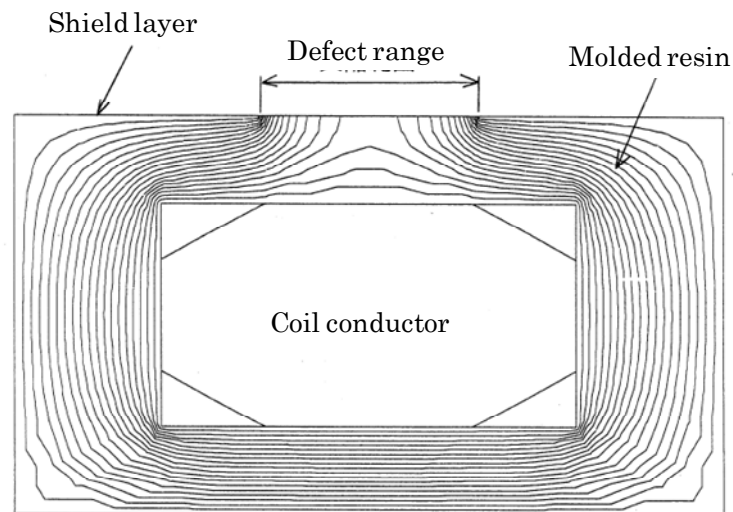


Fig. 6.3 Equipotential distribution of the coil cross section

6.3.1.4 Test results and discussion

(1) Characteristics of $\tan \delta$

The $\tan \delta$ characteristics at the applied voltage of AC20kV for each measurement period is shown in Fig. 6.4. The $\tan \delta$ value tends to increase slightly along with the power supplied period. However, it was observed that some of the specimens with the test cable were affected by the weather conditions. It may be considered that the specimen absorbed moisture temporarily and the dielectric loss increased.

(2) Partial discharge characteristics

The PD characteristics at the applied voltage of AC20kV for each measurement period is shown in Fig. 6.5. There was a tendency of the discharge quantity increase in proportion to the defect area. However, this trend was lost along with the power applied time. It can be considered that the air discharge due to electric field concentration occurring at the edge surface of the defect part and the carbonized layer was formed.

(3) AC breakdown characteristics

After the long-term voltage application, the AC breakdown test was performed on all specimens (if defects were apparent, the defective parts of each specimen were repaired). As a result, there was no significant difference between the specimens including the apparent non-degradation coils. The destructive value was about 80 to 100kV.

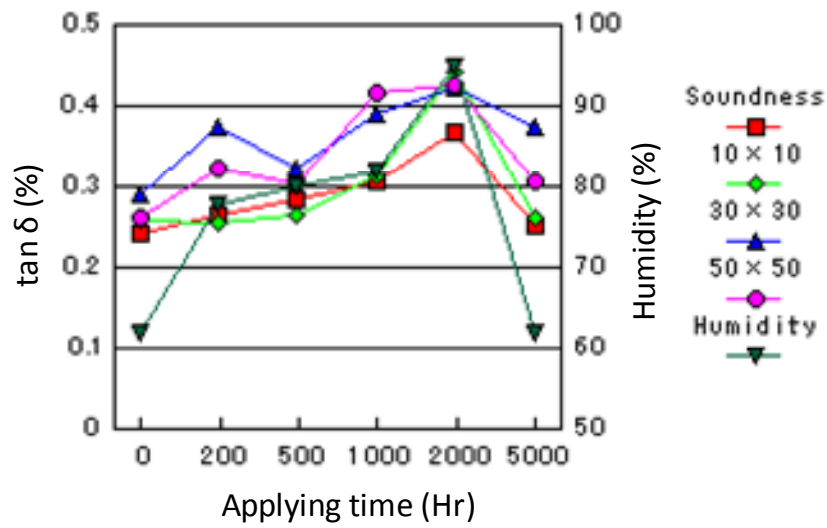


Fig. 6.4 Transition of $\tan \delta$ characteristics

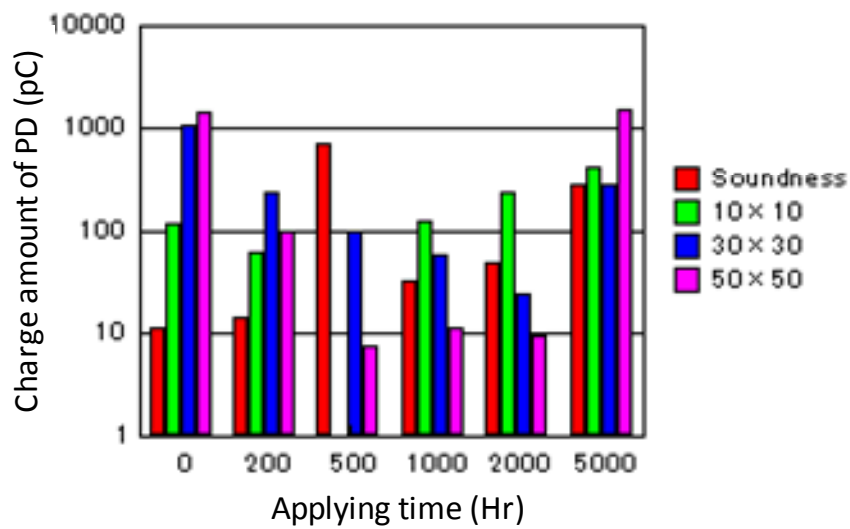


Fig. 6.5 Transition of PD characteristics

6.3.2 Construction defect at cable connection

The defects of the ground coil and cable connecting parts due to improper on-site construction was simulated to examine the correlation between the PD characteristics and the expected abnormalities ⁽⁴⁾.

6.3.2.1 Specimens

The connection specimens of two types were tested.

(1) L-shape connection

The EP rubber outer cone was configured to the cable side to ensure the surface pressure of the interface by the elasticity of the rubber.

(2) PLG coil connection

The silicon rubber inner cone was configured to the cable side to stabilize the contact pressure surface by the spring structure.

6.3.2.2 Simulated abnormal conditions of the interface

The following abnormalities were set to the connecting interface as mentioned above (Fig. 6.6) and performed the connection work.

(1) Linear foreign substance insertion

① hair ($\varphi 0.08$), ② wire ($\varphi 0.25$) or ③ metal rod ($\varphi 0.4$) of length 32mm for each was installed in the longitudinal direction of the surface.

(2) Spherical foreign substance insertion

The chrome steel of ① $\varphi 0.5\text{mm}$, ② $\varphi 1.0\text{mm}$ or ③ $\varphi 2.0\text{mm}$ was set to the center of the interface of each specimen.

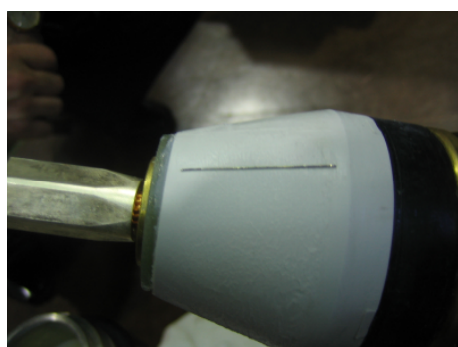
(3) Without lubrication insulating grease

Wipe off the lubrication insulation grease completely from the interface to set to a non-grease state.

6.3.2.3 Partial discharge characteristics

The power frequency voltage was applied to the connected specimens to measure the PD characteristics. As a result, the PD was observed at the L-shape connector when the linear object was inserted. The PD increased

according to the increase of the diameter of the foreign substance (Fig. 6.8). In addition, it was confirmed that the PLG coil connecting part with a high interfacial surface pressure by the spring structure was less susceptible to contamination.



(Linear foreign substance, $\varphi 0.4 \times 32\text{mm}$)



(Spherical foreign substance, $\varphi 2.0\text{mm}$)

Fig. 6.6 External view of interfacial abnormality

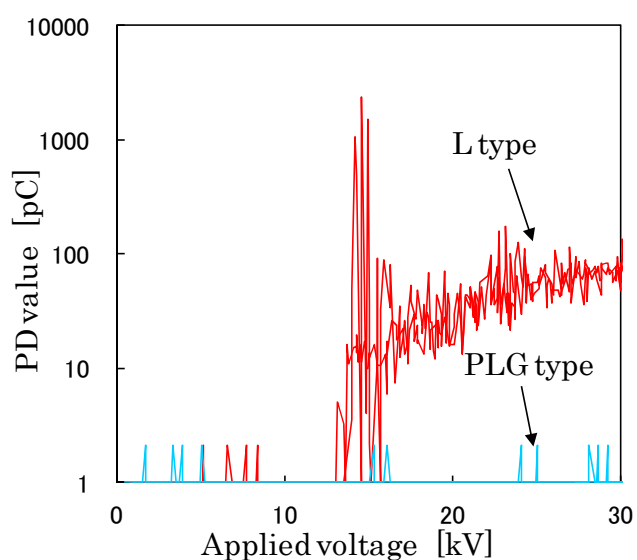


Fig. 6.7 PD characteristic of the cable connection part with defect (linear foreign substance $\varphi 0.4 \times 32\text{mm}$)

6.3.3 Internal defect by the simulated void

The residual void in the resin molding of the ground coil was set as the internal defects, and the defect simulated coil was created to measure the PD characteristics.

6.3.3.1 Creation of the internal defect simulated coil

We simulated an internal defect ⁽⁵⁾ by burying an artificial void in the PLG coil, where PD occurred when high voltage was applied to the coil. Figure 6.8 shows the external view of the defect point. We made the artificial void as follows: (1) the artificial void of which diameter was approximately 0.5mm was made in a small piece of resin, (2) the piece was set in the spacer that supports the winding coil, and (3) the spacer was buried to the specific part in the mold while the winding coil was molded.

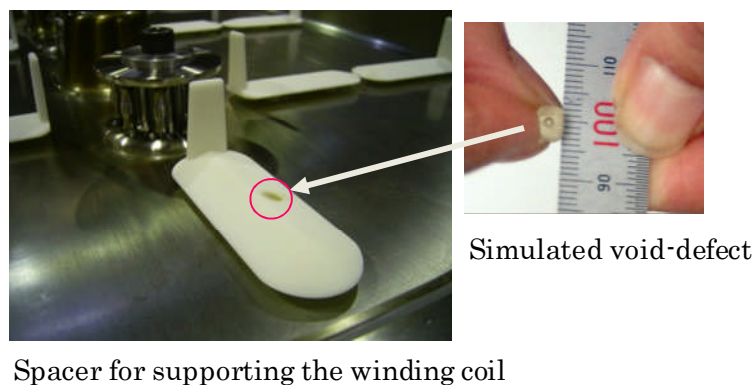
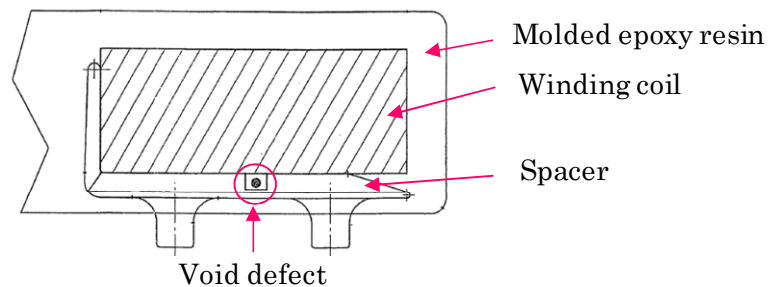


Fig. 6.8 External view of the defect point

6.3.3.2 Electric field distribution of the defect point

An electric field with the void-defect in the molded resin of the ground coil was analyzed. In the analysis, it was presumed that the electric field is equally distributed in the molded resin between the coil conductor and the external shield layer. As a result, it was estimated that the electric field concentration at the void is two times larger than that at the other molded resin area. Figure 6.9 shows an example of analyzing the equipotential distribution in the coil cross section.

6.3.3.3 Partial discharge characteristics of the test coil

We connected the test cable to the sample coil and applied the power-frequency voltage between the coil conductor and the shield layer, and measured the PD characteristic. Figure 6.10 shows the test circuit used for measurement of PD. The discharge current due to the occurrence of PD in the PLG coil was measured after it was passed through the differential circuit connected between the PLG coil and the coupling capacitor. Figure 6.11 shows the relationship between the applied voltage and the apparent charge of PD in the PLG coil. The apparent charge of PD was measured by detecting the electrical discharge pulse at frequencies from 15 kHz to 150 kHz. It is shown that PD occurs from approximately 20kV and the apparent charge of PD increases with the applied voltage.

In the test method described above for measuring the pulse current running through the ground line of the coil, the entire specimen including the test cable will be evaluated. The existence of PD and its quantity can be detected. However, it is difficult to locate the source of PD or identify the cause of PD. Therefore, if it is possible to locate the discharge point and estimate the causes in some way, the reliability of the insulating function can be improved resulting in prevention of any troubles in the manufacturing processes and the actual on-site operation.

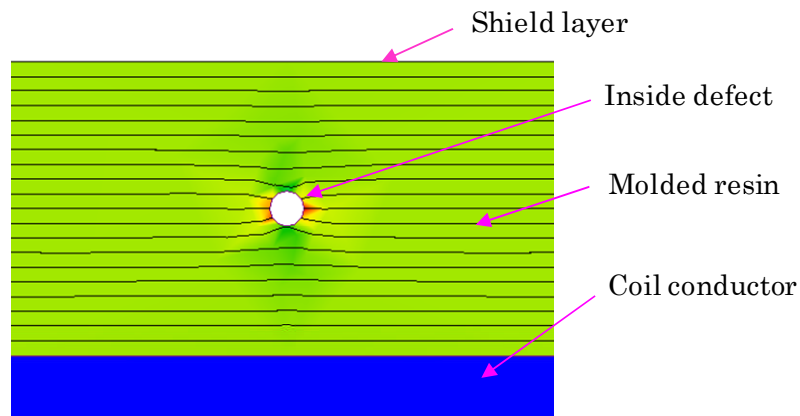


Fig. 6.9 An example of analyzing the equipotential distribution in the coil cross section

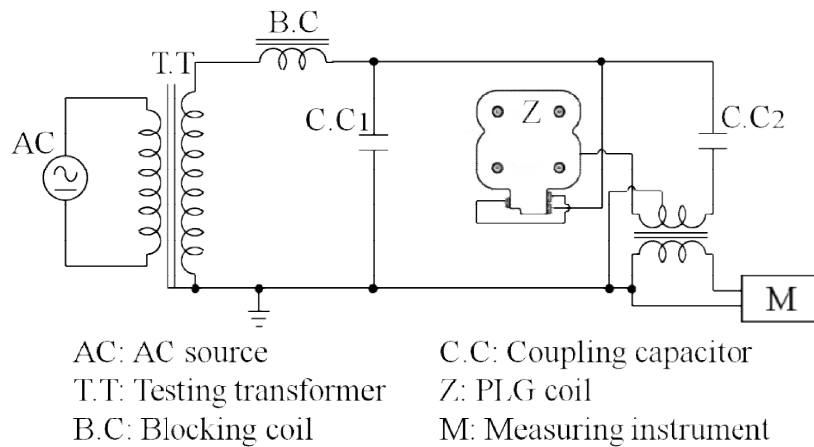


Fig. 6.10 Test circuit used for measurement of PD

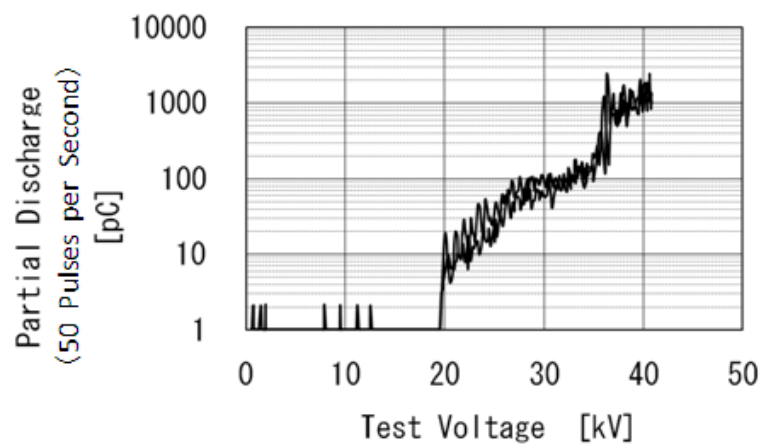


Fig. 6.11 PD characteristic of the test coil

6.4 Locating the defect position by the PD detection

As mentioned in Section 6.2, PD is generated at the defect point of the ground coil due to electric field concentration. Thus, if the defect portion can be identified by the source of the partial discharge, there is a possibility to estimate the cause of defect.

6.4.1 PD detection by the AE sensor

AE (Acoustic Emission) is a phenomenon where an elastic wave sound is generated when the material is deformed or destroyed. This non-destructive evaluation is referred to as the AE method. The phenomenon detection possibility of the propagating elastic waves in the mold resin generated from PD at the defect in the simulated coil using the multiple AE sensors was verified in this section. As a result, if the discharge was not reached 1000pC, it would be difficult to detect the PD by the AE sensor due to insufficient detection sensitivity. The AE attenuation in the mold resin was significant. Therefore, it became clear that this method was not suitable for locating defective positions unless the defective position was approximately located ⁽²⁾. The AE sensors attached on the PLG coil are shown in Fig. 6.12. The AE waveform measured example of PD generated near the defective portion is shown in Fig. 6.13.

6.4.2 PD detection by the UHF sensor

The PD characteristics were currently evaluated by detecting a discharge pulse in the low frequency range of 15 to 150 kHz. Furthermore, in order to identify the source of PD, the PD detection measured as EM waves by expanding the observation frequency band to the Ultra High Frequency (UHF: 300MHz ~ 3GHz) was examined.

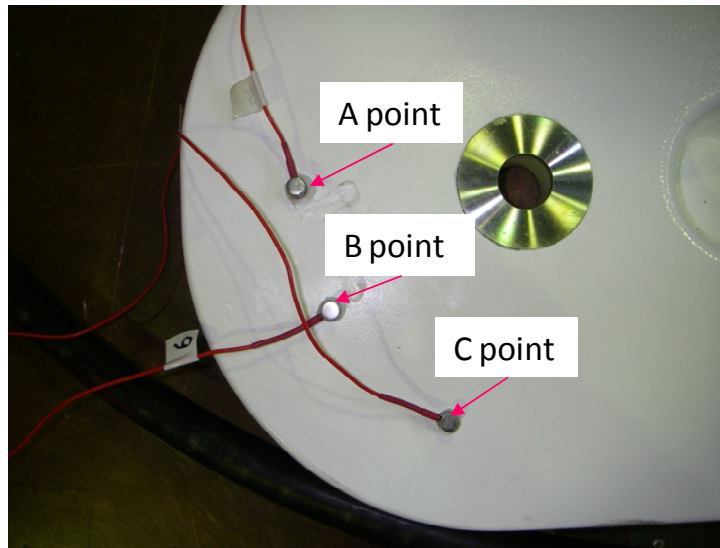


Fig. 6.12 AE sensors attached on the PLG coil

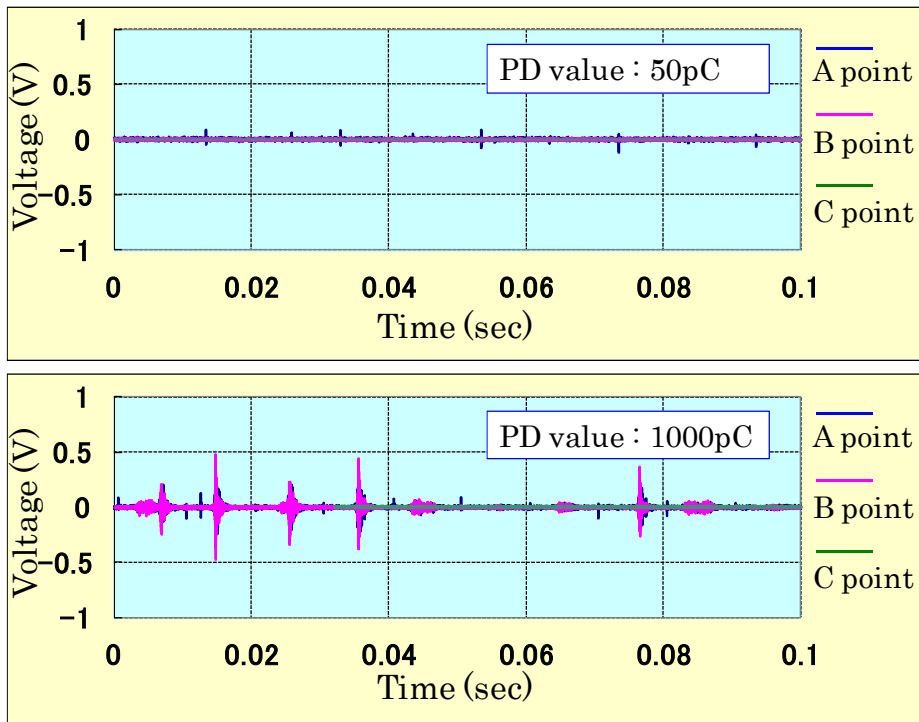


Fig. 6.13 AE waveform example of PD generating part

6.4.2.1 Concept of detection

Figure 6.14 shows the concept for locating void-defect by using a UHF sensor that detects the EM waves emitted from PD ⁽⁶⁾. It is thought that the maximum output of EM waves can be detected at the vicinity of source of PD because emitted EM waves from PD are weak, and attenuates by waves propagation. If it is possible to locate the position of large intensity of EM emission, the defect position causing the PD can be estimated. Figure 6.15 shows the UHF sensor used for locating PD in the PLG coil.

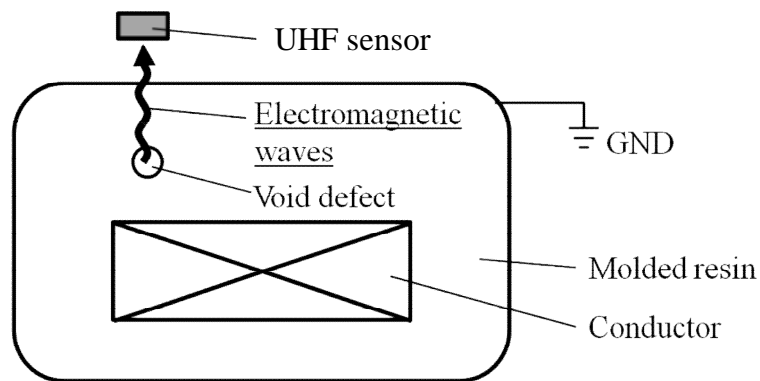


Fig. 6.14 Concept of detection using UHF sensor

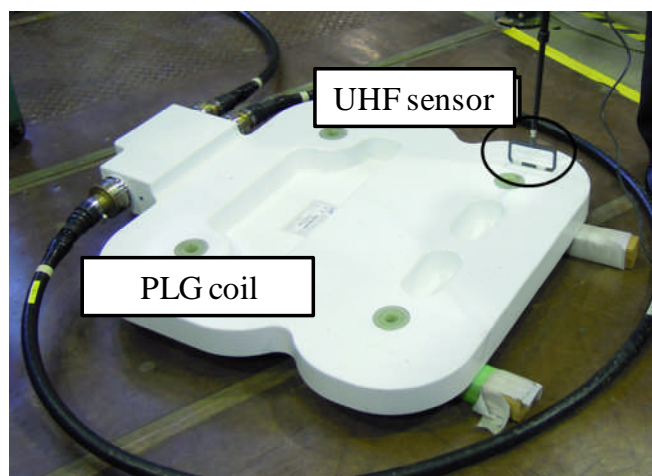
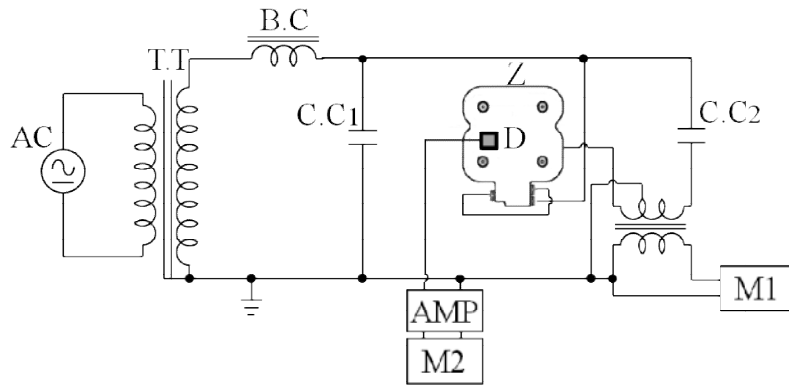


Fig. 6.15 The UHF sensor used for locating PD in the PLG coil

6.4.2.2 Measurement result

Figure 6.16 shows the test circuit used for locating the defect. The UHF sensor was set at some positions roughly within 1cm above the surface of PLG coil while confirming the output voltage of UHF sensor. The position where the output voltage of UHF sensor was high was regarded as the defect position. Furthermore, PD current was recorded simultaneously with the output voltage of the UHF sensor. Figure 6.17 shows the applied voltage, the output voltage converted from the PD current, and the output voltage of the UHF sensor set at the position above the artificial defect. Several pulses of the EM waves were detected per cycle of the applied voltage. The pulses of EM waves synchronize with the PD current. Thus it is presumed that the pulses of the EM waves are emitted from PD. When the UHF sensor was set within horizontally 10mm of PD source of which apparent charge was approximately from 20 to 30pC, the UHF sensor could detect the EM waves emitted from the PD. On the other hand, when the UHF sensor was set at a horizontal distance of approximately 10cm and more from PD source, the detection was difficult, even if the apparent charge of PD was approximately 100pC.



M1: Measuring instrument (partial discharge)
 AMP: Amplifier
 M2: Measuring instrument
 (electromagnetic waves or partial discharge current)

Fig. 6.16 Test circuit used for locating the defect

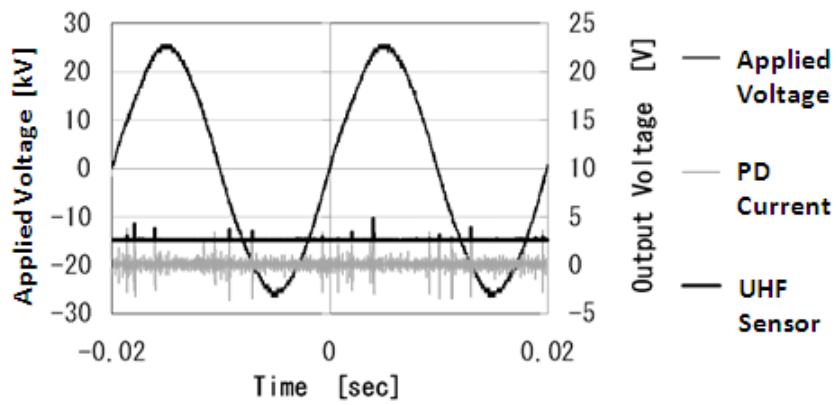


Fig. 6.17 Applied voltage, PD current, and the output voltage of the UHF sensor

6.5 Development of effective insulation diagnosis technique based on the EM wave detection

It is known that PD occurs when there is a defect or deterioration of an insulating material of high-voltage equipment, and it emits broadband EM waves ⁽⁷⁻¹⁰⁾. We investigated a method of locating defect positions inherent in the propulsion ground coil and a method for identifying abnormal coils from the continuously laid coils on the site by detecting the EM waves emitted from PD.

6.5.1 Problems in insulation diagnosis of propulsion ground coils

The conventional insulation confirmation for the initial ground coil installation and for the coil replacement is performed by opening the section switch of the primary side and supplying DC to the load side (coil side) of the corresponding section. However, because the primary purpose of DC withstand voltage tests is screening for installation failures associated with the on-site construction work, it does not fulfill the role of deterioration diagnosis. A pilot study to guide the deterioration diagnosis and maintenance plan for the installation site is also effective by removing the specific coil laid in the commercial operation line periodically to acquire the detailed insulation characteristics. However, evaluation by a well-equipped dedicated laboratory measurement environment is essential. There are problems such as the inspection required for the removal of sample coils at the installation sites and the number of the samples being limited. Furthermore, it is difficult to diagnosis the insulation of the ground coils if they are installed to the actual site because the high voltage is supplied from the substation only when the motor load (counter electromotive force) is generated by the vehicle traveling. Therefore, a development of effective new insulation diagnostic techniques for Maglev which can evaluate the on-site operating ground coils is expected.

6.5.2 Locating defect by using interferometer system

Effectiveness of the insulation diagnostic method using radio sensing has been reported ⁽⁷⁻¹⁰⁾. In this study, we located PD in the PLG coil by using the interferometer system and evaluated the results ⁽¹¹⁻¹³⁾.

6.5.2.1 Concept of locating PD source

Figure 6.18 shows the concept of this measurement method. Two dipole antennas were set near the PD source, and the EM waves emitted from PD were measured. Table 6.1 shows the specifications of antennas. The arrival time of EM waves at antenna 1 and antenna 2 are assumed to be T_1 and T_2 respectively. The time lag between the arrival time at two antennas is given by $\tau_d = (T_1 - T_2)$. The distance difference X_d between the distances from the PD source to each antenna is given by

$$X_d = \tau_d \cdot c \quad (6.1)$$

where c is the velocity of the EM waves. Because a hyperbola is drawn by using the distance difference X_d , PD source can be located as the hyperbola on the horizontal cross-section of ground coil. When the number of antennas for the EM wave detection is increased, PD source can be located with higher accuracy.

6.5.2.2 Measurement result

Figure 6.19 shows the arrangement of PLG coil and dipole antennas. A high voltage was applied to the PLG coil, and the EM waves were measured with two dipole antennas and a digital oscilloscope (frequency bandwidth: 1GHz, sampling rate: 5Gs/s). Figures 6.20 and 6.21 show the examples of background noise and the EM waves emitted from PD. The waveforms of the EM waves emitted from PD are pulse-shape and differ from those of the background noise. Figures 6.22 and 6.23 show the frequency spectra of background noise and the EM waves emitted from PD. The EM waves

emitted from PD have wideband frequency spectra. On the other hand, the background noise has no significant frequency peak except a communication frequency band.

Figure 6.24 shows the location result. The arrival time lag was obtained as $\tau_d = 0.8\text{ns}$ by calculating the difference between the first peak time of the EM waves received with two antennas arranged as shown in Fig. 6.24. As a result, the distance difference was obtained as $X_d = 240\text{mm}$. A curved line of hyperbola that passes through the PLG coil can be drawn by using the distance difference of 240mm. The PD source can be located on the line that passes through the molded resin of PLG coil. The location result is acceptable in practical use, i.e. detecting the PLG coil that has a void-defect.

Furthermore, the PD could be located with an error of several centimeters in the case that the arrangement of antennas was shifted horizontally from that in Fig. 6.24. In the case that the distance between the antenna and PD source was 1m, the PD of which apparent charge was 100pC or more could be located.

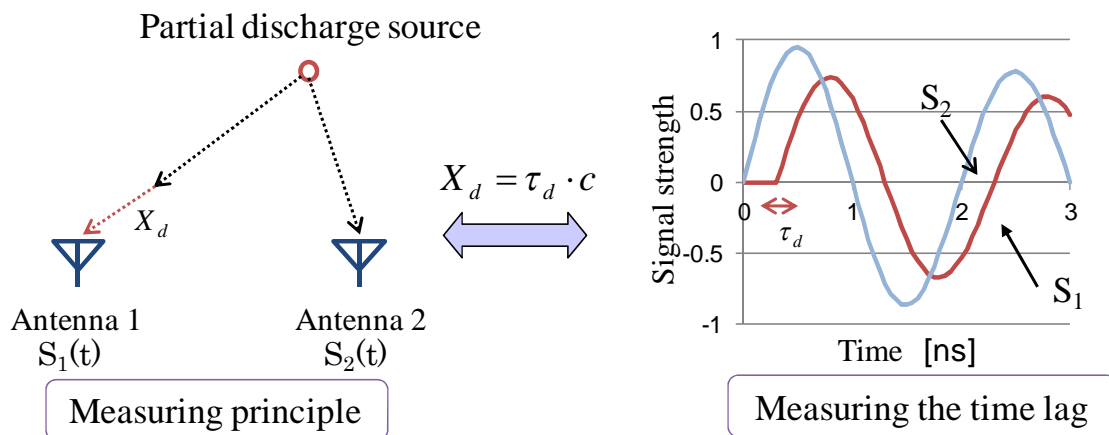


Fig. 6.18 Concept of locating PD source

Table 6.1 Specifications of antenna

Type	Half-length dipole
Frequency range	25-520MHz (variable) 500MHz (in Fig.11)
Impedance	50 Ω
Connector	Type N female
VSWR ratio	2
Gain	0 dB
Coaxial cable type	5D-2W, 10m

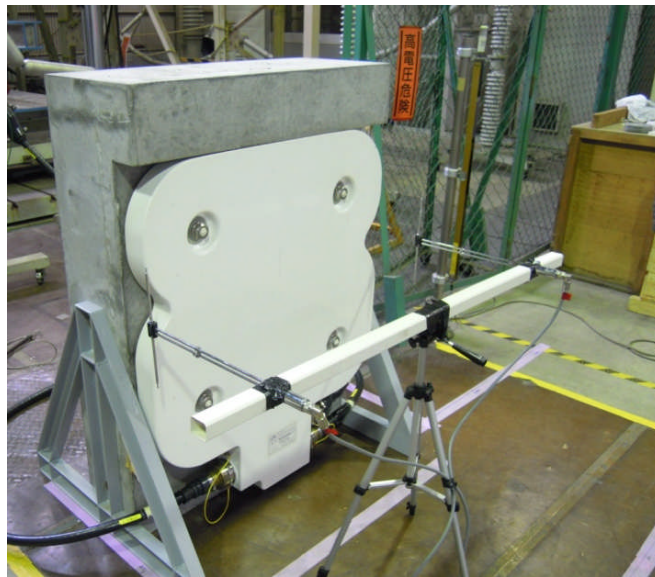


Fig. 6.19 Arrangement of PLG coil and dipole antennas

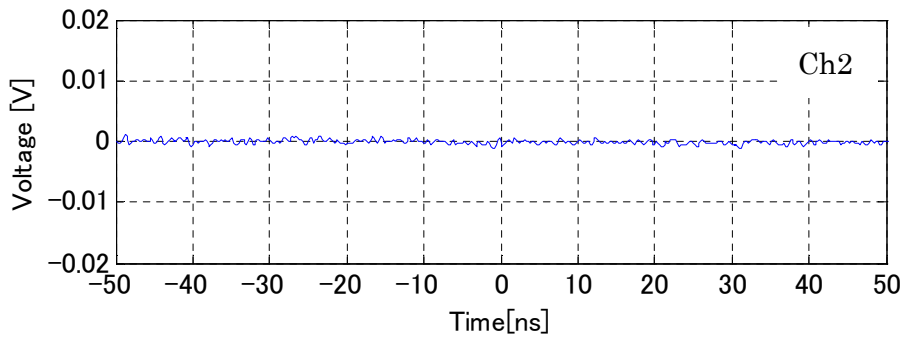
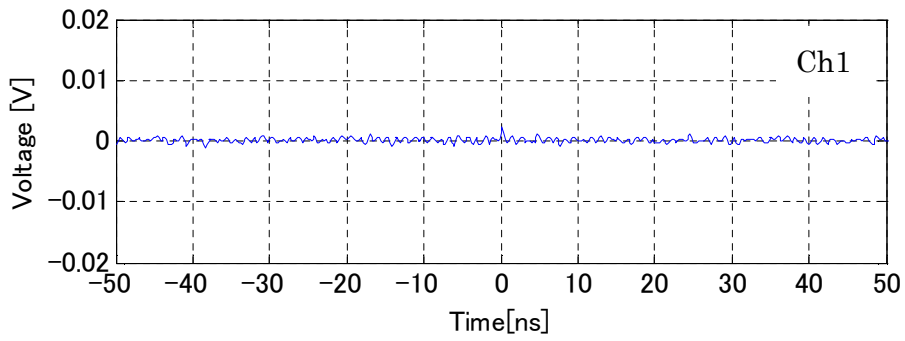


Fig. 6.20 Waveforms of background noise

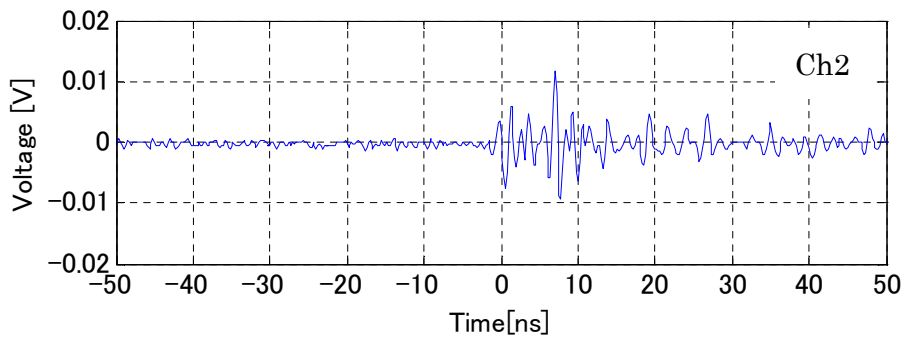
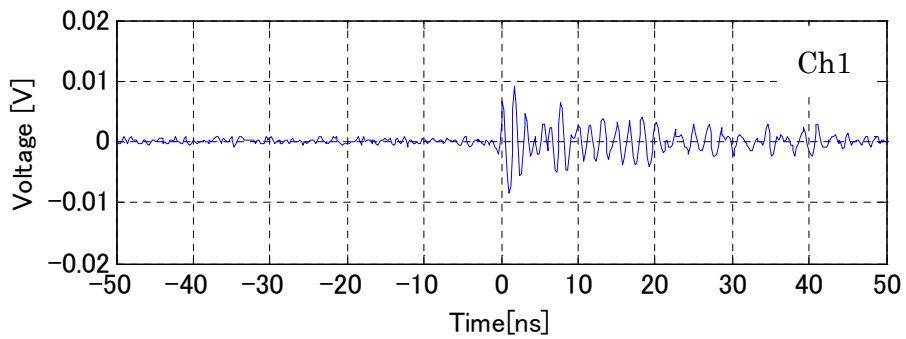


Fig. 6.21 Waveforms of EM waves emitted from PD

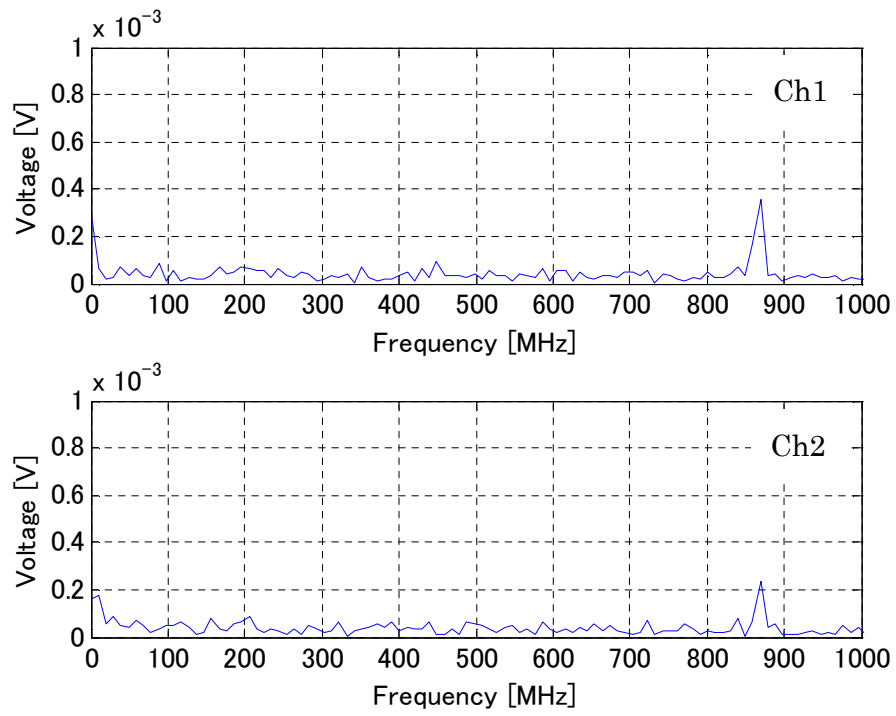


Fig. 6.22 Frequency spectra of background noise

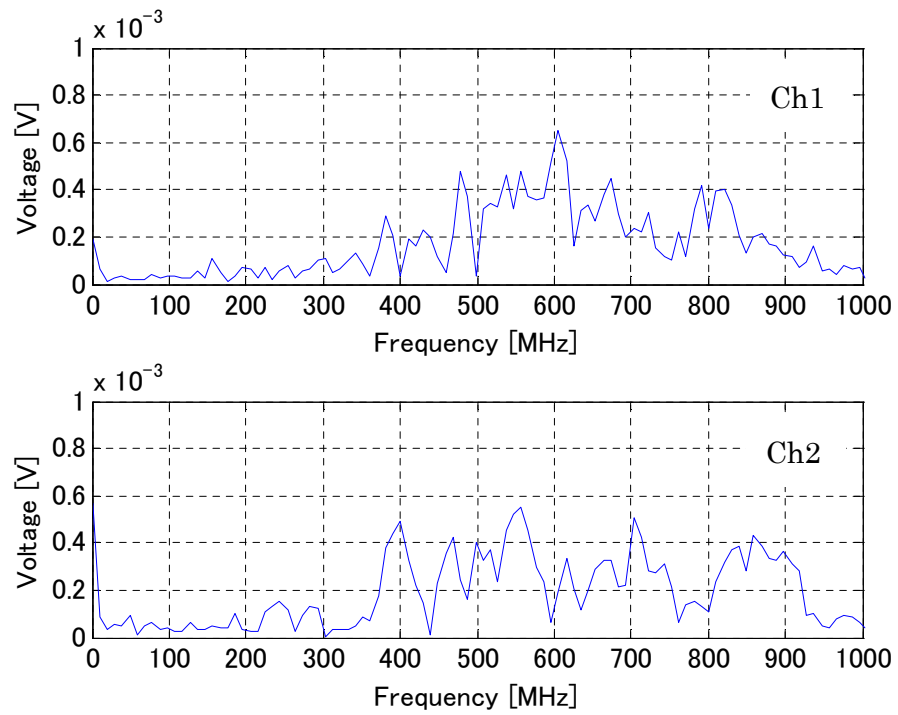


Fig. 6.23 Frequency spectra of EM waves emitted from PD

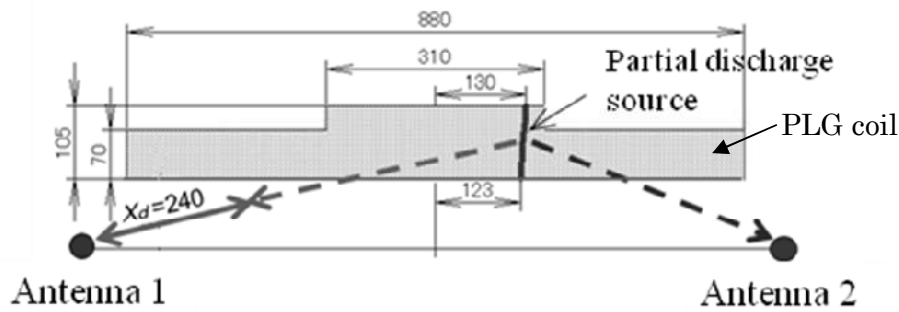


Fig. 6.24 Location of PD source

6.5.3 Preliminary examination in outdoor environment

Prior to the verification examination with the vehicle traveling, the preliminary examination for the PD detection in an outdoor environment was performed using full-size mock guide-way for Maglev System in the site of Railway Technical Research Institute (Kunitachi City, Tokyo) ⁽¹⁴⁾.

6.5.3.1 Purpose of preliminary examination

The PD characteristic of ground coil used to be measured only in a laboratory with special testing equipment. It is the first trial in an outdoor environment. Influence from various air propagated EM waves to the EM wave detection emitted by PD from the ground coil, influence of the guide-way structure and other factors were investigated by this preliminary examination. Furthermore, validity of the test construction for the actual traveling experiment was verified.

6.5.3.2 Test coils

Various insulation abnormalities simulated by five defective mock ground coils were prepared at on-site operation. The specimens were selected which can serve as a source of PD by electric field concentration of the defective

portion. The types of the defective coils and Q_{\max} immediately before the examination are shown in Table 6.2.

6.5.3.3 Test procedure

Aforementioned five defective mock specimens were temporarily installed to the mock guide-way, and voltage was applied to each test specimen through portable type no-corona T.T. The voltage was applied from the generator (50Hz, 100V), insulation Tr (100V to 200V), noise rejection Tr, control panel, No-corona T.T. (0 to 30 kV), post insulator and test specimens in order. The measurement system was configured by 2 sets of one pair (2 poles) of dipole antennas on a straight line of distance 0.1 m from the ground coil surface. The EM waves generated by PD were detected by a digital oscilloscope. Two antenna configurations can estimate the direction of the EM waves. Furthermore, four antenna configurations increased the reliability of the direction of the EM waves, and the EM wave attenuation was also measured. The whole test configuration, test coils and antenna arrangements are shown in Fig. 6.25.

6.5.3.4 Test result

The measurement results of the background noise in an outdoor mock guide-way environment are shown in Fig. 6.26. The waveforms of the background EM waves are shown in Fig. 6.26 (a). The correlation calculated waveforms for period of 8 ns are shown in Fig. 6.26 (b). The frequency spectra of EM waves are shown in Fig. 6.26 (c). The correlation waveforms (time delay - cross correlation, measured by the deviation estimation method) are shown in Fig. 6.26 (d). The correlation waveforms (time delay-cross correlation, measured by the deviation estimation method) are shown in Fig. 6.26 (d). The frequency spectrum of 867.2MHz is observed in Fig.6.26 (c). This frequency corresponds to the movable communication band (860 to 885 MHz, FDMA/TDMA/CDMA type mobile and automobile telephone) according to the Frequency Book ⁽¹⁵⁾. Furthermore, the periodic cross correlation waveform with time delay of 0.5 ns is shown in Fig 6.26 (d).

Fig. 6.26 (c) indicates that the test equipment measured and calculated the signals that were different from the emission of the PD.

The time delay calculation results of the EM wave including PD from void C are shown in Fig. 6.27. The EM waveforms are shown in Fig. 6.27 (a). The correlation calculated waveforms for period of 8 ns are shown in Fig. 6.27 (b). The frequency spectra of EM waves are shown in Fig. 6.27 (c). The correlation waveforms (time delay - cross correlation, measured by the deviation estimation method) are shown in Fig. 6.27 (d). Although the frequency spectrum of 867.2MHz is observed in Fig. 6.27 (c), other frequency spectrums were also observed (indicated with a circled area). The frequency spectrum of Fig. 6.27 (c) is the calculation result of the time range of Fig. 6.27 (a). It is not the extracted frequency spectrum shown in Fig. 6.27 (b). The maximum spectrum is the time delay at 0 ns shown in Fig. 6.27 (d). From this, it can be estimated that a PD existed on the center of the antennas ⁽¹⁶⁾.

The PD was observed in three samples (void B, void C and the shield exfoliation) out of five samples in the preliminary examination. The detectable level by the trigger measurement in an outdoor environment was considered to be about 100 pC of discharge intensity. However, care must be taken in detecting the PD because PD from void B and void C were easily detected but discharge from the shield exfoliation was unstable. No background noise fluctuation irrespective of voltage supply was observed by the voltage supplied experiment without load (AC 30 kV), and nor were there any effects by the guide-way structure (especially steel rods in concrete) to the EM wave detection observed. The validity of this test configuration for the actual on-site test was confirmed from these results.

The PD detection by the antenna mounted bogie being moved along the guide-way was performed as the final test of the preliminary examination. As a result, it was confirmed that the PD could be detected if the antenna approached the discharge source and the EM waves generated by the PD exceeded a preset trigger level. The detected waves had time delay and attenuation.

Table 6.2 Defect type and Q_{\max} of test coils

Test coils	Defect type	Q_{\max} at 15kV
Void A	Single void inside molding	30 pC
Void B	Many voids inside molding	200 pC
Void C	Many voids inside molding	100 pC
Shield exfoliation	Exfoliation of surface shield layer (50mm×50mm)	150 pC
Abnormal connector	Abnormality of cable joint of the coil	10 pC

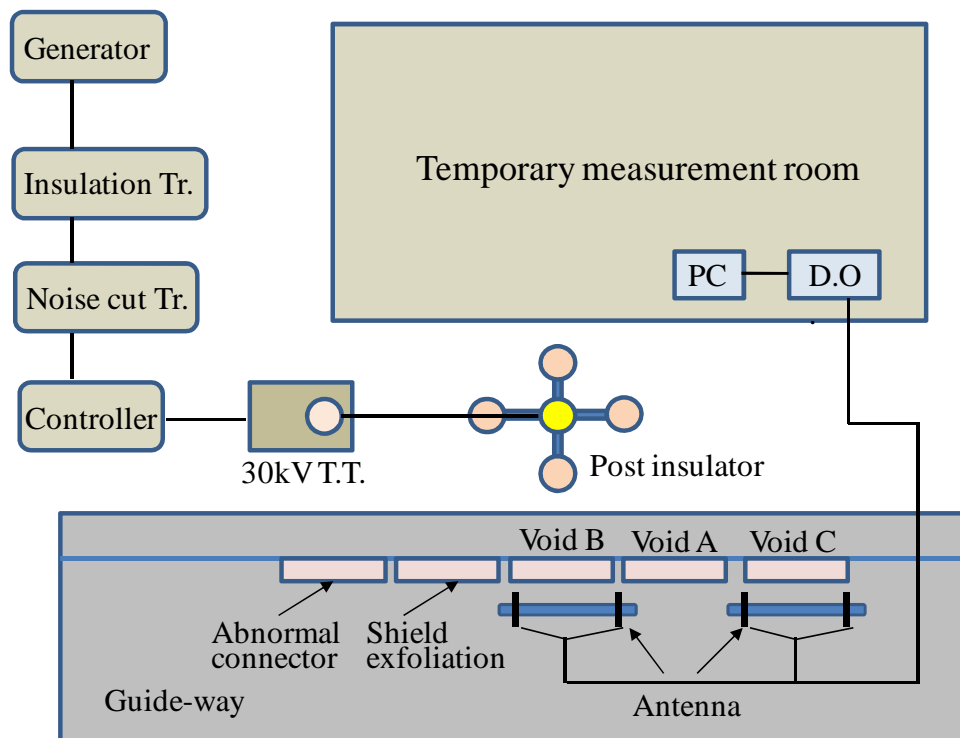
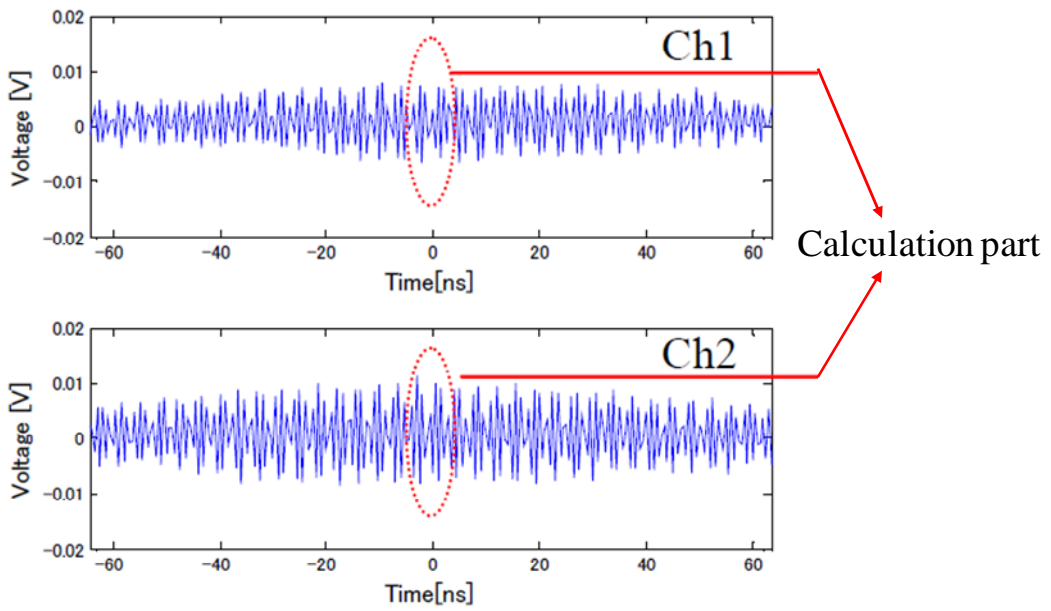
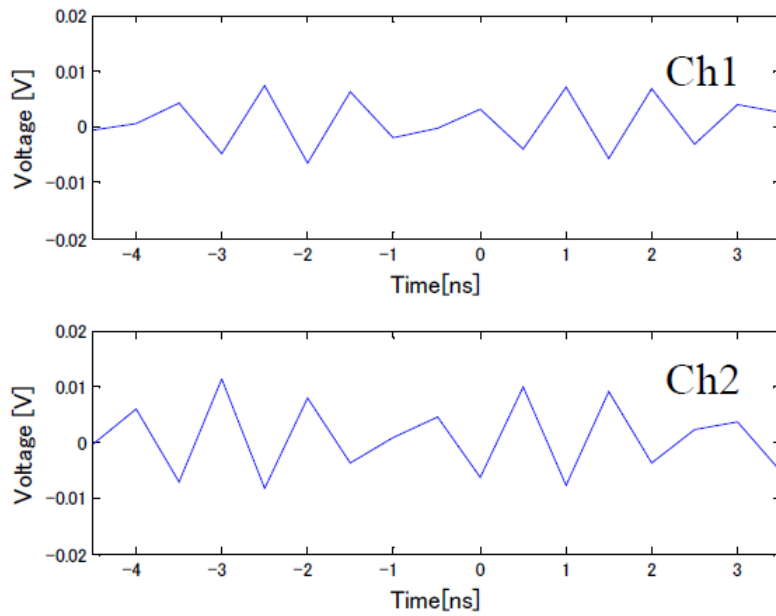


Fig. 6.25 Arrangement of test coil and dipole antennas

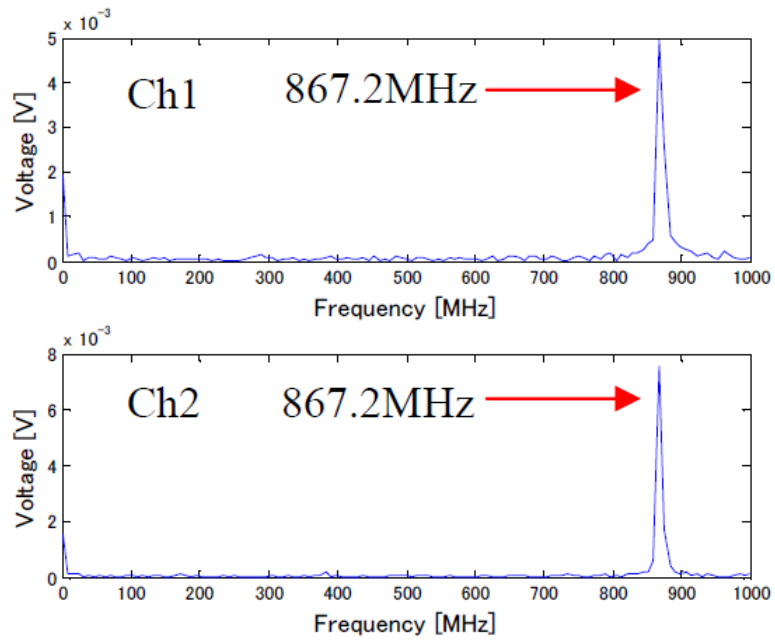


(a) Waveforms of background EM waves

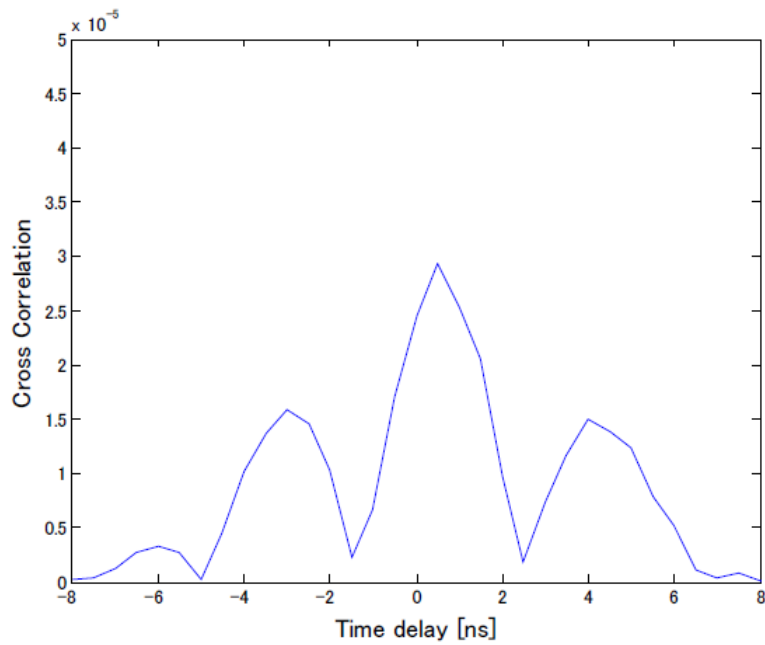


(b) Calculation parts of waveforms

Fig. 6.26 (1) Calculation results of time delay between the received background EM waves

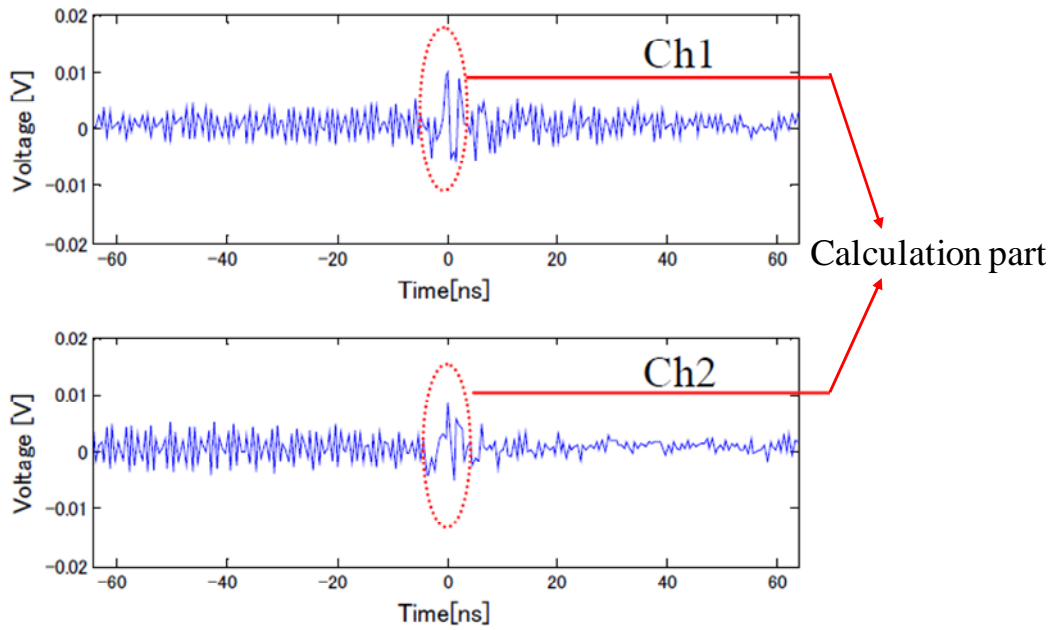


(c) Frequency spectra of EM waves

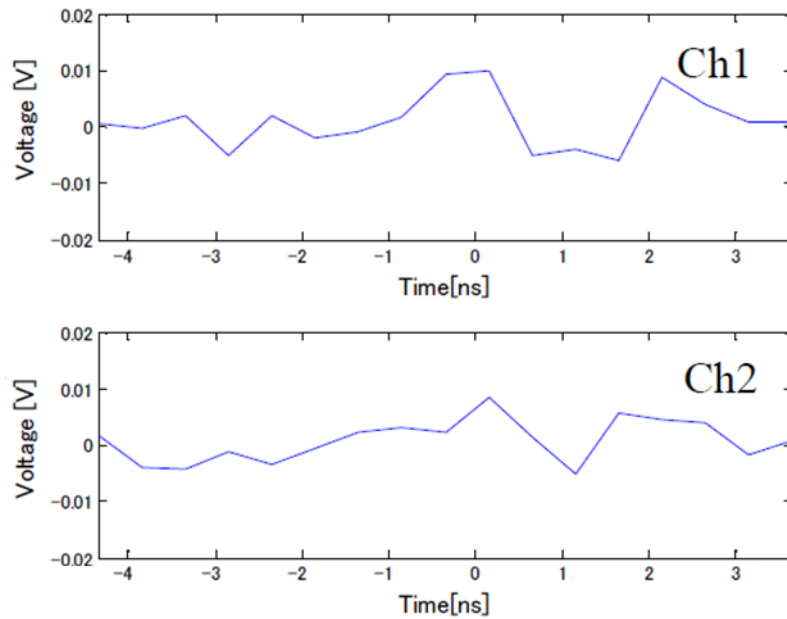


(d) Estimation of time delay

Fig. 6.26 (2) Calculation results of time delay between the received background EM waves

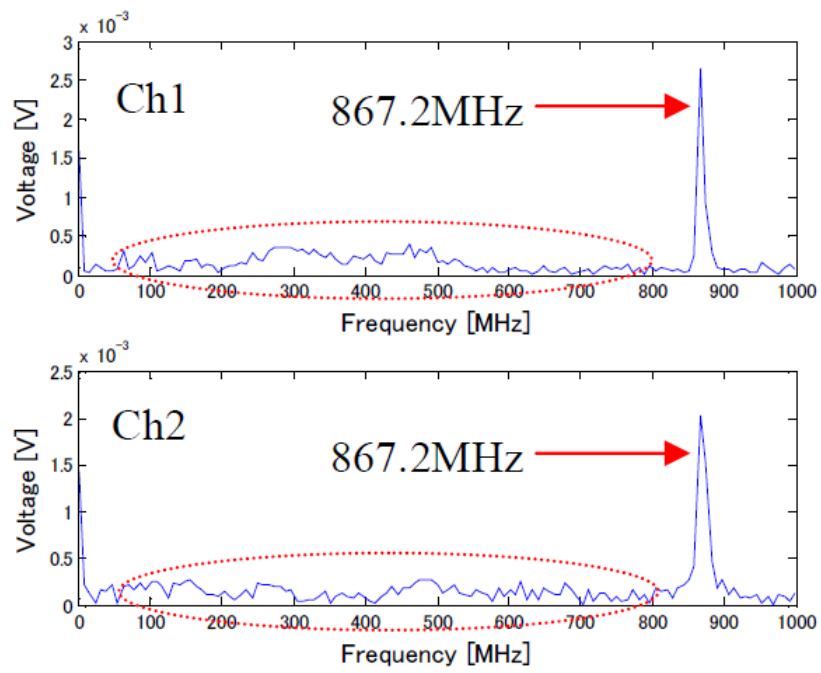


(a) Waveforms of EM waves from PD

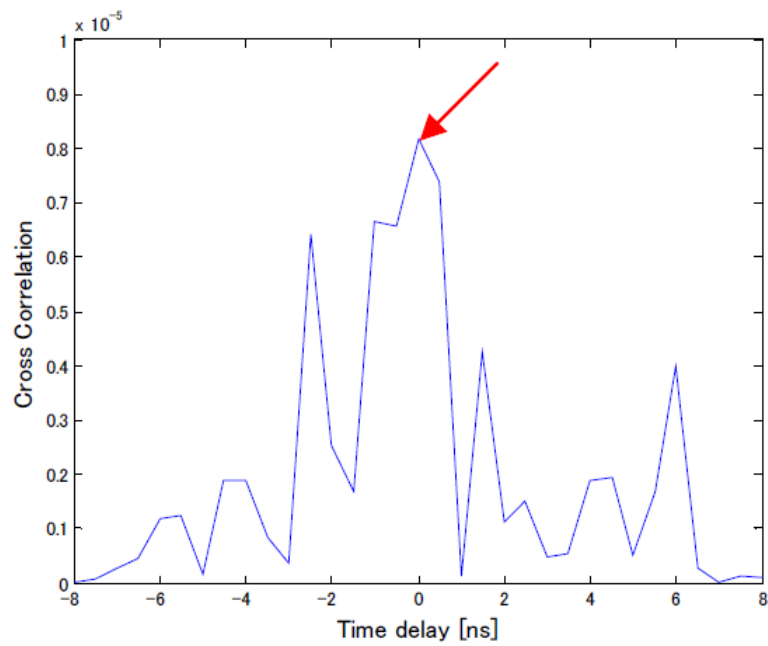


(b) Calculation parts of waveforms

Fig. 6.27 (1) Calculation results of time delay between the received EM waves from PD



(c) Frequency spectra of EM waves



(d) Estimation of time delay

Fig. 6.27 (2) Calculation results of time delay between the received EM waves from PD

6.5.4 Driving test in Miyazaki Test Line

The only condition that can apply a high voltage to the ground coil laid on the site from the substation is to run the vehicle at high speed. Based on the preliminary test results in an outdoor environment, a basic test to detect a ground coil emitting PD by the test vehicle was performed on the track of the Miyazaki Maglev Test Line (Hyuga-shi, Miyazaki) ⁽¹⁴⁾.

6.5.4.1 Purpose of the test run

It is difficult to perform an insulation diagnosis at an on-site installed Maglev System ground coils as mentioned above. Therefore a new concept of an insulation diagnostic technique from the running vehicle to identify the abnormal coil in order to solve this problem was considered. This system was intended to confirm whether the traveling test equipment can detect the PD of the experimentally installed ground coils by EM waves, the same as in the stationary test.

6.5.4.2 Test coils

Five defective mock ground coils that were examined for the preliminary test at the site of the Railway Technical Research Institute were used as specimens considering their reproducibility. The ground coils were experimentally installed on the side wall of the guide-way.

6.5.4.3 Test configuration

The test configuration of the coils, power supplies and EM wave measurement apparatus, etc. were set on the test track of the Miyazaki Maglev Test Line, the same as that of the preliminary test in the site of the Railway Technical Research Institute.

The test coils were installed in equal pitch on the wooden mounts as shown in Fig. 6.28. The top and bottom cable connectors were reversely set because the power was supplied independently from the outside of the side wall. The

power supply configuration was arranged from the power generator to the noise rejection Tr directly under a guide-way, and the configuration from the no-corona T.T. to the test specimen was arranged on a beam. The insulated support increased the insulation creepage distance by preparing a concavo-convex processing in the surface of the fiber reinforced plastic (hereinafter refer to as FRP) pipe. The aluminum PLICA tube was used for the high-voltage bus-bar to suppress electric discharge to the circumference atmosphere. A local electric discharge was prevented by using an electric field relief screw type shield balls at the post electrodes which connected the test cable between a high-voltage bus-bar and each test specimen. The power voltage was controlled by the radio communication between the vehicle and the power supply control room.

The flat bogie and driving vehicle for the EM wave measurement system were borrowed from Tohoku University, which were used for the basic experiment of the aero train by Tohoku University. They were connected as a test vehicle. Dipole antennas furnished with 2 sets of FRP mounts, a power supply for measurement system, a balance weight, a laser displacement gauge for coil position and speed detection, etc. were installed on the flat bogie. The measurement apparatus was set on the driving vehicle. The vibration acceleration sensors were installed to each FRP mount and at the side of the flat bogie in order to monitor the vertical vibration during traveling. The measurement configuration of the test vehicles and test equipment are described in Fig. 6.29. The measurement configuration of the guide-way cross section is shown in Fig. 6.30.



Fig. 6.28 Installation condition of test coils (from the back left, void A, shield exfoliation, void C, void B, abnormal connector)

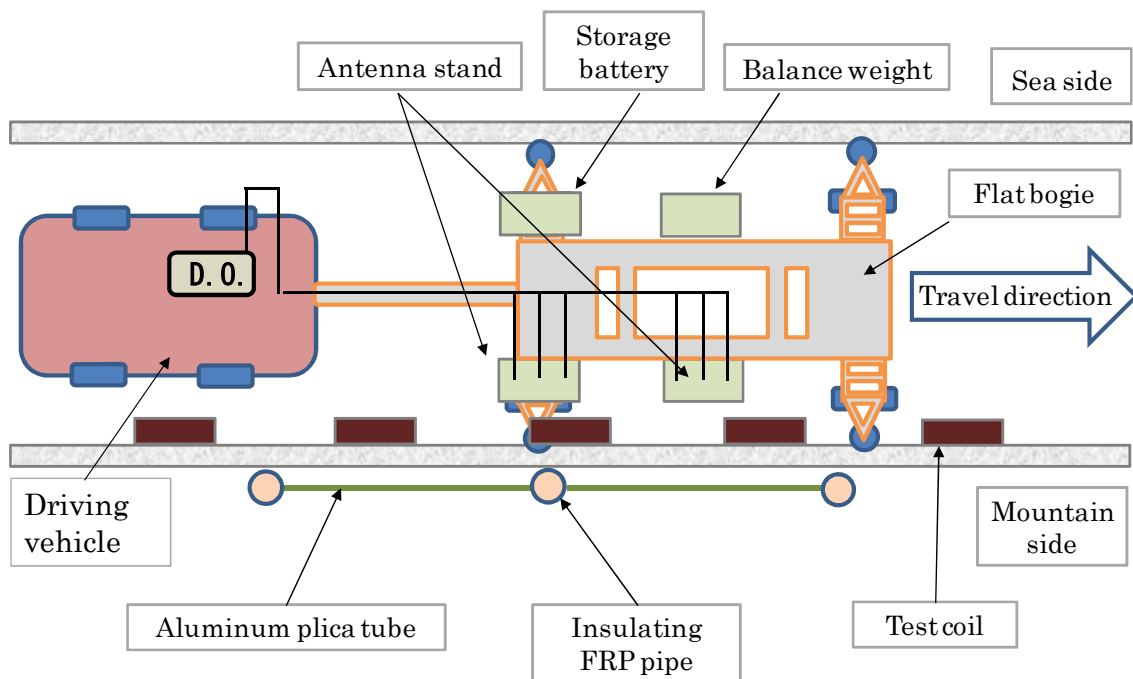


Fig. 6.29 Arrangement of test vehicle and test equipment

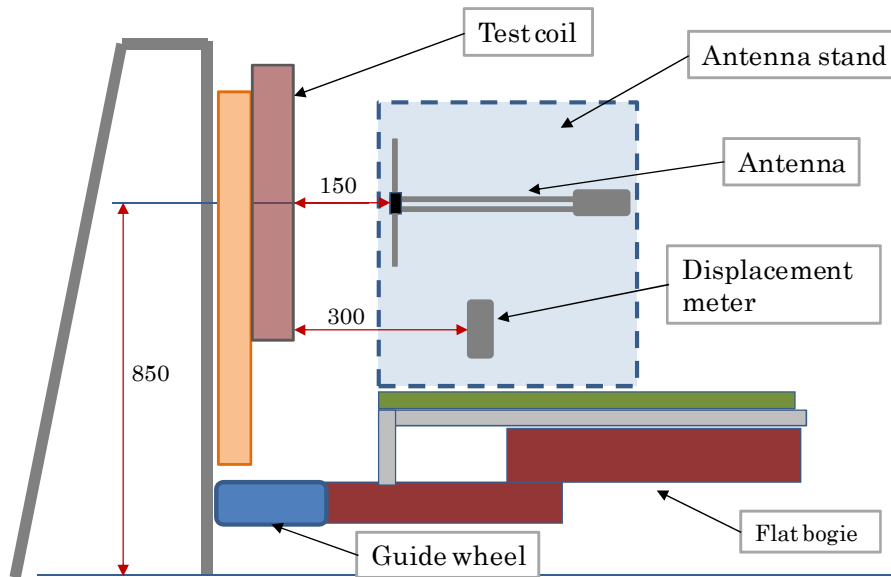


Fig. 6.30 Placement of test coil and antenna (guide-way cross section)

6.5.4.4 Test procedure

The dipole antenna of its resonance frequency of 500 MHz was used the same as the preliminary test. The EM wave signal in each test condition was recorded to two sets of digital oscilloscopes. Each antenna was configured by three elements being set by 0.5 m pitch on a special FRP mount. Two sets of antenna arrays were arranged 0.15 m laterally from the test coil surface along the moving direction, and they were fixed to the coil side of the flat bogie with vibration proof hard rubber. Although the emission directions of EM waves could be detected with two antennas, the three-antenna configuration was used to improve the detection reliability of the signal directions. Furthermore, the attenuation in EM wave propagation was examined by setting two sets of the antenna arrays.

In addition, dummy antennas with the same specification were installed to the opposite side of the measuring antenna on the flat bogie in order to easily distinguish other EM waves from the EM wave emitted from the ground coil. A laser type displacement gauge was installed to the antenna mount in order to scan the center projection on the surface of the ground coils to enable the

detection of the relative position between the ground coil and the antenna at the time of the trigger signal being detected.

Prior to the test run, the same performance of EM detection at the time of the preliminary test carried out in the site of the Railway Technical Research Institute was confirmed by stopping the antenna installed test vehicle at the test coils installed zone. No influence to the measurement system was confirmed by using the electrical discharges in the atmosphere with the standard gap. No influence to the power supply system was also confirmed by applying voltage (30 kV rated) with no load.

In the test run, the EM wave emissions were measured by two digital oscilloscopes with the same trigger level at the time of the test vehicle passing the test coils. The passing speed was increased from 20 km/h to 60 km/h in units of 20 km/h while vibration of the flat bogie and the measurement data were monitored.

6.5.4.5 Test result

(1) Stationary test

PD was observed in three samples (void B, void C and the shield exfoliation) in the stationary examination. Data acquisition from void B and void C was easy. However, it took time to acquire data from the shield exfoliation. Therefore, target coils for the traveling test were set to void B and void C.

(2) Traveling test

First, the test vehicle traveling without applying voltage to the ground coils was investigated to monitor the changes in the measurement environment. The equipment and antennas were secured to the flat bogie with rubber plates and/or wood blocks in order to avoid electromagnetic noise generation caused by directly contacting (friction or impact) the frame of the bogie. The vertical vibration acceleration while traveling was a maximum 10m/s^2 at 60km/h. No change in the measurement environment caused by the vibration during vehicle traveling was observed. The voltage was applied individually to void B and void C respectively to detect the EM wave. As a result, it was confirmed that the EM waves generated from the PD could be

relatively easily detected regardless of the traveling speed. The PD detected waveform example of the traveling test is shown in Fig. 6.31. However, the ambient noises (arc welding, cutting trees and weeding by engine cutters, etc.) largely exceeding the detection level of PD were detected during the on-site measurement for multiple days and they affected the measurement environment.

(3) Locating the PD generating point

Locating the PD was performed from the stationary detected EM waves for void B. The frequency spectrum and detected EM waveform is shown in Fig. 6.32. The circled area in Fig. 6.32 (a) was used to acquire the time difference. The time width was set to 6.4ns. Fig. 6.32 (b) shows that a wideband signal was detected. The time delay between the arrival times of the EM wave at the antennas is shown in Fig. 6.33. From the figure the time delay is -0.2ns, -1.2ns and -1.6ns respectively. Since the distance between antennas was 0.5m for Ch4 and Ch5 and for Ch5 and Ch6, the maximum time delay was set to 1.6 ns ($= 0.5\text{m} / 3 \times 10^8\text{m/s}$). Furthermore, since the distance between antennas Ch4 and Ch6 was 1 m, the maximum time delay was set to 3.2 ns. The acquired time delay lines are shown in Fig. 6.34. These time delay lines by the values of Ch4 and Ch5 (-0.2ns) and Ch5 and Ch6 (-1.6ns) shows the passing through the coil. The arrival time delay line of Ch5 and Ch6 (-1.2ns) does not pass through the coil, but it passes within 10cm or less. From these facts, the source of EM waves can be presumed to be the PD in the coil.

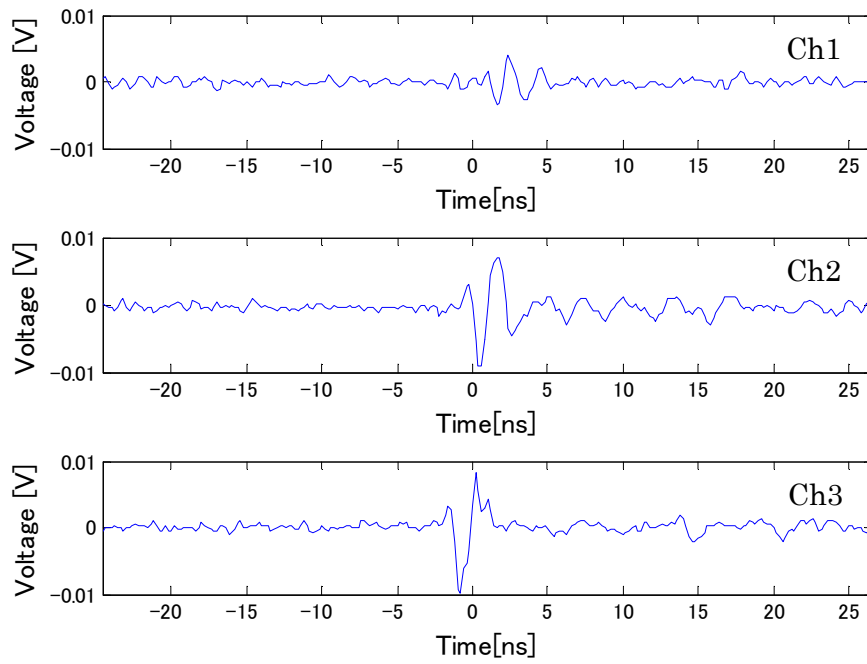
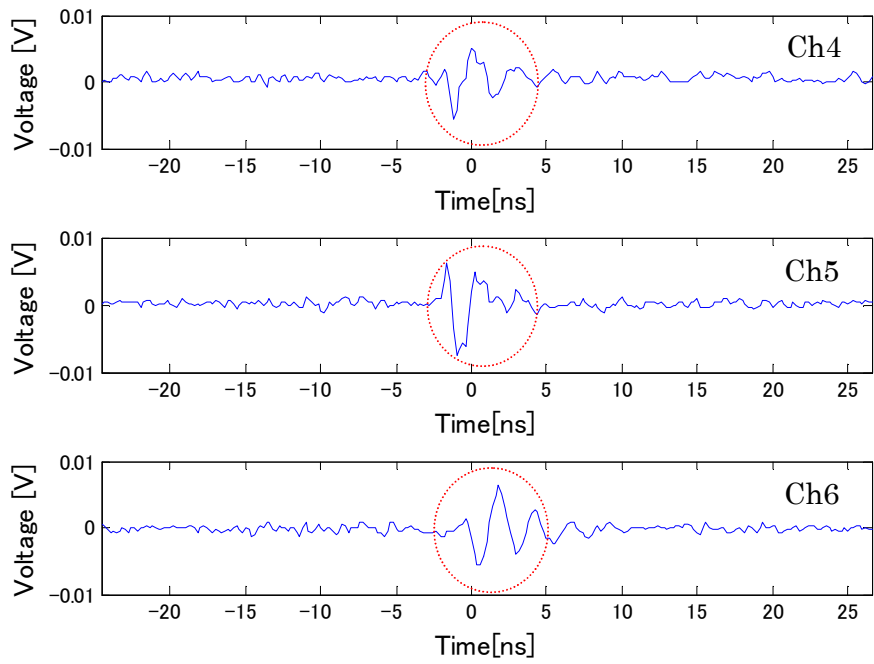
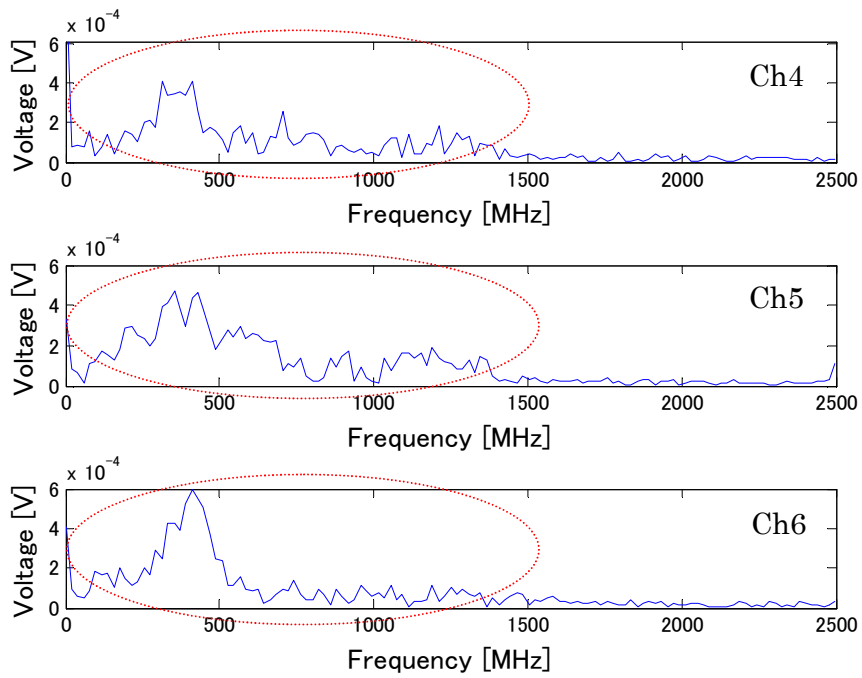


Fig. 6.31 Waveforms of EM waves emitted from PD in void C coil while driving



(a) Waveforms of EM waves emitted by PD



(b) Frequency spectra of EM waves

Fig. 6.32 Waveforms and frequency spectra of EM waves emitted from PD in void B coil

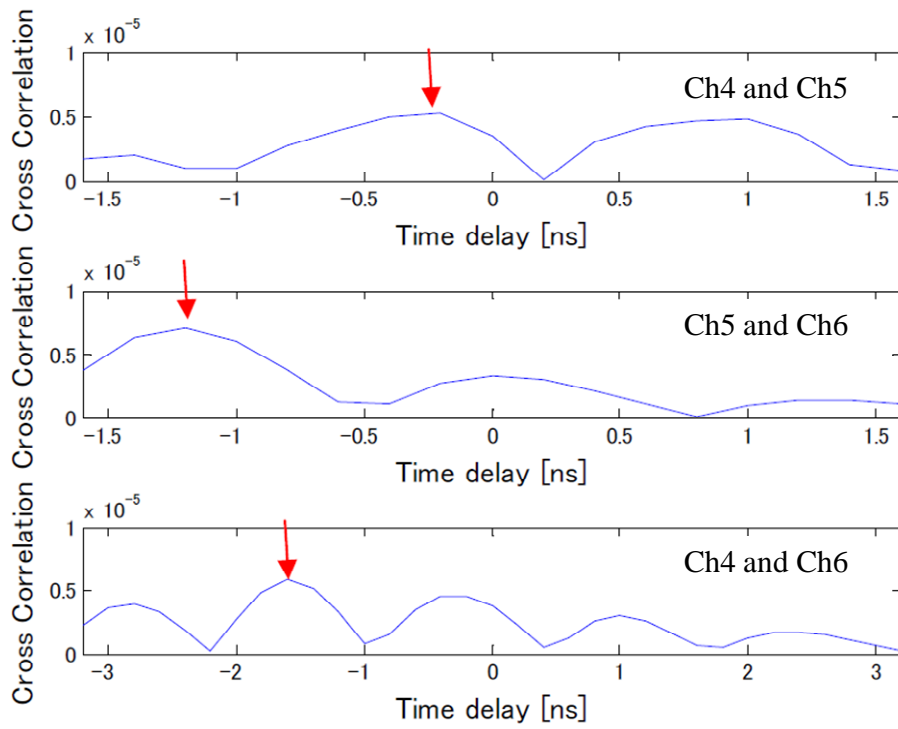


Fig. 6.33 Estimation of time delay between the each antenna

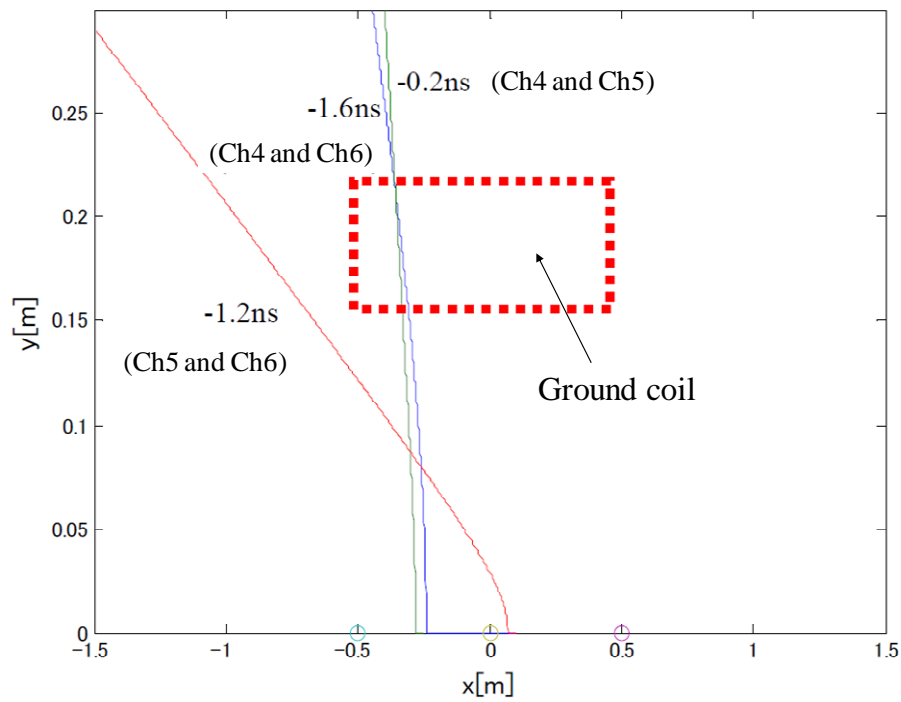


Fig. 6.34 Results of PD location using the time delay lines

6.5.5 Insulation diagnosis configuration intended for commercial operation

The research on new insulation diagnostic method for propulsion ground coils has been conducted and a prospect for practical applications has been gained from various test results. The insulation diagnostic configuration that can detect abnormal coils from the commercial vehicle and/or the general test vehicle during high-speed traveling assuming the commercial operation were investigated.

6.5.5.1 Antenna arrangement and configuration of the insulation diagnosis

It is a known fact that the probability of discharge from the propulsion system ground coil is high in the phase of (either + and - sides) immediately after the applied voltage crosses the zero-point as shown in Fig. 6.35. On the other hand, the current phase of the ground coils as viewed from the vehicle is constant because the superconducting Maglev uses a primary ground linear synchronous motor as a drive source. That is, it is possible to arrange the dipole antenna to oppose any phase position of the ground coil by adjusting the positional relationship of the traveling direction against the SCM. The positional relationship between the SCM (there are four poles in practice, but shown as two poles for explanation) on the vehicle and propulsion coils laid in the guide-way, the dipole antenna for detecting EM waves and other units are displayed in Fig. 6.36. Figure 6.37 shows the three-phase alternating current supplied to the propulsion coils. If the current phase applied to each coil is the same as the applied voltage, it is presumed that the PD may occur in each phase of the pitch of 60 degrees (① to ⑥) as shown in the figure (1/2 of the ground coils laid pitch: D). The positional relationship between the vehicle and each phase of the ground coil is shown in Fig. 6.38. For example, discharge can occur easily in the U-phase coil (①). It can be easily assumed that the PD will be detected in the order of a, b and c from the reaching time delay to the antenna. Similarly, it is easy to discharge in the W-phase coil (②). The PD will be detected in the order of c, b and a. And it is easy to discharge in the V-phase coil (③). The PD will be detected in the order of a, b and c. It is possible to locate the presence and

intensity of discharge from a particular coil by using the three dipole antennas. It was assumed that the applied voltage to the ground coils was in the same phase with the electric current in this explanation. However, if a constant phase shift is expected, it will be sufficient to consider the installation position of the antenna based on the phase shift.

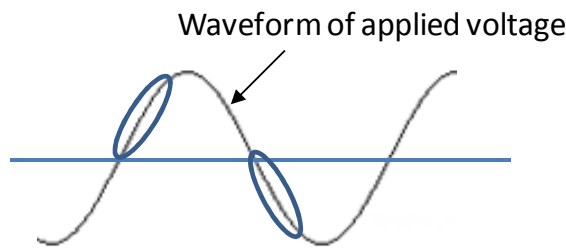


Fig. 6.35 Occurrence phase of PD

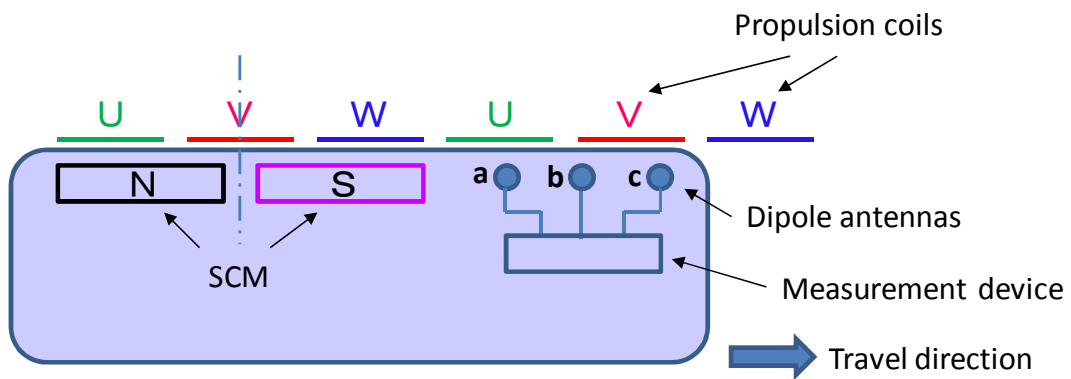


Fig. 6.36 Detection configuration of PD

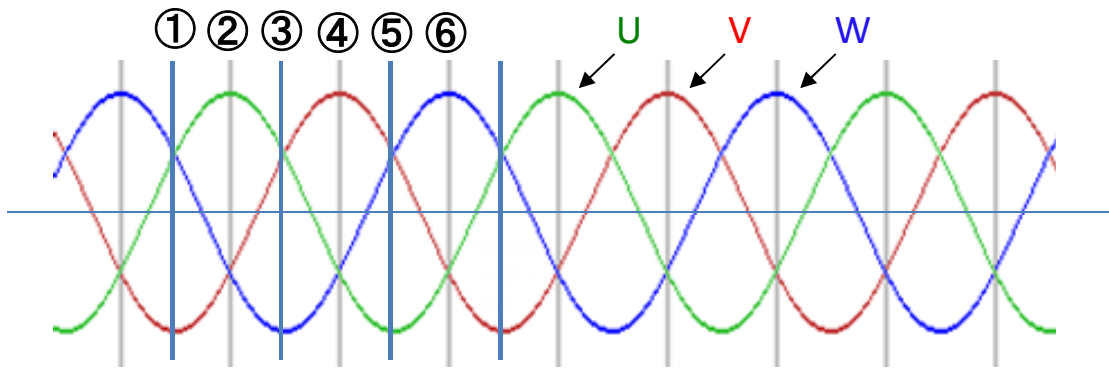


Fig. 6.37 Three-phase alternating current supplied to the propulsion coil

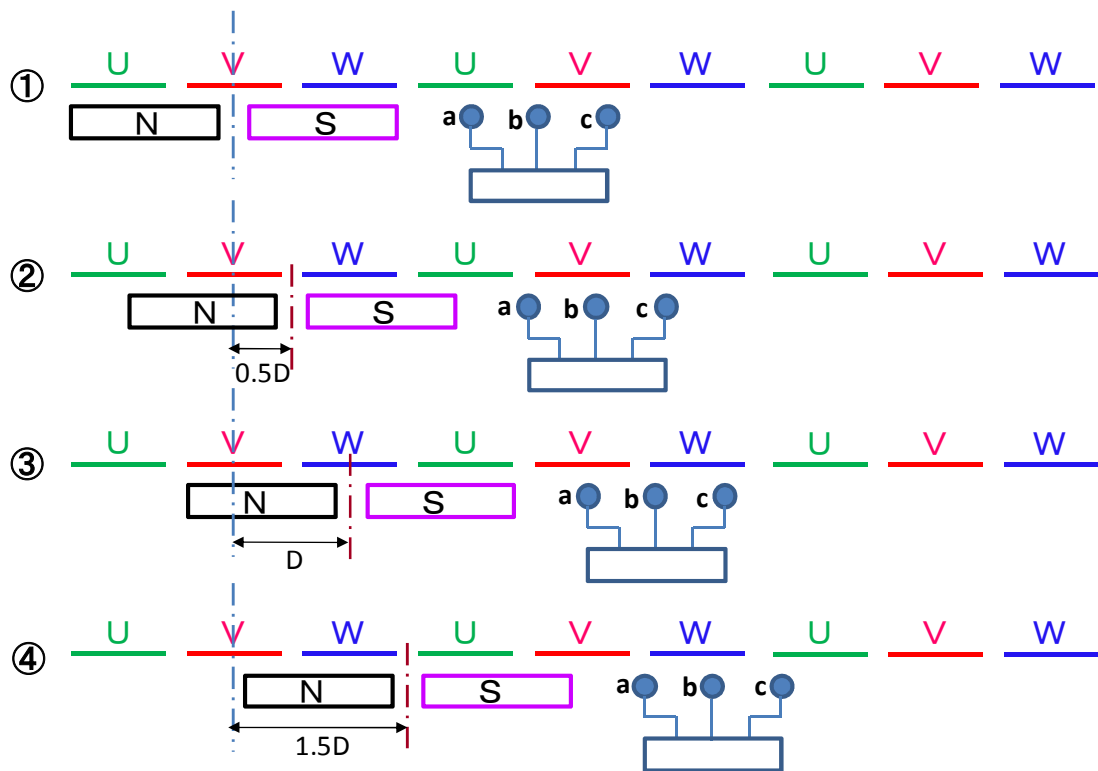


Fig. 6.38 Positional relationship between the vehicle and the voltage phase of the propulsion coil

6.5.5.2 Study of noise removal

Discharged quantity associated with the PD is small in the order of pC (10^{-12} C) and its measurement is easily affected by noises (aerial propagation waves). It is important to consider the method for removing noise effectively. The example studies of noise removal are shown below.

(1) Application of an EM wave shielding material

The actual vehicle simulated mock-up was created (Fig. 6.39) to measure the PD in an environment that includes outdoor noise. As a result, it was confirmed that the combination of an aluminum shielding plate and an EM wave absorbing material simulating the vehicle body removed the noises effectively from the back and sides of the antenna.

(2) Application of digital signal processing

It is possible to extract the frequency components to be acquired by applying a mathematical process to the sampled digital data. The FIR (Finite-duration impulse response) filter was applied as a digital filter. It was confirmed that the main noise component (the communication signal frequency of 867.2MHz) was eliminated. Furthermore, it is presumed that the noise components can be relatively easily removed for commercial operation by examining driving inverters, wireless communication, and on-site specific noise sources.

6.5.5.3 Quantitative estimation of partial discharged quantity

The actual PD management system must determine instantaneously whether the EM wave level of the PD from the ground coil is at a problem level while the vehicle is commercially operated. As described above, the conventional PD measurements evaluated the low-frequency range (15kHz to 150kHz). However, it is necessary to understand the correlation between detected intensity and discharged quantity for detecting the UHF band high-frequency EM waves. There is a plan to evaluate the quantitative PD by preparing a test body and performing the insulation breakdown test by

simultaneous measurement of the aforementioned two methods.

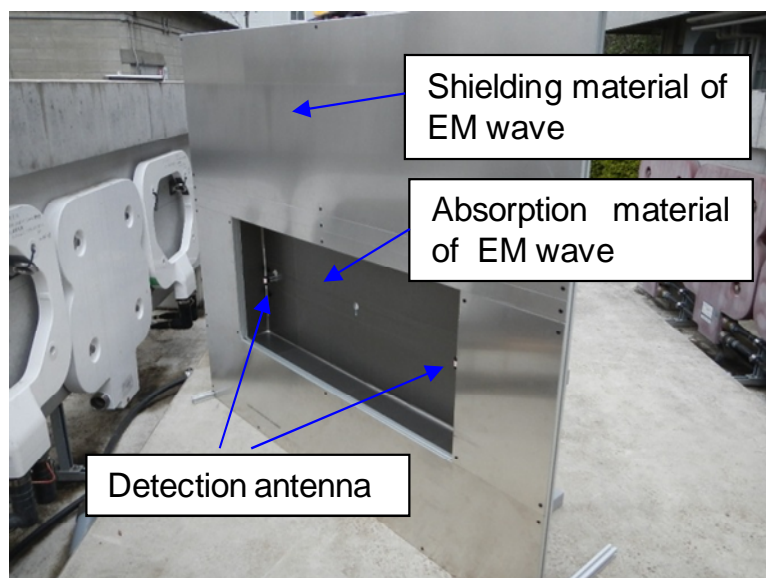


Fig. 6.39 Mock-up of the linear body

6.6 Summary

The propulsion ground coil requires insulation stability as special high-voltage equipment. As there is no means for applying a high voltage to the propulsion coil from the substation while the vehicle is stopped in the current Maglev system, development of effective on-site insulation diagnostic procedures is required.

There is a possibility that the inherent defect factors become apparent by adding load during operation since the ground coil is operated in a special environment. The insulation abnormalities to be considered are voids or foreign substances in the molded resin, conductor exfoliation, peeling of the shield layer, on-site construction failures and other elements.

The defects simulated specimens simulating the various abnormalities were manufactured and the influences on the insulation properties and the chronological change were investigated. The PD was generated for all specimens due to electric field concentration in the vicinity of the defect portions leading to temporal changes in that portion.

There is a possibility that the defect type can be estimated if the defective point can be located from the source of the PD. As a result of position location test by the AE sensor, it was found that the AE sensor was unsuitable for locating defect position of the ground coil due to large attenuation of acoustic waves in the mold resin. As a result of the location test by UHF sensor, it was found that the discharge position near the discharge source was located with relatively high accuracy. However, it was difficult to detect if the sensor was positioned 10cm away from the discharge source.

As a new insulation diagnostic technique, applying a radio interferometer system for evaluating on-site ground coils was examined. First, the effectiveness of this method in the location of discharge source was confirmed by measuring the time delay of the EM wave using the two dipole antennas. The advantage of this method is that it can maintain a large offset distance from the detection antennas to the source of the PD. Then, a similar PD detection in an outdoor environment was performed using the simulated guide-way of the Railway Technical Research Institute. As a result, it was confirmed that the position of the PD generated by the defect simulated coil

was located in spite of receiving influences from external noises. Furthermore, the defect simulated multiple coils were temporarily installed to part of the Miyazaki Test Line for a basic study of PD from the traveling test vehicle to detect PD. As a result, it was confirmed that the multiple antennas on the vehicle detected the EM waves that could be considered as PD from the ground coils and the time delay corresponding to the antenna distance was confirmed.

Assuming future actual commercial operations, the insulation diagnostic configuration capable of detecting abnormal coils from the high-speed traveling vehicle was investigated. Because the Maglev system employs a linear synchronous motor for the primary ground coils, the current phase of the propulsion coils and moving vehicle are synchronized. Therefore, if the EM wave detection antenna is installed to the vehicle, it is possible to adjust the voltage phase of the ground coils so that the voltage phase that generates PD can be easily detected. In addition, it was confirmed that application of the EM wave shielding material to the back and sides of the antenna and the digital signal processing of the sampling data were effective measures for removal of noises at the time of insulation diagnosis.

Chapter 7 Conclusions

This study summarizes the high functionality aimed at reliability improvement and cost reduction, efforts to endurance verification, research results on the insulation diagnostic technology targeting the superconducting Maglev ground coil.

In Chapter 1, I stated the purpose and background of the study and the structure of this paper.

In Chapter 2, the operational environment that is the basic of various designs on the ground coil was examined and specific load of superconducting linear system was indicated. Ground coils that receive mechanical, electrical and environmental composite loads are exposed to a special operational environment. Therefore, when designing the ground coil, it is necessary to scrutinize the operating and environmental conditions over a long time and set appropriate specifications. In particular, one must be careful in considering what molding resin materials is necessary for the integral molding of the coil in terms of not only in the decrease in strength due to environmental impact but also the degradation of specific polymeric material due to various loads.

In Chapter 3, two cases of research and development from different aspects were illustrated in order to reduce the cost of the ground coil. The RIM system coil has a special feature of simplified winding coil configuration and shortened molding cycle. Reduction of the production costs can be expected. The thermally cured molding method by self-heating reaction has advantages for application to the ground coils in the following points in addition to a cost reduction due to its quick molding time.

(1) While having strength equal to or greater than the conventional SMC method, it can reduce the elastic modulus of the resin in half. Consequently, it is possible to reduce the continuous loads such as residual stress, bolt tightening stress, thermal stress significantly.

(2) This coil has a significant advantage to the impact strength compared with the mold for other resins owing to the elastomer component contained in the raw material.

The PLG system coil has an advantage by sharing three functions, propulsion, levitation and guidance in the same coil. It is possible to reduce the required number

of ground coils to half. In the development of practical type PLG coil, the coil configuration was changed from conventional double eight shape to the eight shape and the upper and lower unit coils were configured asymmetrically with the aim of improving characteristics of the lift-to-drag ratio and reduction of the vibration force to SCM. The monolayer arrangement assuming a surface protective layer of PLG coil was developed, and the superior performance of a shock absorbing layer was confirmed.

In Chapter 4, research and development cases for high functionality of the ground coil for increasing performance and reliability were illustrated within a limited cost and design conditions. First, durability improvements in compact linear cable connection unit were developed to enhance its reliability in an environment with EM vibration. In this connection unit, the surface pressure of the insulating surface was increased by a spring mechanism, and the unit was significantly downsized due to reduction of the creepage distance. Similarly, the vibration proof fastening unit based on the comparative evaluation of the fastening models was developed for the bolt fastening portion of the ground coil. The superiority of the laminated FRP bush by the SW process was confirmed due to stress generated in the fastening vicinity being greatly reduced while avoiding bolt looseness. From the viewpoint of reducing the running cost of the system, it is necessary to minimize the eddy currents generated in the conductor of the ground coils. Quantitative evaluation results of eddy current loss using wire samples showed the superiority of a round twisted wire for the ground coil applications. Furthermore, we expect to balance the performance and stabilization of the ground coils and reduction of eddy current loss by applying a compression molding to the winding coil using the selected wire material. In addition, it is necessary to introduce unique management techniques never before utilized in order to maintain a huge number of on-site installed ground coils stably and properly. The basic development of the IT utilizing ground coil maintenance and management system was examined. Development of the IC tag applied ID management method provided prospect for an effective and simplified reliable ID management system for commercial operation. Then, the ultimate coil self monitoring and diagnostic system to detect, forecast and transmit the abnormality prior to initiating any problems was verified. The

dimensions of the power supply of the sensing unit were reduced following the conceptual design. Concerning the independent operation of abnormality sensor embedded into the ground coil, the outlook for functional forecast was obtained. The development challenges for the future shall be the establishment of the precise determination method by enhancing the reliability of the detection of abnormalities for a large number of objects according to the self-diagnostic method. On the other hand, the increase in the performance of the molded resin material is required by improving the reliability of the ground coils, because the molded epoxy resin having hard but fragile physical properties shall be applied to the ground coil with air-core structure. Therefore low elastic core-shell particles were arranged with resin that provided the prospect of improving greatly the toughness of the epoxy resin.

In Chapter 5, research and development cases for the durability verification for actual commercial operation from materials to the actual coil were illustrated. First, basic configuration of durability verification and mutual equality were considered, and verification methods unique to ground coils were systematized. Then, the environmental degradation factors of the molding resin material were examined. The degradation progress was not uniform in the thickness direction and was limited to the surface layer. Furthermore, the resin block simulating the cross-sectional shape of the ground coil was also created and the water absorption characteristic with a parameter of the immersion temperature was acquired. Then, the reaction kinetics was verified by the time to reach to the certain water absorption ratio and the immersion temperature based on the water absorption characteristics. As a result, it was confirmed that the correlation between the two elements followed the Arrhenius law substantially. The effectiveness of the application of this correlation to set the accelerated aging conditions necessary to evaluate the long-term durability in short time was confirmed. In addition, the evaluation method for the fatigue strength of mold resin material that took into account the actual operational environment of the ground coil was verified. As a result, the common assessment method for the fatigue strength used in metal and other materials was not applicable and the need of a strength evaluation method specific to the mold resin material

was indicated. The durability verification for the actual coil was also demonstrated. The verification of dynamic durability in consideration of the actual operational environments of the ground coil was essential. Therefore, the ground coil EM vibration equipment simulating the real traveling stationary was developed. It was confirmed that the dynamic durability of the coil fastening and cable connection portions could be verified effectively. In addition, we have developed the weathering test equipment of ultra-promotion type for ground coil intended to measure long-term outdoor use. This instrument makes it possible to facilitate magnification of about 100 times of outdoor exposure by greatly increasing the emission efficiency of the ultraviolet region that affects the degradation of the molding resin material while satisfying the equivalence to the actual use. In addition, as a thermal durability verification, the long-term outdoor power supply test which was applied to the development test for the cable connection part was applied to the heat cycle load for the propulsion coil. This verification test assuming the electrical load during commercial operation will be an effective verification means including screening for defects in the insulation design of the development phase. There is an urgent need to establish the durability inspection criteria and verification method in order to cope with the development of new functional materials and high-performance ground coils, the need growing more and more.

In Chapter 6, examples of research and development concerning the effective insulation diagnostic technique for the propulsion coil that requires insulation stability as special high-voltage equipment were illustrated. First, the insulating abnormalities to be considered in actual operation were enumerated. Then simulated defect specimens assuming abnormalities were provided to investigate the effect on the insulating characteristics and chronological degradation. Then, various non-destructive testing methods for identifying PD generated at the defect part were verified and compared for their advantages and disadvantages. As a result, it was found that the location test using AE or UHF sensors, which were commonly able to detect PD, were unsuitable for locating the defect of the ground coil due to limited sensing distance from the discharge source. In addition, as a new insulation diagnostic technique, applying a radio interferometer system for evaluating

on-site ground coils was examined. First, the effectiveness of this method in the location of discharge source was confirmed by measuring the time delay of the EM wave using the two dipole antennas. The advantage of this method is that it can maintain a large offset distance from the detection antennas to the source of the PD. Furthermore, the basic tests for detecting PD generated from the ground coils were conducted through traveling test vehicles at the Miyazaki Test Line after completion of the basic preliminary studies in an outdoor environment in order to verify the effectiveness of this diagnostic method. As a result, it was confirmed that the multiple antennas on the vehicle detected the EM waves emitted from PD in the ground coils. Based on these results, the insulation diagnosis configuration capable of detecting abnormal coil from a high-speed traveling vehicle was studied assuming future commercial operations. Because the Maglev system uses a linear synchronous motor whose primary windings are connected to a power source on the ground side, it is possible to align the antenna for detecting EM waves on the vehicle with the voltage phase where the PD from the ground coil may be generated. This is believed to be the dominant condition for applying this diagnostic method. In addition, it was confirmed that application of the EM wave shielding material to the back and sides of the antenna and the digital signal processing of the sampling data were effective measures for removal of noises at the time of insulation diagnosis. From the experimental results, the prospect of the establishment of an effective insulation diagnosis that can evaluate the on-site state of the ground coils was obtained.

References

Chapter 1

- [1] K. Nagashima, "Story of friendly superconducting Maglev (part 1)," Superconductivity web 21, pp.1-3 (2011-2) (in Japanese)
- [2] M. Suzuki, "Durability Evaluation of Ground Coils for Superconducting Magnetically Levitated Transportation System," TEST, Vol.12, pp.3-6 (2009-7) (in Japanese), Japan Testing Machinery Association

Chapter 2

- [1] S. Fujiwara and T. Fujimoto, "Characteristics of the Combined Levitation and Guidance System Using Ground Coils on the Side Wall of the Guideway," RTRI REPORT, Vol.3, No.11, pp.16-21 (1989.11) (in Japanese)
- [2] S. Fujiwara and T. Fujimoto, "Influence of the superconducting coil shape in side wall levitation system," The 1990 IEEJ Annual Meeting Record, 7-771, (1990-3)

Chapter 3

- [1] M. Suzuki, "Cost reduction of ground coils," RRR of RTRI, Vol.58, No.9, pp.11-14 (2001-9) (in Japanese)
- [2] M. Yamato and K. Okumura, "ZEON-RIM system and PENTAM," Reinforced Plastics, Vol.36, No.1, pp.22-27 (1988-1) (in Japanese), JRPS
- [3] M. Kagawa, M. Niimura, and M. Yamato, "Development of a RIM system as a raw material DCPD," NIKKEI NEW MATERIALS 19, pp.61-70 (1989-6) (in Japanese)
- [4] M. Yamato, "RIM Method," MACROMOLECULAR Vol.39, pp.434-435 (1990-6) (in Japanese)
- [5] M. Suzuki, T. Yoshikawa, H. Suwa, and T. Fujimoto, "Development of the ground

- coil by RIM method,” RTRI REPORT, Vol.7, No.9, pp.53-58 (1993.9) (in Japanese)
- [6] M. Suzuki, K. Hirata, T. Yoshikawa, and M. Yamato, “Development of the Ground Coil by RIM Method,” Proc. of the International Conference on Speedup Technology for Railway and Maglev Vehicles of JSME. 1, pp.156-161, Yokohama, Japan, (1993)
- [7] M. Suzuki and T. Yoshikawa, “Development of the Ground Coil by RIM Method,” QR of RTRI, Vol.35, No.3, pp.178-184 (1994-8)
- [8] M. Suzuki, T. Yoshikawa, T. Fujimoto, M. Torii, and A. Nishibe, “DEVELOPMENT OF A LOW COST GROUND COIL BY RIM METHD,” Proc. of 4th Japan International SAMPE Symposium, pp.1240-1245 (1995-9)
- [9] M. Suzuki, K. Sawada, T. Fujimoto, Y. Nakamura, and N. Aihara, “Development of a low cost ground coil by RIM method,” RTRI REPORT, Vol.10, No.1, pp.41-46 (1996-1) (in Japanese)
- [10] M. Suzuki, T. Fujimoto, K. Sawada, and N. Aihara, “Development of practical ground coil by RIM method,” Proc. of the 29th International SAMPE Technical Conference, Orland, FL. pp.375-382 (1997-10)
- [11] M. Suzuki, T. Fujimoto, and H. Suwa, “Development of Levitation Coil by Reaction Injection Molding Method,” RTRI REPORT, Vol.13, No.9, pp.9-14 (1999.9) (in Japanese)
- [12] M. Suzuki, T. Fujimoto, and H. Suwa, “Development of Levitation Coil by Reaction Injection Molding Method,” QR of RTRI, Vol.41, No.2, pp.57-62 (2000-6)
- [13] M. Suzuki and T. Fujimoto: “Durability Verification of the Practical Ground Coil by RIM Method,” 8th International Conference on Composite or Nano Engineering, Tenerife, Spain (2001-8)
- [14] M. Suzuki and T. Fujimoto, “Durability Verification of the Ground Coil by RIM Method,” 8th Jointed Railway Technology Symposium (2001-12) (in Japanese)
- [15] T. Fujimoto, T. Murai, and M. Suzuki, “Development of combined Propulsion, Levitation and Guidance coil in EDS Maglev,” Proc. of the 16th International Conference on Magnetically Levitated Systems and Linear Drives, Rio de Janeiro, Brazil pp.275-280 (2000-6)
- [16] T. Murai, M. Aiba, H. Suzuki, M. Suzuki, T. Fujimoto, K. Umeki, and H. Natsuhara, “Characteristics of Null-Flux EDS with an Asymmetric Figure,” RTRI REPORT, Vol.14, No.11, pp.5-10 (2000.11) (in Japanese)
- [17] M. Aiba and M. Suzuki, “Durability Verification of Combined Propulsion, Levitation and Guidance Ground Coil,” RTRI REPORT, Vol.19, No.6, pp.19-24

(2005.6) (in Japanese)

- [18] M. Suzuki, M. Aiba, M. Tanaka, and S. Okada, "Fundamental Development of the PLG Coil with a Surface Protection Layer," Proc. of the 12th Jointed Railway Technology Symposium, pp.21-22 (2005-12) (in Japanese)
- [19] M. Aiba, M. Suzuki, M. Tanaka, and S. Okada, "Development of the Ground Coil Combining Propulsion, Levitation and Guidance with a Surface Protection Layer for the Maglev System," Proc. of the 14th Jointed Railway Technology Symposium, pp.319-320 (2007-12) (in Japanese)
- [20] N. Takahashi and M. Suzuki, "The shock strength evaluation of a ground coil with the protective layer," Proc. of the 16th Jointed Railway Technology Symposium, pp.413-414 (2009-12) (in Japanese)
- [21] M. Suzuki, M. Aiba, and N. Takahashi, "Development of the PLG Coil with a Surface Protection Layer for Maglev System," Proc. of the 18th International Conference on Composite or Nano Engineering, pp.715-716 Anchorage, Alaska, USA (2010-7)

Chapter 4

- [1] M. Aiba, T. Murai, M. Suzuki, and N. Takahashi, "Development of the Ground Coil for Practical Use by the Combined Propulsion, Levitation and Guidance System for the Superconducting Maglev," Proc. of the 10th Jointed Railway Technology Symposium, pp.313-316 (2003-12)
- [2] M. Suzuki, H. Suzuki, M. Aiba, H. Matsue, M. Tanaka, and S. Okada, "Development of the Vibration-proof Fixing Part for Ground Coil," Proc. of the 13th Jointed Railway Technology Symposium, pp.265-266 (2006-12) (in Japanese)
- [3] M. Suzuki, H. Suzuki, M. Aiba, H. Matsue, and S. Okada, "Development of the Vibration-proof Fixing Part for Ground Coil," 15th International Conference on Composite or Nano Engineering, Hainan, China (2007-7)
- [4] H. Matsue, M. Aiba, and M. Suzuki, "Stress Evaluation on the PLG Ground Coil with FRP Fastening Devices," RTRI REPORT, Vol.22, No.11, pp.17-22 (2008.11) (in Japanese)
- [5] T. Fujimoto, "Measurement of Magnetic Drag Force of Metals in Track Caused by Eddy Currents," RTRI REPORT Vol.5, No.4 pp.3-10 (1991.4) (in Japanese)

- [6] Morisawa, "AC Theory," Electrical Shoin pp.453 (1974) (in Japanese)
- [7] M. Suzuki, M. Aiba, N. Takahashi, and S. Ota, "Development of Low Eddy Current Loss Ground Coil Which Applied Compression Molding by Winding Coils," Proc. of the 17th Jointed Railway Technology Symposium, pp.157-158 (2010-12) (in Japanese)
- [8] A. Komura, Y. Furukawa, K. Hattori, H. Fukumoto, S. Tsujimoto, H. Tsuruga, M. Terai, and K. Umeki, "Development of Low Loss Type Levitation Coil with Strand Wires and Estimation of Loss in Levitation Coil", pp.25-30, LD-98-82 (1998.12) (in Japanese)
- [9] M. Aiba and M. Suzuki, "Reduction of Eddy Current Loss of Ground Coil Winding for the Maglev System by Compression Molding," Proc. of the 16th Jointed Railway Technology Symposium, pp.357-358 (2009-12) (in Japanese)
- [10] M. Suzuki, M. Aiba, N. Takahashi, S. Ota, and S. Okada, "Development of Ground Coils with Low Eddy Current Loss by Applying the Compression Molding Method after the Coil Winding," IEEJ Trans. on Industry Applications, Vol.132, No.2, pp185-193 (2012-2) (in Japanese)
- [11] M. Suzuki, M. Aiba, M. Tanaka, and S. Ota, "Development of the Maintenance Management Method for Ground Coil Applied Information Technology," RTRI REPORT, Vol.24, No.1, pp.17-22 (2010.1) (in Japanese)
- [12] M. Suzuki, M. Aiba, and M. Tanaka, "Development of the Individual Information Management Device Application to IC Tag for Ground Coil," Proc. of the 14th Jointed Railway Technology Symposium, pp.605-606 (2007-12) (in Japanese)
- [13] M. Tanaka, N. Takahashi, M. Suzuki, R. Ikeda, and S. Nagasaka, "Development of the On-board Maintenance Management System for Ground Coils of Maglev by Using RFID Technology," RTRI REPORT, Vol.25, No.3, pp.29-34 (2011.3) (in Japanese)
- [14] S. Ota and M. Aiba, "Downsizing of Power Unit for a Detection Sensor of Ground Coil Abnormalities," Proc. of the 16th Jointed Railway Technology Symposium, pp.315-316 (2009-12) (in Japanese)
- [15] M. Tanaka, S. Ota, M. Aiba, and M. Suzuki, "Development of a Power Supply Unit for an Anomaly Detection Sensor in a Ground Coil," Proc. of the 2010 Japan Industry Applications Society Conference, 257-258 (2010-8) (in Japanese)
- [16] M. Tanaka and M. Suzuki, "Development of Power Supply Unit for Anomaly Detection Sensor in Ground Coils of superconducting Maglev," RTRI REPORT,

Chapter 5

- [1] T. Fujimoto, "Verify the durability of the ground coil," RRR of RTRI, Vol.58, No.9, pp.4-7 (2001-9) (in Japanese)
- [2] M. Suzuki, "Environmental Degradation Characteristics of the Mold Resin for Ground Coil," RTRI REPORT, Vol.20, No.8, pp.23-28 (2006.8) (in Japanese)
- [3] Y. Kanuma, "How to Proceed Efficiently Reliability Accelerated Test, and Its Actual," Nippon Techno Center, pp.35-38 (1997-10) (ISBN4- 931443-00-1 C3050)
- [4] M. Suzuki, "Durability Verification of the Ground Coil," Proc. of the 146th Monthly Presentation of the RTRI, pp.30-33 (2002.1)
- [5] M. Suzuki, T. Fujimoto, and H. Ishihara, "Durability Verification of the Practical Ground Coil for Propulsion," Paper number: PP05105 the 17th International Conference on Magnetically Levitated Systems and Linear Drives, Lausanne, Switzerland (2002.9)
- [6] H. Suzuki, M. Suzuki, and N. Aihara, "Durability Evaluation Tests of Mold Resin for Ground Coil," RTRI REPORT, Vol.21, No.9, pp.17-22 (2007.9) (in Japanese)
- [7] M. Tanaka, M. Aiba, and M. Suzuki, "Development of Electromagnetic Vibration Test Apparatus to Verify Durability of Ground Coils," RTRI REPORT, Vol.20, No.8, pp.17-22 (2006.8) (in Japanese)
- [8] M. Suzuki, "Dynamic durability verification of the ground coil by electromagnetic vibration test," RRR of RTRI, Vol.64, No.12, pp.28-31 (2007-12) (in Japanese)
- [9] M. Suzuki, S. Ota, and N. Takahashi, "Dynamic Durability Examination of Cable Connection for Propulsion Ground Coils," The 2012 IEEJ Annual Meeting Record, 5-160, (2012-3)
- [10] M. Suzuki, "Durability Evaluation of Ground Coils for Superconducting Magnetically Levitated Transportation System," TEST, Vol.12, pp.3-6 (2009-7) (in Japanese), Japan Testing Machinery Association
- [11] M. Aiba and M. Suzuki, "A Long Duration Dielectric Test with Current Flow of the Ground Coils for the Maglev System," The 2005 IEEJ Annual Meeting Record, 5-205, (2005-3)

Chapter 6

- [1] M. Suzuki, S. Ota, R. Ikeda, and M. Kawada, "Internal Defect Position Evaluation of Ground Coil by Detecting Electromagnetic Waves from Partial Discharge," *IEEJ Trans. on Fundamentals and Materials*, Vol.133-A, No.5, pp.307-312, (2013-5)
- [2] M. Suzuki, S. Ota, R. Ikeda, and M. Kawada, "Study on Locating Internal Defect of Ground Coil by Detecting Electromagnetic Waves," *RTRI REPORT*, Vol.27, No.7, pp.11-16 (2013.7) (in Japanese)
- [3] M. Suzuki, "Long-term Insulation Test of Ground Coil Mock-up with Artificial Defects," *Proc. of the 1998 National Convention Record IEEJ*, III-266 (1998-8) (in Japanese)
- [4] M. Suzuki, M. Aiba, and S. Ota, "Partial Discharge Characteristics of Ground Coil / Cable Joint which Simulated an Interfacial Abnormality," *The 2009 IEEJ Annual Meeting Record*, 5-059, (2009-3)
- [5] M. Suzuki, H. Matsue, and M. Aiba, "Partial Discharge Characteristics of Ground Coil Simulated Inside Defect," *The 2007 IEEJ Annual Meeting Record*, 5-281, (2007-3)
- [6] S. Ota and M. Suzuki, "Examination of Defect Estimation within Ground Coil for Superconducting Maglev," *The 19th MAGDA Conference* (2010-11)
- [7] M. Kawada, Z. Kawasaki, K. Matsuura, and M. Kawasaki, "Non-Contact Detection of Electromagnetic Noise Occurrence due to Partial Discharges by Spatial Phase Difference Method," *T.IEEJ*, Vol.115-B, No.10, pp.1168-1173, 1995
- [8] M. Kawada, "Fundamental Study on Locating Partial Discharge Source Using VHF-UHF Radio Interferometer System," *IEEJ Trans. on Power and Energy*, vol.122-B, No.5, pp.629-636, 2002
- [9] M. Kawada, Z. Kawasaki, K. Matsuura, S. Kuroki, T. Osawa, and H. Tanaka, "On-Line Partial Discharge Detection of Turbine Generator using GHz-Band Spatial Phase Difference Method," *IEEJ Trans. on Power and Energy*, vol.118-B, No.11, pp.1243-1248, (1998)
- [10] M. Kawada, Z. Kawasaki, K. Matsuura, S. Kuroki, T. Osawa, H. Tanaka, and T. Musashiya, "Insulation Diagnosis Method for the Generator Winding by Measuring Microwave Associated with Dielectric Breakdown," *IEEJ Trans. on Power and Energy*, vol.118-B, No.3,

- pp274-281, (1998)
- [11] M. Kawada, M. Suzuki, and S. Ota, "Measurement of Electromagnetic Waves Emitted from Partial Discharge Generated in PLG Type Ground Coil for Superconducting Maglev," Proc. of the 30th IEEE Electrical Insulation Conference, pp.412-416, Annapolis, MD, USA, (2011-6).
 - [12] M. Suzuki, S. Ota, R. Ikeda, and M. Kawada, "Internal Defect Position Evaluation of the Ground Coil by Detecting the Electromagnetic Waves from the Partial Discharge," Proc. of 2011 International Symposium on Electrical Insulating Materials, pp.181-184, Kyoto, Japan, (2011-9).
 - [13] M. Kawada, M. Suzuki, and S. Ota, and R. Ikeda, "Locating Partial Discharge Generated in PLG Type Ground Coil for Superconducting Maglev Using Radio Interferometer System," Conference Record of the 2012 IEEE International Symposium on Electrical Insulation, pp.99-103, San Juan, Puerto Rico, (2012-6).
 - [14] M. Suzuki, R. Ikeda, N. Takahashi, M. Tanaka, and M. Kawada, "Examination of Insulation Diagnosis for Ground Coil by Detecting Partial Discharge in Maglev System," Proc. of 2012 Annual Conference Fundamentals and Materials Society IEEJ, pp.389-394, Akita, (2012-9) (in Japanese)
 - [15] "Frequency Book," Three powers books, 2000
 - [16] M. Kawada, M. Suzuki, and R. Ikeda, "Location of Partial Discharge Occurring in Ground Coil of Superconducting Maglev System under Noise Environment using Radio Interferometer System," Proc. of the 31st IEEE Electrical Insulation Conference, pp.142-146, Ottawa, Canada, (2013-6).

Acknowledgment

I deeply appreciate Masatake Kawada, Associate Professor at the University of Tokushima, who gave me the opportunity to write this thesis and advised me with numerous, polite and kind guidance to summarize this paper. I also deeply appreciate Professor Naoyuki Shimomura, Professor Masaki Hashizume, Professor Takashi Yasuno, at the University of Tokushima for the continued opinions and criticism concerning the contents of this paper.

This paper summarizes the results of research that I was involved in Maglev ground coils consistently for about 25 years while I have been a member of the Levitated Railway Laboratory of Railway Technical Research Institute. This paper was achieved with direct and indirect support by everyone, especially the executives of Railway Technical Research Institute whom I have been blessed with and given me a place to do research activities.

In particular, I appreciate Dr. Shunsuke Fujiwara, the chief at the time, who had guided the EM force characteristics and Maglev system since I was assigned to the laboratory.

In addition, I sincerely appreciate the great support of Mr. Hiroshi Nakashima, Mr. Kanichiro Kaminishi, Mr. Kazuo Sawada, General Manager of the Maglev Development Division, Mr. Hiroshi Suwa, manager of the Electromagnetic Guide-way Division, Mr. Kiyoshi Takahashi, manager of the Researching Division, Mr. Tsutomu Furuki, manager of the engineering Division, Mr. Kunio Hirata, Mr. Tsuyoshi Fujimoto, Laboratory Head, Dr. Toshiaki Murai, Senior Researcher and everyone of the Maglev Development Division at the time of execution of this studies over the years.

In addition, I appreciate Dr. Takashi Sasakawa, Mr. Masayuki Aiba, Mr. Hiroyuki Suzuki, Mr. Noriyuki Takahashi, Mr. Hitoshi Matsue, Dr. Minoru Tanaka, Mr. Satoru Ota, Mr. Ryohei Ikeda, and those involved with TESS Ltd. for their great cooperation at the time of practical implementation of the research.

I furthermore deeply appreciate Dr. Fuminao Okumura, Executive

Director of the Railway Technical Research Institute, Dr. Kimitoshi Ashiya, Director of the Research and Development Promotion Division, Dr. Masaru Iwamatsu, Deputy Director of the Planning Division, Dr. Ken Nagashima, Director of the Maglev System Technology Division, Mr. Masahiko Nakauchi and Mr. Shingo Matsumoto, Planning Division of the Yamanashi Maglev Test Center, for their understanding and great consideration in order to summarize a series of studies for this paper.

Finally, I express great gratitude to my family, my wife Yasuko, my son Yutaka and my daughter Miho for their understanding and cooperation for my preparation efforts for this paper.

This study had been financially supported in part from the Ministry of Land, Infrastructure, Transport and Tourism of Japanese Government, and JSPS KAKENHI Grant Number 24560335.

List of Publications

Original papers on this thesis

[A] Transactions and Journals

- [1] Y. Nakamichi, H. Shigeeda, K. Ajiki, and M. Suzuki, “Surge Characteristics of Propulsion Coils Including Mutual Coupling for Maglev,” IEEJ Trans. on Industry Applications, Vol.119, No.11, pp.1315-1326 (1999-11) (in Japanese)
- [2] M. Suzuki, “Durability Evaluation of Ground Coils for Superconducting Magnetically Levitated Transportation System,” TEST, Vol.12, pp.3-6 (2009-7) (in Japanese), Japan Testing Machinery Association
- [3] M. Suzuki, M. Aiba, N. Takahashi, S. Ota, and S. Okada, “Development of Ground Coils with Low Eddy Current Loss by Applying the Compression Molding Method after the Coil Winding,” IEEJ Trans. on Industry Applications, Vol.132, No.2, pp.185-193 (2012-2) (in Japanese)
- [4] M. Suzuki, S. Ota, R. Ikeda, and M. Kawada, “Internal Defect Position Evaluation of Ground Coil by Detecting Electromagnetic Waves from Partial Discharge,” IEEJ Trans. on Fundamentals and Materials, Vol.133-A, No.5, pp.307-312, (2013-5)

[B] International Conferences

- [1] M. Suzuki, K. Hirata, T. Yoshikawa, and M. Yamato, “Development of the Ground Coil by RIM Method,” Proc. of the International Conference on Speedup Technology for Railway and Maglev Vehicles of JSME. 1, pp.156-161, Yokohama, Japan, (1993)
- [2] M. Suzuki, T. Yoshikawa, T. Fujimoto, M. Torii, and A. Nishibe, “DEVELOPMENT OF A LOW COST GROUND COIL BY RIM METHD,” Proc. of 4th Japan International SAMPE Symposium, Harumi, Japan, pp.1240-1245

- (1995-9)
- [3] M. Suzuki, T. Fujimoto, K. Sawada, and N. Aihara, "Development of practical ground coil by RIM method," Proc. of the 29th International SAMPE Technical Conference, Orland, FL. pp.375-382 (1997-10)
 - [4] T. Fujimoto, T. Murai, and M. Suzuki, "Development of combined Propulsion, Levitation and Guidance coil in EDS Maglev," Proc. of the 16th International Conference on Magnetically Levitated Systems and Linear Drives, Rio de Janeiro, Brazil pp.275-280 (2000-6)
 - [5] M. Suzuki and T. Fujimoto, "Durability Verification of the Practical Ground Coil by RIM Method," 8th International Conference on Composite or Nano Engineering, Tenerife, Spain (2001-8)
 - [6] M. Ando, Y. Nakamichi, K. Ajiki, H. Shigeeda, and M. Suzuki, "Simulation Model for Surge Propagation of Propulsion Coils for Maglev," 5th World Congress on Railway Research, Cologne, Germany (2001-11)
 - [7] M. Suzuki, T. Fujimoto, and H. Ishihara, "Durability Verification of the Practical Ground Coil for Propulsion," Paper number: PP05105 the 17th International Conference on Magnetically Levitated Systems and Linear Drives, Lausanne, Switzerland (2002.9)
 - [8] Y. Jizo, K. Yoshikawa, and M. Suzuki, "Outline of the Ground Coils for the Yamanashi Test Line," 11st US-Japan Conference on Composite Materials & TEXCOMP-7, Yamagata, Japan (2004-9)
 - [9] M. Aiba, T. Murai, M. Suzuki, and N. Takahashi, "Development of the Ground Coil for Practical Use by the Combined Propulsion, Levitation and Guidance System," Proc. of the 18th International Conference on Magnetically Levitated Systems and Linear Drives, Shanghai, China pp.849-855 (2004-10)
 - [10] M. Tanaka, M. Aiba, and M. Suzuki, "Development of Electromagnetic Vibration Apparatus for Ground Coils of Maglev," 7th World Congress on Railway Research, Montreal, Canada (2006-6)
 - [11] K. Takahashi, A. Inoue, and M. Suzuki, "Diagnosis and Evaluation Technique for Superconducting Magnet and Ground Coils," 19th International Conference on Magnetically Levitated Systems and Linear Drives, Dresden, Germany (2006-9)
 - [12] M. Tanaka, M. Suzuki, and M. Aiba, "Electromagnetic Vibration Test for

- Durability Verification of Ground Coil,” 19th International Conference on Magnetically Levitated Systems and Linear Drives, Dresden, Germany (2006-9)
- [13] M. Suzuki, H. Suzuki, M. Aiba, H. Matsue, and S. Okada, “Development of the Vibration-proof Fixing Part for Ground Coil,” 15th International Conference on Composite or Nano Engineering, Hainan, China (2007-7)
- [14] H. Matsue, M. Aiba, and M. Suzuki, “Stress Evaluation of the PLG Ground Coil Inserted GFRP Fastening Devices,” 20th International Conference on Magnetically Levitated Systems and Linear Drives, San Diego, USA (2008-12)
- [15] H. Matsue, M. Aiba, and M. Suzuki, “Stress Evaluation of the PLG Ground Coil with GFRP Fastening Devices,” The 9th International Conference on Speedup Technology for Railway and Maglev Vehicles of JSME. Niigata, Japan, (2009-6)
- [16] M. Suzuki, M. Aiba, and N. Takahashi, “Development of the PLG Coil with a Surface Protection Layer for Maglev System,” Proc. of the 18th International Conference on Composite or Nano Engineering, pp.715-716 Anchorage, Alaska, USA (2010-7)
- [17] M. Kawada, M. Suzuki, and S. Ota, “Measurement of Electromagnetic Waves Emitted from Partial Discharge Generated in PLG Type Ground Coil for Superconducting Maglev,” Proc. of the 30th IEEE Electrical Insulation Conference, pp.412-416, Annapolis, MD, USA, (2011-6).
- [18] M. Suzuki, S. Ota, R. Ikeda, and M. Kawada, “Internal Defect Position Evaluation of the Ground Coil by Detecting the Electromagnetic Waves from the Partial Discharge,” Proc. of 2011 International Symposium on Electrical Insulating Materials, pp.181-184, Kyoto, Japan, (2011-9).
- [19] N. Takahashi, M. Suzuki, and M. Aiba, “Development of Ground Coil Type of PLG for Maglev,” 21st International Conference on Magnetically Levitated Systems and Linear Drives, Daejeon, Korea (2011-10)
- [20] M. Kawada, M. Suzuki, and S. Ota, and R. Ikeda, “Locating Partial Discharge Generated in PLG Type Ground Coil for Superconducting Maglev Using Radio Interferometer System,” Conference Record of the 2012 IEEE International Symposium on Electrical Insulation, pp.99-103, San Juan, Puerto Rico, (2012-6).

- [21] M. Tanaka, M. Suzuki, N. Takahashi, and R. Ikeda, "RFID Based Maintenance Management System for Ground Coils of Superconducting Maglev," IEEE International Conference on RFID-Technology and Applications 2012, pp.330-334, Nice, France, (2012-11)
- [22] M. Kawada, M. Suzuki, and R. Ikeda, "Location of Partial Discharge Occurring in Ground Coil of Superconducting Maglev System under Noise Environment using Radio Interferometer System," Proc. of the 31st IEEE Electrical Insulation Conference, pp.142-146, Ottawa, Canada, (2013-6).

[C] Domestic Conferences

- [1] M. Suzuki, "Composite Degradation of Propulsion Coil for Magnetically Levitated Transportation System," The 1996 IEEJ Annual Meeting Record, 5-158, (1996-3) (in Japanese)
- [2] M. Suzuki, "Thermal Dependence on Insulation Characteristic of the Ground Coil for Propulsion," The 1997 IEEJ Annual Meeting Record, 2-214, (1997-3) (in Japanese)
- [3] T. Murai, T. Fujimoto, and M. Suzuki, "Electromagnetic Force acting on the Superconducting Coil to the Propulsion Coil Short-circuit," 9th Symposium on Electromagnetics and Dynamics, Sapporo, (1997-6) (in Japanese)
- [4] M. Suzuki, "Long-term Insulation Test of Ground Coil Mock-up with Artificial Defects," Proc. of the 1998 National Convention Record IEEJ, III-266 (1998-8) (in Japanese)
- [5] M. Suzuki, and H. Suzuki, "Transformation on Insulation Characteristic of the Ground Coils for Actual Use," The 1999 IEEJ Annual Meeting Record, 2-164, (1999-3) (in Japanese)
- [6] M. Ando, K. Ajiki, H. Shigeeda, Y. Nakamichi, and M. Suzuki, "Fundamental Study on Surge Characteristics between Propulsion Coil and Levitation Coil for Maglev," Proc. of the 6th Jointed Railway Technology Symposium, (1999-12) (in Japanese)
- [7] M. Ando, K. Ajiki, H. Shigeeda, Y. Nakamichi, and M. Suzuki, "Surge Characteristics between Propulsion Coils through Levitation Coils for Maglev," The 2000 IEEJ Annual Meeting Record, (2000-3) (in Japanese)

- [8] M. Aiba, T. Murai, M. Suzuki, T. Fujimoto, T. Herai, and K. Nagashima, "The Electromagnetic Vibration Test of a Ground Coil by Using the Magnetic Field of Superconducting Magnets," Linear Drive Joint Seminar of Superconducting Power Equipment, (2001-1) (in Japanese)
- [9] M. Suzuki, and T. Fujimoto, "Degradation Characteristics by Water Absorption on the Ground Coil for Propulsion," The 2001 IEEEJ Annual Meeting Record, 5-248, (2000-3) (in Japanese)
- [10] M. Aiba, T. Murai, M. Suzuki, T. Fujimoto, T. Herai, and K. Nagashima, "The Electromagnetic Vibration Test of a Ground Coil by Using the Magnetic Field of Superconducting Magnets," 13th Symposium on Electromagnetics and Dynamics, Chiba, (2001-6) (in Japanese)
- [11] M. Suzuki and T. Fujimoto, "Durability Verification of the Ground Coil by RIM Method," 8th Jointed Railway Technology Symposium (2001-12) (in Japanese)
- [12] M. Aiba, T. Murai, M. Suzuki, and N. Takahashi, "Development of the Ground Coil for Practical Use by the Combined Propulsion, Levitation and Guidance System for the Superconducting Maglev," Proc. of the 10th Jointed Railway Technology Symposium, pp.313-316 (2003-12) (in Japanese)
- [13] M. Tanaka, M. Aiba, T. Murai, and M. Suzuki, "A Study on the Durability Test of a Propulsion Coil Using an Electromagnetic Vibration Apparatus, The 11th Jointed Railway Technology Symposium, (2004-12) (in Japanese)
- [14] M. Aiba, T. Murai, M. Suzuki, and N. Takahashi, "Development of a 120-degree-pitch Ground Coil of the Combined Propulsion, Levitation and Guidance System," Linear Drive Joint Seminar of Semiconductor Power Conversion, (2004-12) (in Japanese)
- [15] M. Aiba and M. Suzuki, "A Long Duration Dielectric Test with Current Flow of the Ground Coils for the Maglev System," The 2005 IEEEJ Annual Meeting Record, 5-205, (2005-3) (in Japanese)
- [16] M. Tanaka, M. Aiba, M. Suzuki, and H. Suzuki, "Electromagnetic Vibration Test of Ground Coil combining Propulsion, Levitation and Guidance by Using Magnetic Field of Superconducting Magnets," Proc. of the 17th Symposium on Electromagnetics and Dynamics, pp.77-78 (2005-6) (in Japanese)
- [17] M. Aiba and M. Suzuki, "Soundness Evaluation of Combined Propulsion,

- Levitation and Guidance Coils for the Maglev System,” Proc. of the 2005 Japan Industry Applications Society Conference, pp.III-277-278 (2005-8) (in Japanese)
- [18] M. Suzuki, M. Aiba, M. Tanaka, and S. Okada, “Fundamental Development of the PLG Coil with a Surface Protection Layer,” Proc. of the 12th Jointed Railway Technology Symposium, pp.21-22 (2005-12) (in Japanese)
- [19] M. Suzuki, H. Suzuki, M. Aiba, H. Matsue, M. Tanaka, and S. Okada, “Development of the Vibration-proof Fixing Part for Ground Coil,” Proc. of the 13th Jointed Railway Technology Symposium, pp.265-266 (2006-12) (in Japanese)
- [20] M. Suzuki, H. Matsue, and M. Aiba, “Partial Discharge Characteristics of Ground Coil Simulated Inside Defect,” The 2007 IEEEJ Annual Meeting Record, 5-281, (2007-3) (in Japanese)
- [21] M. Aiba, M. Suzuki, M. Tanaka, H. Matsue, H. Suzuki, and S. Okada, “Development of a High Performance Ground Coil Combining Propulsion, Levitation and Guidance for the Maglev System,” Proc. of the 2007 Japan Industry Applications Society Conference, pp.III-167-168 (2007-8) (in Japanese)
- [22] M. Aiba, M. Suzuki, M. Tanaka, and S. Okada, “Development of the Ground Coil Combining Propulsion, Levitation and Guidance with a Surface Protection Layer for Maglev System,” Proc. of the 14th Jointed Railway Technology Symposium, pp.319-320 (2007-12) (in Japanese)
- [23] M. Suzuki, M. Aiba, and M. Tanaka, “Development of the Individual Information Management Device Application to IC Tag for Ground Coil,” Proc. of the 14th Jointed Railway Technology Symposium, pp.605-606 (2007-12) (in Japanese)
- [24] M. Suzuki, and H. Matsue, “Acceleration Deterioration Test Results of Ground Coil by Partial Discharge Stress,” The 2008 IEEEJ Annual Meeting Record, 5-061, (2008-3) (in Japanese)
- [25] H. Matsue, M. Aiba, and M. Suzuki, “Measurement of Thermal Stress on the PLG Ground Coil with GFRP Fastening Devices,” Proc. of the 2008 Japan Industry Applications Society Conference, pp.III-143-144 (2008-8) (in Japanese)
- [26] M. Aiba, and M. Suzuki, “Examination of a Power Unit for Sensing in a Detection System of Ground Coil Abnormalities,” Proc. of the 15th Jointed Railway Technology Symposium, pp.159-160 (2008-12) (in Japanese)

- [27] M. Suzuki, M. Aiba, and S. Ota, "Partial Discharge Characteristics of Ground Coil / Cable Joint which Simulated an Interfacial Abnormality," The 2009 IEEEJ Annual Meeting Record, 5-059, (2009-3) (in Japanese)
- [28] M. Aiba, and M. Suzuki, "Trial Manufacture of a Prototype of a Power Unit for Sensing in a Ground Coil," The 2009 IEEEJ Annual Meeting Record, 5-057, (2009-3) (in Japanese)
- [29] N. Takahashi, and M. Suzuki, "Impact Resistance Test of High Performance Ground Coil, The 2009 JSCE Annual Meeting Record, pp.715-716 (2009-9)
- [30] N. Takahashi, and M. Suzuki, "The shock strength evaluation of a ground coil with the protective layer," Proc. of the 16th Jointed Railway Technology Symposium, pp.413-414 (2009-12) (in Japanese)
- [31] M. Aiba and M. Suzuki, "Reduction of Eddy Current Loss of Ground Coil Winding for the Maglev System by Compression Molding," Proc. of the 16th Jointed Railway Technology Symposium, pp.357-358 (2009-12) (in Japanese)
- [32] M. Tanaka, S. Ota, M. Aiba, and M. Suzuki, "Development of a Power Supply Unit for an Anomaly Detection Sensor in a Ground Coil," Proc. of the 2008 Japan Industry Applications Society Conference, pp. III -257-258 (2010-8) (in Japanese)
- [33] S. Ota and M. Suzuki, "Examination of Defect Estimation within Ground Coil for Superconducting Maglev," The 19th MAGDA Conference (2010-11) (in Japanese)
- [34] M. Tanaka, N. Takahashi, and M. Suzuki, "Maintenance Management System for Maglev Ground Coils by Using RFID Technology," Proc. of the 17th Jointed Railway Technology Symposium, pp.153-154 (2010-12) (in Japanese)
- [35] M. Suzuki, M. Aiba, N. Takahashi, and S. Ota, "Development of Low Eddy Current Loss Ground Coil Which Applied Compression Molding to Winding Coils," Proc. of the 17th Jointed Railway Technology Symposium, pp.157-158 (2010-12) (in Japanese)
- [36] S. Ota, M. Aiba, and M. Suzuki, "Interface Pressure Characteristics of Cable Joint for Maglev Ground Coil," The 2011 IEEEJ Annual Meeting Record, 5-071, (2011-3) (in Japanese)

- [37] M. Suzuki, M. Tanaka, and M. Aiba, "Environment Characteristics of IC Tag for Individual Information Management of Ground Coils," The 2011 IEEJ Annual Meeting Record, 5-072, (2011-3) (in Japanese)
- [38] N. Takahashi, M. Suzuki, and M. Aiba, "Cable Installation Verification of the PLG Ground Coil," The 2011 JSCE Annual Meeting Record, pp.307-308 (2011-9)
- [39] M. Tanaka, M. Suzuki, and R. Ikeda, "Development of Anomaly Detection Sensors in Ground Coils of Maglev," Proc. of the 2011 Japan Industry Applications Society Conference, pp.III-273-274 (2011-9) (in Japanese)
- [40] M. Tanaka, M. Suzuki, N. Takahashi, and R. Ikeda, "Development of On-board Maintenance Management System for Maglev Ground Coils Using RFID Technology," The 2012 IEEJ Annual Meeting Record, 5-159, (2012-3) (in Japanese)
- [41] M. Suzuki, S. Ota, and N. Takahashi, "Dynamic Durability Examination of Cable Connection for Propulsion Ground Coils," The 2012 IEEJ Annual Meeting Record, 5-160, (2012-3)
- [42] N. Takahashi, and M. Suzuki, "Recycling of Ground Coils of Mold Resin as a concrete additive," The 2012 JSCE Annual Meeting Record, (2012-9)
- [43] M. Tanaka and M. Suzuki, "A study of abnormality detection accelerometers for Maglev ground coils," Proc. of the 2012 Japan Industry Applications Society Conference, pp.III-375-376 (2012-8) (in Japanese)
- [44] M. Suzuki, R. Ikeda, N. Takahashi, M. Tanaka, and M. Kawada, "Examination of Insulation Diagnosis for Ground Coil by Detecting Partial Discharge in Maglev System," Proc. of 2012 Annual Conference Fundamentals and Materials Society IEEJ, pp.389-394, Akita, (2012-9) (in Japanese)
- [45] M. Tanaka and M. Suzuki, "Condition monitoring system for railway equipment by using a sensor tag," Proc. of the 19th Jointed Railway Technology Symposium, No. 1610 (2012-12) (in Japanese)
- [46] N. Takahashi, and M. Suzuki, "Examination about the recycling of the ground coil," Proc. of the 19th Jointed Railway Technology Symposium, No. 1517 (2012-12) (in Japanese)
- [47] R. Ikeda, M. Suzuki, and S. Ota, "Deterioration of Mold Resin for Ground Coil," Proc. of the 19th Jointed Railway Technology Symposium, No.

2506 (2012-12) (in Japanese)

- [48] M. Tanaka and M. Suzuki, “Development of Condition Monitoring System for Maglev Ground Coils at High Speed Section,” The 2013 IEEEJ Annual Meeting Record, (2013-3)
- [49] N. Takahashi, and M. Suzuki, “Study to Improve the Recyclability of the Ground Coil Mold Resin at Normal Pressure Weld Solution,” The 2013 JSCE Annual Meeting Record, pp.189-190 (2013-9)

[D] Railway-specialized Publication Papers

- [1] M. Suzuki, T. Yoshikawa, H. Suwa, and T. Fujimoto, “Development of the ground coil by RIM method,” RTRI REPORT, Vol.7, No.9, pp.53-58 (1993-9) (in Japanese)
- [2] M. Suzuki, and T. Yoshikawa, “Development of the ground coil by RIM method,” Quarterly Report of RTRI, Vol. 35, No. 3, pp.178-184, (1994-8)
- [3] M. Suzuki, K. Sawada, T. Fujimoto, Y. Nakamura, and N. Aihara, “Development of a Low Cost Ground Coil by RIM Method,” RTRI REPORT, Vol.10, No.10, pp.41-46 (1996-1) (in Japanese)
- [4] T. Yoshikawa, H. Suwa, N. Aihara, and M. Suzuki, “Durability of Moulding Resins for Ground Coils of Maglev,” Quarterly Report of RTRI, Vol. 40, No. 2, (1999-2)
- [5] M. Suzuki, T. Fujimoto, and H. Suwa, “Development of Levitation Coil by Reaction Injection Molding Method,” RTRI REPORT, Vol.13, No.9, pp.9-14 (1999-9) (in Japanese)
- [6] M. Suzuki, T. Fujimoto, and H. Suwa, “Development of Levitation Coil by Reaction Injection Molding Method,” QR of RTRI, Vol.41, No.2, pp.57-62 (2000-6)
- [7] T. Murai, M. Aiba, H. Suzuki, M. Suzuki, T. Fujimoto, K. Umeki, and H. Natsuhara, “Characteristics of Null-Flux EDS with an Asymmetric Figure,” RTRI REPORT, Vol.14, No.11, pp.5-10 (2000.11) (in Japanese)
- [8] M. Ando, Y. Nakamichi, K. Ajiki, H. Shigeeda, and M. Suzuki, “Simulation Model for Surge Propagation of Propulsion Coils for Maglev,” RTRI REPORT, Vol.14, No.11, pp.17-22 (2000.11) (in Japanese)
- [9] M. Aiba, T. Murai, M. Suzuki, T. Fujimoto, T. Herai, and K. Nagashima, “The Electromagnetic Vibration Test of a Ground Coil by Using the

- Magnetic Field of Superconducting Magnets,” RTRI REPORT, Vol.14, No.11, pp.33-38 (2000.11) (in Japanese)
- [10] M. Suzuki, “Cost reduction of ground coils,” RRR of RTRI, Vol.58, No.9, pp.11-14 (2001-9) (in Japanese)
- [11] M. Ando, Y. Nakamichi, K. Ajiki, H. Shigeeda, and M. Suzuki, “Surge Characteristic Propagation on Coils Including Mutual Coupling for Maglev,” QR of RTRI, Vol.43, No.1, pp.13-19 (2002-2)
- [12] M. Aiba and M. Suzuki, “Durability Verification of Combined Propulsion, Levitation and Guidance Ground Coil,” RTRI REPORT, Vol.19, No.6, pp.19-24 (2005.6) (in Japanese)
- [13] M. Tanaka, M. Aiba and M. Suzuki, “Development of Electromagnetic Vibration Test Apparatus to Verify Durability of Ground Coils,” RTRI REPORT, Vol.20, No.8, pp.17-22 (2006.8) (in Japanese)
- [14] M. Suzuki, “Environmental Degradation Characteristics of the Mold Resin for Ground Coil,” RTRI REPORT, Vol.20, No.8, pp.23-28 (2006.8) (in Japanese)
- [15] M. Tanaka, M. Aiba and M. Suzuki, “Development of Electromagnetic Vibration Test Apparatus for Ground Coils Applied to Maglev System,” QR of RTRI, Vol.48, No.2, pp.110-114 (2007-5)
- [16] H. Suzuki, M. Suzuki, and N. Aihara, “Durability Evaluation Tests of Mold Resin for Ground Coil,” RTRI REPORT, Vol.21, No.9, pp.17-22 (2007.9) (in Japanese)
- [17] M. Suzuki, “Dynamic durability verification of the ground coil by electromagnetic vibration test,” RRR of RTRI, Vol.64, No.12, pp.28-31 (2007-12) (in Japanese)
- [18] H. Suzuki, M. Suzuki, and N. Aihara, “Durability Evaluation Tests of Mold Resin for Ground Coil,” QR of RTRI, Vol.49, No.2, pp.119-126 (2008-5)
- [19] H. Matsue, M. Aiba, and M. Suzuki, “Stress Evaluation on the PLG Ground Coil with FRP Fastening Devices,” RTRI REPORT, Vol.22, No.11, pp.17-22 (2008.11) (in Japanese)
- [20] M. Suzuki, M. Aiba, M. Tanaka, and S. Ota, “Development of the Maintenance Management Method for Ground Coil Applied Information Technology,” RTRI REPORT, Vol.24, No.1, pp.17-22 (2010.1) (in Japanese)
- [21] N. Takahashi, M. Suzuki, and M. Aiba, “Shock Assessment-resistant of a Surface Protection Layer for the Maglev System Ground Coil,” RTRI

- REPORT, Vol.24, No.1, pp.11-16 (2010.1) (in Japanese)
- [21] M. Suzuki, “Forefront, Electromagnetic Guide-way Technology to Support the Superconducting Maglev,” RRR of RTRI, Vol.68, No.2, pp.30-35 (2011-2) (in Japanese)
- [22] M. Tanaka, N. Takahashi, M. Suzuki, R. Ikeda, and S. Nagasaka, “Development of the On-board Maintenance Management System for Ground Coils of Maglev by Using RFID Technology,” RTRI REPORT, Vol.25, No.3, pp.29-34 (2011.3) (in Japanese)
- [23] M. Tanaka, N. Takahashi, and M. Suzuki, “Take Advantage of RFID to the Maintenance of Railway Equipment,” RRR of RTRI, Vol.68, No.4, pp.26-29 (2011-4) (in Japanese)
- [24] M. Tanaka, N. Takahashi, M. Suzuki, and R. Ikeda, “Development of On-board Maintenance Management System for Ground Coils of Maglev by Using RFID Technology,” QR of RTRI, Vol.53, No.1, pp.46-51 (2012-2)
- [25] N. Takahashi and M. Suzuki, “Construction-related Inspection of Cable Wiring of Ground Coil Type of PLG,” RTRI REPORT, Vol.26, No.5, pp.29-34 (2012.5) (in Japanese)
- [26] M. Suzuki, N. Takahashi, M. Aiba, and S. Ota, Development of Ground Coil with Low Eddy Current Loss by Applying the Compression Molding Method after the Coil Winding,” RTRI REPORT, Vol.26, No.5, pp.35-40 (2012.5) (in Japanese)
- [27] N. Takahashi and M. Suzuki, “Verification of Practical Applicability of Cable Wiring for PLG Ground Coils to Maglev System,” QR of RTRI, Vol.54, No.1, pp.52-58 (2013-2)
- [28] M. Suzuki, S. Ota, R. Ikeda, and M. Kawada, “Study on Locating Internal Defect of Ground Coil by Detecting Electromagnetic Waves,” RTRI REPORT, Vol.27, No.7, pp.11-16 (2013.7) (in Japanese)
- [29] M. Tanaka, and M. Suzuki, “Development of Power Supply Unit for Anomaly Detection Sensor in Ground Coils of superconducting Maglev,” RTRI REPORT, Vol.27, No.7, pp.17-22 (2013.7) (in Japanese)

[E] Public Presentations

- [1] M. Suzuki, “Development of the ground coil by RIM method,” 48th RTRI Monthly Presentation Meeting, (1992-6, Kokubunji, RTRI, Tokyo) (in Japanese)
- [2] M. Suzuki, “Durability Verification of the Ground Coil,” 146th RTRI Monthly Presentation Meeting, (2002-1, Kogakuin University, Shinjuku, Tokyo) (in Japanese)
- [3] M. Suzuki, “Examination of the Maintenance Management Method for Ground Coil Applied Information Technology,” 223th RTRI Monthly Presentation Meeting, (2009-5, S-TEC Joho Building Shinjuku, Tokyo) (in Japanese)
- [4] M. Suzuki, and S. Ota, “Ultra-accelerated Weathering Test Equipment,” RTRI Technology Exchange Meeting of Research and Diagnostic, (2010-9, Kokubunji, RTRI, Tokyo) (in Japanese)

[F] Books

- [1] Railway Technical Research Institute, “Linear,” pp.85-92, Kotsu Shinbunsha, 2006 (ISBN: 978-4-330-90506-8)

Original papers unrelated this thesis

- [1] M. Suzuki, S. Ota, S. Katayama, T. Usuki, S. Hase, and H. Shigeeda, “Development of the Insulation Horizontal Pipe for Overhead Contact System Manufactured by Sheet Winding Process,” Proc. of the 16th Jointed Railway Technology Symposium, pp.307-308 (2009-12) (in Japanese)
- [2] T. Usuki, S. Katayama, M. Suzuki, S. Ota, S. Hase, and H. Shigeeda, “DC Field Test of Metal Attachment for an Insulation Pipe,” Proc. of the 16th Jointed Railway Technology Symposium, pp.309-310 (2009-12) (in Japanese)
- [3] S. Katayama, T. Usuki, I. Matsumura, S. Hase, H. Shigeeda, H. Tanaka, M. Suzuki, and S. Ota, “Provision against Corrosion of Fittings for Insulator,” Proc. of the 2011 Japan Industry Applications Society Conference, pp. III-185-186 (2011-9) (in Japanese)
- [4] S. Katayama, T. Usuki, I. Matsumura, S. Hase, H. Shigeeda, H. Tanaka, M. Suzuki, and S. Ota, “Provision against Corrosion of Supporting

- Equipment Overhead Contact System,” Proc. of 2011 Annual Conference Fundamentals and Materials Society IEEJ, Tokyo, (2011-9) (in Japanese)
- [5] S. Katayama, T. Usuki, I. Matsumura, M. Suzuki, and S. Ota, “Development of Anti-corrosive Supporting Equipment Overhead Contact Line for Narrow Section Tunnels,” RTRI REPORT, Vol.26, No.6, pp.47-52 (2012.6) (in Japanese)

List of Patents

Patents on this thesis

Japanese

- [1] M. Suzuki and T. Fujimoto, “Wiring configuration of guidance combined use for magnetic levitation coil,” Patent registration number 02033498, (1996-3) (in Japanese)
- [2] M. Suzuki and S. Fujiwara, “Fixing method of ground coil,” Application number 178299, (1990-7) (in Japanese)
- [3] M. Suzuki, “Molding method of ground coil for Maglev system and its ground coil,” Patent registration number 02558008, (1996-5) (in Japanese)
- [4] M. Suzuki, “Ground coil,” Application number 214575, (1992-7) (in Japanese)
- [5] M. Suzuki and T. Fujimoto, “Reaction injection molding method,” Patent registration number 03741817, (2005-11) (in Japanese)
- [6] M. Suzuki and T. Fujimoto, “Manufacturing method of molded product for Maglev coil,” Patent registration number 03631351, (2004-12) (in Japanese)
- [7] M. Suzuki and T. Fujimoto, “Production method of reaction injection molded with built winding coil,” Application number 124811, (1997-4) (in Japanese)
- [8] M. Suzuki and T. Fujimoto: “Manufacturing method of molded product for Maglev coil,” Patent registration number 03939811, (2007-4) (in Japanese)

- [9] M. Suzuki and T. Fujimoto, "Manufacturing method of molded product for Maglev coil," Application number 125066, (1997-4) (in Japanese)
- [10] M. Suzuki and T. Fujimoto, "Manufacturing method of molded product for Maglev coil," Application number 140921, (1997-5) (in Japanese)
- [11] M. Suzuki and T. Fujimoto, "The ground coil system of Maglev," Patent registration number 03833360, (2006-7) (in Japanese)
- [12] T. Murai, T. Fujimoto, and M. Suzuki, "Electromagnetic vibration test equipment for ground coil," Patent registration number 03732735, (2005-10) (in Japanese)
- [13] M. Suzuki, N. Takahashi, M. Aiba, and T. Murai, "Joint device," Patent registration number 04469557, (2010-3) (in Japanese)
- [14] M. Suzuki, M. Aiba, N. Takahashi, and T. Murai, "Contact state detection jig of insulation between the cable joint," Patent registration number 04015049, (2007-9) (in Japanese)
- [15] M. Suzuki, M. Aiba, and M. Tanaka, "Ground coil device for superconducting Maglev and its manufacturing method," Patent registration number 04335162, (2009-7) (in Japanese)
- [16] M. Suzuki, H. Suzuki, and M. Aiba, "Structure of the fastening portion for Maglev ground coils," Patent registration number 04541265, (2010-7) (in Japanese)
- [17] M. Suzuki, H. Matsue, and M. Tanaka, "Structure of the fastening portion for Maglev ground coils," Patent registration number 04588593, (2010-9) (in Japanese)
- [18] M. Suzuki, M. Aiba, and M. Tanaka, "Joint device," Patent registration number 05102962, (2012-10) (in Japanese)
- [19] M. Suzuki and M. Tanaka, "The abnormality detection sensor of ground coil for Maglev and its detection system," Patent registration number 04912805, (2012-1) (in Japanese)
- [20] M. Suzuki and M. Aiba, "IC tagged ground coil for Maglev," Patent registration number 04964543, (2012-4) (in Japanese)
- [21] M. Suzuki and M. Aiba, "Ground coil system with the surface protection layer of the superconducting Maglev and evaluation method of the positioning accuracy of the protective plate," Patent registration number 05073364, (2012-8) (in Japanese)

- [22] M. Suzuki and M. Aiba, "Power supply system of an abnormality detection sensor for the Maglev ground coil," Application number 064055, (2008-3) (in Japanese)
- [23] M. Aiba, and M. Suzuki, "The device and method for measuring the SCM position of the Maglev vehicle," Patent registration number 05198100, (2013-2) (in Japanese)
- [24] M. Suzuki, "Suppression method of temperature rise for magnetic levitation ground coils," Patent registration number 05191824, (2013-2) (in Japanese)
- [25] M. Aiba, and M. Suzuki, "The apparatus and method for measuring the simulated eddy current loss of the ground coil conductor in superconducting Maglev," Patent registration number 05165614, (2012-12) (in Japanese)
- [26] M. Suzuki and M. Aiba, "Manufacturing method of the ground coil for Maglev," Patent registration number 05242490, (2013-4) (in Japanese)
- [27] M. Suzuki and M. Aiba, "Fatigue test apparatus by electromagnetic vibration using magnetic field of the SCM," Patent registration number 05225949, (2013-4) (in Japanese)
- [28] M. Suzuki and N. Takahashi, "Variable frequency fatigue test apparatus using the electro-dynamic vibration generator," Patent registration number 05275940, (2013-5) (in Japanese)
- [29] S. Ota, M. Suzuki and N. Takahashi, "Vibration test apparatus of the cable joint for superconducting Maglev ground coil," Application number 064055, (2008-3) (in Japanese)
- [30] M. Tanaka, M. Suzuki and N. Takahashi, "Management system of maintenance information for Maglev ground coils," Application number 227899, (2010-10) (in Japanese)
- [31] M. Suzuki, S. Ota, R. Ikeda, and M. Kawada, "Insulation diagnosis method of the ground coil and its apparatus," Application number 188489, (2011-8) (in Japanese)
- [32] M. Suzuki, N. Takahashi, and M. Tanaka, "Test equipment and test method of dynamic durability for superconducting Maglev ground coil," Application number 274327, (2012-12) (in Japanese)
- [33] S. Fujiwara and M. Suzuki, "The guide-way for Maglev," Application number

of utility model 134537, (1988-10) (in Japanese)

- [34] S. Fujiwara and M. Suzuki, “Ground coil,” Utility model registration number 02029981, (1994-8) (in Japanese)
- [35] M. Suzuki and S. Fujiwara, “Fixing method of the ground coil,” Application number of utility model 040752, (1989-4) (in Japanese)
- [36] M. Suzuki, “Ground coil,” Utility model registration number 02087988, (1995-11) (in Japanese)

International

- [1] M. Suzuki, “Molding method of ground coil for Maglev system and its ground coil,” Patent registration number 05178072, (1993-1) (USA)
- [2] M. Suzuki, “Molding method of ground coil for Maglev system and its ground coil,” Patent registration number 2054460, (1998-7) (Canada)
- [3] M. Suzuki, “Molding method of ground coil for Maglev system and its ground coil,” Patent registration number 41359895, (1995-11) (Germany)

Patents unrelated this thesis (Japanese)

- [1] M. Suzuki and T. Usuki, “The Apparatus and manufacturing method of Insulation Horizontal FRP Pipe for Overhead Contact System,” Application number 243257, (2012-11) (in Japanese)
- [2] K. Mizuno, M. Ogata, M. Suzuki, and R. Ikeda, “Norbornene-based Resin-impregnated Superconducting Coil,” Application number 143418, (2013-7) (in Japanese)